

---

**Transport through Hybrid  
Superconducting/Normal Nanostructures**

---

Von der Fakultät für Physik  
der Universität Duisburg-Essen  
genehmigte

**Dissertation**

zur Erlangung des Grades  
Doktor der Naturwissenschaften

von  
**Dipl.-Phys. David Futterer**  
aus Münster

**Duisburg 2013**

Referent:	Prof. Dr. J. König
Korreferent:	Prof. Dr. K. Flensberg
Tag der mündlichen Prüfung:	29.01.2013



---

## Deutsche Zusammenfassung

In dieser Arbeit untersuchen wir hauptsächlich den Transport durch wechselwirkende Quantenpunkte. Dafür erweitern wir eine bereits existierende Theorie, um mit dieser den elektrischen Transport durch proximisierte Quantenpunkte mit normalen- und supraleitenden Zuleitungen zu beschreiben. Dadurch sind wir in der Lage, den Einfluss einer starken Coulombwechselwirkung auf Josephson- und Andreevströme zu studieren. Dies ist eine besonders interessante Themenstellung, da hier zwei gegensätzliche Mechanismen aufeinandertreffen: In Supraleitern erfahren Elektronen paarweise eine anziehende Wechselwirkungskraft, wodurch sie sich zu Cooper-Paaren zusammenschließen, wohingegen sich zwei Elektronen auf dem Quantenpunkt durch die Coulomb-Kraft gegenseitig abstoßen. Das suggeriert, dass elektrische Transportprozesse, die Cooper-Paare involvieren, unterdrückt sein müssten. Allerdings ist es möglich, den supraleitenden Proximityeffekt in Nichtgleichgewichtssituationen auf dem Dot zu induzieren.

Zunächst untersuchen wir ein System, das aus einem Quantenpunkt besteht, der an eine normale-, eine ferromagnetische- und eine supraleitende Zuleitung gekoppelt ist. Im Limes einer unendlich großen Energielücke des Supraleiters wird die Kopplung zum Supraleiter durch die vorgestellte Theorie exakt beschrieben. In diesem Limes formieren sich Andreev-gebundene Zustände (ABS), die es erlauben, einen Spinstrom, der durch keinen Ladungsstrom begleitet wird, zu generieren.

Als nächstes führen wir, ausgehend vom Limes unendlich großer Energielücken, eine Störungsentwicklung des Gaps um unendlich durch. Anhand der Josephson- und Andreevströme überprüfen wir, wie gut die Vorhersagen der Rechnungen im Limes unendlich großer Energielücken für reale Systeme mit kleinen Energielücken sind. Wir finden Hinweise auf eine Renormierung der ABS und stellen einen Resummationsansatz vor, der es erlaubt, die ABS für eine endliche Energielücke abzuschätzen. Da abgesehen von der Renormierung die Änderungen der Ströme relativ klein sind, folgern wir, dass mit den Rechnungen im Limes unendlich großer Gaps auch für Systeme mit endlichen Gaps verlässliche Vorhersagen getroffen werden können. Neben den endlichen Gaps ist es auch möglich, Renormierungen durch die Kopplung des Quantenpunkts an eine normale Zuleitung herbeizuführen. Um diese zu untersuchen, berechnen wir die Korrekturen, die sich durch die Kopplung an die normale Zuleitung ergeben und identifizieren Renormierungen der  $0 - \pi$ -Übergänge des Josephsonstroms, der Extrema des Andreevstroms und der gemittelten Ladung auf dem Quantenpunkt.

In unserer letzten Arbeit betrachten wir ein hybrides System, bestehend aus einem p-dotierten Halbleiter, der sich an einer Grenzfläche zu einem Supraleiter befindet. Dieses System untersuchen wir auf mögliche Andreevreflexionen von leichten- und schweren Löchern für beliebige Injektionswinkel. Dazu lösen wir die Bogoliubov-de Gennes-Gleichung für ein  $6 \times 6$ -Kane-Modell und entdecken, dass sowohl leichte Löcher, wie auch schwere Löcher Andreev reflektiert werden und dabei auch ineinander umgewandelt werden können. Es stellt sich heraus, dass senkrecht injizierte schwere Löcher nicht Andreev reflektiert werden können, und dass es zweierlei kritische Winkel gibt. Einen kritischen Winkel für umwandlungsfreie Andreevreflexionen und einen kritischen Winkel, oberhalb dem schwere Löcher nicht mehr in leichte Löcher umgewandelt werden können.

---

---

## English abstract

We mainly investigate transport through interacting quantum dots proximized by superconductors. For this purpose we extend an existing theory to describe transport through proximized quantum dots coupled to normal and superconducting leads. It allows us to study the influence of a strong Coulomb interaction on Andreev currents and Josephson currents. This is a particularly interesting topic because it combines two competing properties: in superconductors Cooper pairs are formed by two electrons which experience an attractive interaction while two electrons located on a quantum dot repel each other due to the Coulomb interaction. It seems at first glance that transport processes involving Cooper pairs should be suppressed because of the two competing interactions. However, it is possible to proximize the dot in nonequilibrium situations.

At first, we study a setup composed of a quantum dot coupled to one normal, one ferromagnetic, and one superconducting lead in the limit of an infinitely-large superconducting gap. Within this limit the coupling between dot and superconductor is described exactly by the presented theory. It leads to the formation of Andreev-bound states (ABS) and an additional bias scheme opens in which a pure spin current, i.e. a spin current with a vanishing associated charge current, can be generated.

In a second work, starting from the infinite-gap limit, we perform a systematic expansion of the superconducting gap around infinity and investigate Andreev currents and Josephson currents. This allows us to estimate the validity of infinite-gap calculations for real systems in which the superconducting gap is usually a rather small quantity. We find indications that a finite gap renormalizes the ABS and propose a resummation approach to explore the finite-gap ABS. Despite the renormalization effects the modifications of transport by finite gaps are rather small. This result lets us conclude that the infinite-gap calculation is a valuable tool to study transport through proximized interacting quantum dots. Not only does a finite superconducting gap give rise to renormalization effects but also the coupling to the normal lead can evoke renormalizations. To explore these we calculate the correction terms arising from the coupling to the normal lead and identify renormalizations of the  $0 - \pi$  transitions of the Josephson current, the extrema of the Andreev current, and the average dot charge.

In the previous works the occurring normal conducting leads are assumed to be metallic so that the shape of the band structure can be neglected. If the normal conducting region is a semiconductor, the shape of the band structure plays an important role. In our last calculation we consider a p-type semiconductor–superconductor interface and study oblique injections of light holes and heavy holes. Solving the Bogoliubov-de Gennes equations for a  $6 \times 6$  Kane model we find that light holes and heavy holes can be Andreev reflected and in this process converted into each other. Moreover, in perpendicular incidence heavy holes cannot be Andreev reflected. Two types of critical angles occur. First, a critical angle above which conversion-less Andreev reflection is no longer possible and, second, a critical angle above which heavy holes cannot be converted into light holes anymore.



# Contents

<b>1</b>	<b>Introduction</b>	<b>1</b>
<b>2</b>	<b>Hybrid systems containing quantum dots and superconductors</b>	<b>5</b>
2.1	superconductivity . . . . .	5
2.1.1	BCS-theory . . . . .	5
2.1.2	DC Josephson effect . . . . .	8
2.1.3	Andreev reflection . . . . .	8
2.2	Quantum dots . . . . .	9
2.2.1	Basic concepts . . . . .	10
2.2.2	Transport through single-level quantum dots . . . . .	11
2.3	Quantum dots coupled to superconductors . . . . .	13
2.3.1	Experiments on quantum dots coupled to superconductors . . . .	14
	Supercurrent reversal in quantum dots . . . . .	14
	Cooper pair beam splitter . . . . .	15
	Observation of Andreev-bound states in quantum dots . . . . .	15
2.3.2	Interacting quantum dots in the infinite-gap limit . . . . .	16
	Model . . . . .	17
	Reduced density matrix and current formula . . . . .	18
	Isospin . . . . .	18
	Andreev bound states . . . . .	19
<b>3</b>	<b>Diagrammatic technique</b>	<b>23</b>
3.1	Model . . . . .	23
3.2	Effective Hamiltonian . . . . .	24
3.3	Reduced density matrix . . . . .	25
3.4	Interaction picture and Keldysh time . . . . .	25
3.5	Generalized master equation . . . . .	27
3.6	Current formula . . . . .	28
3.7	Diagrammatic rules . . . . .	28
3.8	Large-gap limit . . . . .	30
<b>4</b>	<b>Generation of pure spin currents by superconducting proximity effect in quantum dots</b>	<b>33</b>
4.1	Model and method . . . . .	34
4.2	Results . . . . .	35
4.3	Conclusions . . . . .	39

---

<b>5</b>	<b>Renormalization effects in interacting quantum dots coupled to superconducting leads</b>	<b>41</b>
5.1	Model and Method . . . . .	42
5.1.1	Hamiltonian . . . . .	42
5.1.2	Diagrammatic Technique . . . . .	43
	Effective Dot Hamiltonian . . . . .	43
	Generalized Master Equation . . . . .	44
	Current formulae . . . . .	45
5.2	Finite-gap effects . . . . .	46
5.2.1	$1/\Delta$ Expansion . . . . .	46
5.2.2	Renormalization of Andreev Bound States . . . . .	49
	Exact Green's function for the noninteracting dot . . . . .	49
	Hartree-Fock approximation . . . . .	49
	Resummation Approach . . . . .	50
5.3	Beyond weak coupling to the normal lead . . . . .	52
5.4	Conclusions . . . . .	57
<b>6</b>	<b>Band-mixing-mediated Andreev reflection of semiconductor holes</b>	<b>59</b>
6.1	Model . . . . .	60
6.2	Results . . . . .	65
6.3	Conclusions . . . . .	71
<b>7</b>	<b>Conclusions</b>	<b>73</b>
<b>A</b>	<b>Calculating diagrams via Mathematica</b>	<b>75</b>
<b>B</b>	<b>Diagrams contributing to the resummation approach</b>	<b>90</b>
	<b>Bibliography</b>	<b>92</b>

# 1 Introduction

In superconductors electrons experience an attractive interaction and form Cooper pairs. At the Fermi energy Cooper pairs are energetically more favorable than single-particle excitations so that the formation of Cooper pairs is accompanied by the formation of an energy gap inside which no single-particle excitations exist. Electrical sub-gap transport between a superconductor and a normal conductor is thus not carried by single electrons but sustained by a process known as *Andreev reflection*. In an Andreev reflection process a Cooper pair of the superconductor is split and two electrons with opposite spin and momentum are transferred into the normal conductor or vice versa. We are interested in studying the impact of Coulomb repulsion between electrons on Andreev reflection. In superconductors the two electrons forming a Cooper pair are usually spatially separated. Therefore, the experienced Coulomb repulsion between the two electrons is rather small. This motivates the inclusion of quantum dots between the superconductor and the normal conductor: quantum dots are small systems that confine occupying electrons to effectively zero dimensions. In fact, quantum dots can be so small that the Coulomb repulsion between two electrons on the dot can become the dominating energy scale of the system. It makes hybrid systems composed of quantum dots coupled to superconducting and normal conducting reservoirs especially interesting setups to study because here the competition between the attractive interaction of the Cooper pairs and the Coulomb repulsion of the dot can be investigated. Such hybrid superconductor-quantum dot systems have frequently been studied during past years.<sup>1,2</sup>

Experimentally, highly controllable quantum dots have been realized e.g. in semi-conducting two-dimensional electron gases (2DEG).<sup>3</sup> Since superconductivity usually cannot be found in semiconductors, 2DEGs are rather inappropriate to create quantum dots contacted to superconducting reservoirs. Experimental groups were nevertheless able to couple quantum dots to superconductors in realizing quantum dots in semiconductor nanowires or carbon nanotubes which can be contacted to superconductors.<sup>1</sup> Recent examples of experiments involving superconductor-dot-normal conductor junctions are the search for signatures of Majorana fermions,<sup>4</sup> Cooper pair beam splitters,<sup>5-8</sup> and the investigation of Andreev-bound states (ABS).<sup>9,10</sup> The formation of the last mentioned ABS is a direct consequence of the superconducting proximity effect, which will be in the focus of this thesis. Carbon nanotubes can also be coupled to ferromagnetic electrodes<sup>11-13</sup> so that even hybrid superconducting-ferromagnetic quantum dot systems can be investigated<sup>14</sup> to study the interplay of spin-dependent currents and superconductivity in combination with the Coulomb interaction.

From the theoretical point of view transport through non-interacting quantum dots can be solved exactly by means of a scattering approach.<sup>15</sup> To get an impression of how the finite Coulomb interaction acts on transport it can be treated on a perturbative

## 1 Introduction

---

level.<sup>16–21</sup> However, in systems where the Coulomb interaction is large compared to other quantities this approach is no longer justified. In these systems transport can be calculated in the weak-coupling limit, where the coupling between dot and leads is treated perturbatively.<sup>22</sup> The aim of this thesis is to investigate strongly proximized interacting quantum dots in which ABS are formed. Since the formation of ABS requires tunneling processes of high order, the weak-tunneling limit for the coupling between dot and the superconductors is not an appropriate choice. One possible regime that can account for a large on-site Coulomb interaction as well as a large coupling between dot and superconductors is the infinite-gap limit. In Ref. 23 it has been shown that in this limit the coupling between dot and superconductors can be resummed exactly for arbitrary Coulomb interactions.

In the present thesis we reformulate the diagrammatic language introduced in Ref. 23 in the eigenbasis of an effective Hamiltonian<sup>24–32</sup> which already includes the coupling between dot and superconductors. It has the great advantage that the rather lavish resummation can be skipped.

In the first result chapter we demonstrate how the formation of ABS can lead to a pure spin current. To this end we consider a hybrid setup composed of an interacting quantum dot coupled to a superconducting, a normal and a ferromagnetic lead in the infinite-gap limit and identify a biasing scheme which enables the generation of pure spin currents, i.e. a finite spin current with no associated charge current, in the normal lead.

In real systems the superconducting gap is usually not the largest energy scale so that it is not clear whether the infinite-gap limit enables an appropriate description of real systems. To address this question we perform an expansion of the superconducting gap around infinity to arrive at a first estimation of the influence of a finite gap. It turns out that a finite gap renormalizes the ABS and that despite this renormalization the infinite-gap calculations already lead to quantitatively good results. Furthermore, we present a resummation approach that allows to explore the finite-gap ABS. We compare the so obtained ABS with the Hartree-Fock approximation of Ref. 9 and with the NRG data of Ref. 33, 34. In the above mentioned works the coupling to the normal conducting leads is always assumed to be weak and only leading-order tunneling processes are being accounted for. To study the impact of a normal lead on the superconducting proximity effect induced on an interacting quantum dot we perform a perturbation expansion in the coupling to the normal lead to determine the corrections arising from the coupling to the normal lead. In our analyses of the results we focus on renormalization effects occurring in the Josephson current, Andreev current and the average dot charge.

Despite the issue of how Andreev reflection processes are influenced by an on-site Coulomb repulsion an other interesting aspect to investigate is the question of how Andreev reflections depend on the band structure of the normal conductor. The shape of the band-structure of typical normal conducting metallic electrodes can usually be neglected, but for semiconductors, which have a much smaller Fermi energy, it is important. Blonder *et al.* have formulated a scattering approach<sup>35</sup> based on the Bogoliubov-de Gennes equations<sup>36</sup> to study the scattering amplitudes of normal conductor–superconductor interfaces. Further studies analyzed oblique Andreev re-

flections and found that critical angles may occur above which Andreev reflection is no longer possible. Here, we turn our attention to a p-type semiconductor directly contacted to a superconductor. In p-type semiconductors transport is mediated by quasiparticle holes which possess a spin-3/2 degree of freedom. Particles with spin projection of 1/2 are light holes, while particles with spin projection 3/2 are heavy holes. The holes stem from the semiconductor's valence band and mix with conduction-band states which enables them to be Andreev reflected. We investigate the conditions required for light holes and heavy holes to be Andreev reflected and determine the angle dependence of the possible Andreev processes. Hereby, we identify two different types of critical angles.

This thesis is structured as follows. In Chapter 2 we start with a short introduction to superconductivity. In particular, we focus on the BCS theory including the Bogoliubov transformation and on the Josephson effect and the process of Andreev reflection. Furthermore, in this chapter we motivate the use of quantum dots with a special focus on hybrid systems containing quantum dots coupled to superconductors. We will give several examples of experimental realizations of such systems as well as a short summary of the theoretical investigation of a three-terminal setup composed of a quantum dot coupled to one normal and two superconducting leads. The theory describing interacting quantum dots coupled to normal, superconducting, and ferromagnetic leads is presented in Chapter 3. It includes the formulation of the diagrammatic technique in the basis of the above mentioned effective Hamiltonian. In Chapter 4 a hybrid system composed of an interacting quantum dot coupled to one normal, one ferromagnetic, and one superconducting lead is investigated in the infinite-gap limit with the objective of finding a pure spin current in the normal lead. Renormalization effects arising from a systematic  $1/\Delta$  expansion on the one hand and from the corrections arising from the coupling to the normal lead on the other hand is presented in Chapter 5. Next, in a hybrid system composed of a p-type semiconductor–superconductor interface we study the circumstances under which light holes and heavy holes can undergo the process of Andreev reflection. These results are given in Chapter 6. In the final Chapter 7 the conclusions will be drawn.

## 1 Introduction

---

# 2 Hybrid systems containing quantum dots and superconductors

## 2.1 superconductivity

Certain materials completely lose their electrical resistance below a critical temperature  $T_c$ . These materials are called *superconductors*. From the discovery of superconductivity in 1911 by H. K. Onnes<sup>37</sup> until today the field of superconductivity is of great interest for scientific researches. About 22 years after its discovery W. Meißner and R. Ochsenfeld were able to prove that superconductivity is not just the effect of vanishing electrical resistance but superconductivity is a thermodynamical state: when a magnetic field penetrates a superconducting material in its normal state and then the material is cooled down below the critical temperature the magnetic field will be repelled from this material.

Superconductors divide into the two subgroups: type I and type II superconductors. Type I superconductors have only one critical temperature  $T_c$  that separates the superconducting state from the normal conducting state. In the superconducting state the magnetic field inside the superconductor vanishes. Examples of type I superconductors are metallic superconductors like aluminum, mercury or lead. In contrast to type I superconductors type II superconductors possess two critical temperatures  $T_{c1}$  and  $T_{c2}$ . Below the lower critical temperature  $T_{c1}$  the material is superconducting and magnetic fields are repelled completely. Between the two critical temperatures the superconductor is in a mixed state, the so called vortex state. Here the material is still superconducting but, additionally, magnetic fields can penetrate into the superconductor in form of vortices. For temperatures above  $T_{c2}$  the material is normal conducting. Examples of type II superconductors are the high-temperature ceramic superconductors<sup>38</sup> and the iron-based superconductors.<sup>39</sup>

In this thesis we mainly consider setups containing superconductors tunnel coupled to quantum dots. In order to be able to calculate the transport properties of such systems it is important to have a microscopic theory for the superconductors. The BCS theory is just such a microscopic theory, and in this work we will solely focus on conventional superconductors that can be described with the BCS theory.

### 2.1.1 BCS-theory

In this section we will give a short summary of the derivation of the mean-field BCS Hamiltonian following Ref. 40. We start from the Fröhlich Hamiltonian

$$H = \sum_{k,\sigma} \epsilon_k c_{k,\sigma}^\dagger c_{k,\sigma} + \sum_{k,q,\sigma} \left[ M(q) c_{k+q,\sigma}^\dagger c_{k,\sigma} b_q + M(-q) c_{k-q,\sigma}^\dagger c_{k,\sigma} b_q^\dagger \right] + \sum_q \hbar \omega_q b_q^\dagger b_q, \quad (2.1)$$

## 2 Hybrid systems containing quantum dots and superconductors

---

where  $c_{k,\sigma}^{(\dagger)}$  are annihilation (creation) operators for electrons with momentum  $k$  and spin  $\sigma$ ,  $\epsilon_k$  the corresponding single-particle energies,  $b_q^{(\dagger)}$  the annihilation (creation) operators for phonons with momentum  $q$ ,  $\hbar\omega_q$  the corresponding energies and  $M(q)$  is the electron-phonon coupling. In second order perturbation theory an effective Hamiltonian for the electrons can be derived from the Fröhlich Hamiltonian:

$$H = \sum_{k,\sigma} \epsilon_k c_{k,\sigma}^\dagger c_{k,\sigma} - \frac{V_{k,k',q}}{2} \sum_{\sigma,\sigma'} \sum_{k,k',q} c_{k+q,\sigma}^\dagger c_{k'-q,\sigma'}^\dagger c_{k',\sigma'} c_{k,\sigma}, \quad (2.2)$$

with

$$V_{k,k',q} = |M(q)|^2 \frac{-2\hbar\omega_q}{(\epsilon_{k+q} - \epsilon_k)^2 - (\hbar\omega_q)^2}. \quad (2.3)$$

The second sum of Eq. (2.2) describes an effective electron-electron interaction that results from the electron-phonon coupling. For  $|\epsilon_{k+q} - \epsilon_k| < \hbar\omega_q$  this electron-electron interaction becomes attractive. Two electrons attracting each other are called *Cooper pair*. A Cooper pair can be the energetically more favorable state for two electrons close to the Fermi energy. As a consequence the Fermi sea becomes unstable and electrons close to the Fermi energy condense into a macroscopic state formed by Cooper pairs. It can be shown<sup>40</sup> that the optimal condition for Cooper pairs to be formed is that the participating electrons have opposite momenta. Furthermore, since the total wave functions of the participating electrons need to be antisymmetric the two electrons must have opposite spins. Though in general triplet superconductivity<sup>41,42</sup> is possible, in this thesis we will always consider the common case where Cooper pairs consist of spin singlets.

The preceding considerations lead to the BCS<sup>43,44</sup> Hamiltonian

$$H = \sum_{k,\sigma} \epsilon_k c_{k\sigma}^\dagger c_{k\sigma} - V \sum_{k,k'} c_{k'\uparrow}^\dagger c_{-k'\downarrow}^\dagger c_{-k,\downarrow} c_{k\uparrow}, \quad (2.4)$$

where the phonon-mediated interaction  $V$  is assumed to be independent of  $k, k'$ , and  $q$ . Applying the mean-field theory to the BCS Hamiltonian and introducing the pair potential  $\Delta = V \sum_{k'} \langle c_{-k'\downarrow} c_{k'\uparrow} \rangle$  yields the mean-field BCS Hamiltonian

$$H = \sum_{k,\sigma} \epsilon_k c_{k\sigma}^\dagger c_{k\sigma} - \Delta^* \sum_k c_{-k,\downarrow} c_{k\uparrow} - \Delta \sum_k c_{k\uparrow}^\dagger c_{-k,\downarrow}^\dagger + \frac{|\Delta|^2}{V}. \quad (2.5)$$

With respect to the Fröhlich Hamiltonian of Eq. (2.1) the mean-field BCS Hamiltonian has simplified a lot. It will be the Hamiltonian that we will use to model the superconductors appearing in the context of this thesis. The pairing of electrons to Cooper pairs is captured by the terms containing two annihilation or accordingly two creation operators. A problem of the mean-field BCS Hamiltonian is that it is not conserving the number of particles. For this reason we take the Fermi energy of the occurring superconductors always as reference energy, i.e.  $E_F^S = 0$ . This guarantees energy conservation even if the number of particles is not being conserved.

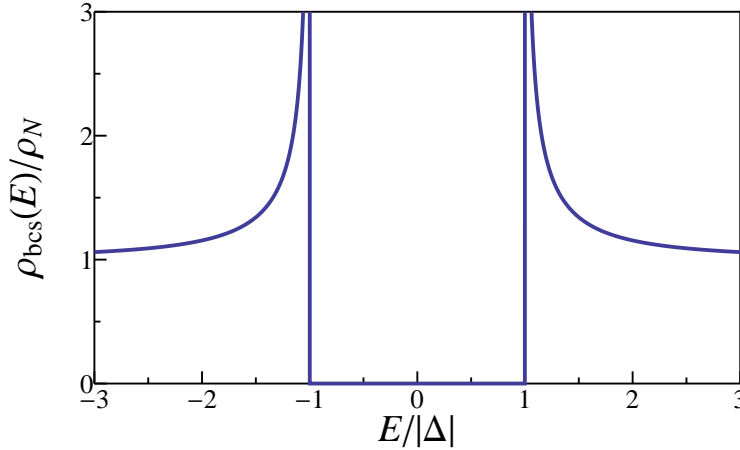


Figure 2.1: Density of states in a BCS superconductor.

The mean-field Hamiltonian can be diagonalized to

$$H = \sum_k E_k \left( \gamma_{k\uparrow}^\dagger \gamma_{k\uparrow} + \gamma_{k\downarrow}^\dagger \gamma_{k\downarrow} \right), \quad (2.6)$$

by transforming the electronic operators into quasiparticle operators with the Bogoliubov transformation

$$\gamma_{k\uparrow} = u_k c_{k\uparrow} - v_k c_{-k\downarrow}^\dagger \quad (2.7)$$

$$\gamma_{-k\downarrow} = u_k c_{-k\downarrow} + v_k c_{k\uparrow}^\dagger. \quad (2.8)$$

In Eq. (2.6) we have introduced the quasiparticle energy  $E_k = \sqrt{\epsilon_k^2 + |\Delta|^2}$  and neglected additive constants. The quasiparticle operators  $\gamma_{k\sigma}$  behave like fermionic operators if  $|v_k|^2 + |u_k|^2 = 1$  holds.

The superconducting density of states is then given by

$$\rho_{\text{bcs}} = \rho_N \frac{|E|}{\sqrt{E^2 - |\Delta|^2}} \Theta(|E| - |\Delta|), \quad (2.9)$$

where  $\rho_N$  is the normal state density of states.

For large energies  $|E| \gg |\Delta|$  the density of states of the quasiparticles converges towards the normal state density of states, see Fig. 2.1. At the points  $E = \pm|\Delta|$  the density of states of the quasiparticles diverges and in between the two points a gap is formed. This means that directly at the Fermi level of the superconductor, i.e.  $E = 0$ , single-particle excitations are suppressed and there transport is carried solely by Cooper pairs. Thus, the superconducting pair potential  $\Delta$  determines the size of the energy gap and in the course of this thesis we will often refer to it as the *superconducting gap*.

## 2 Hybrid systems containing quantum dots and superconductors

---

### 2.1.2 DC Josephson effect

In this section we study transport between two superconductors. In a so-called Josephson junction two superconductors are coupled to each other via a non-superconducting barrier. The Cooper pairs on each side can be described by macroscopic wave functions  $\psi_L$  and  $\psi_R$ , respectively, which obey the time-dependent Schrödinger equation

$$i\hbar \frac{\partial}{\partial t} \psi_L = E_L \psi_L + K \psi_R \quad (2.10)$$

$$i\hbar \frac{\partial}{\partial t} \psi_R = E_R \psi_R + K \psi_L, \quad (2.11)$$

with  $K$  being the coupling between the two superconductors. The resulting current flowing from the left into the right superconductor is then given by

$$I_L = e \frac{\partial}{\partial t} |\psi_L|^2 \quad (2.12)$$

$$= \frac{K}{i\hbar} (\psi_1^* \psi_2 - \psi_2^* \psi_1), \quad (2.13)$$

which can be simplified to

$$I_L = \frac{2eK}{\hbar} |\psi_L| |\psi_R| \sin(\phi_R - \phi_L), \quad (2.14)$$

where  $\phi_{L(R)}$  is the phase of the wave function in the left (right) lead. Eq. (2.14) tells us that without applying a bias voltage a Cooper-pair current can flow between the two superconductors that depends on the phase difference. This effect is known as the dc Josephson effect.<sup>45</sup>

### 2.1.3 Andreev reflection

How is transport sustained between a superconductor and a normal conductor? At the Fermi level single electrons from the normal conductor cannot enter the superconductor due to the superconducting gap. However, two electrons with opposite spin and opposite momentum can be transferred into the superconductor in form of a Cooper pair. Such a combined process is known as *Andreev reflection*.<sup>46,47</sup> Technically, it is useful to interpret the process as a reflection process rather than a process where two electrons approach the interface at the same time: an electron with spin  $\sigma$  and momentum  $k$  impinging at the normal conductor–superconductor interface from the normal-conducting side can be retroreflected, i.e. the momentum is reversed, as a time-reversed electron with reversed spin, often referred to as “hole” that has all properties of the time-reversed partner of the incident particle. During this reflection process two electrons with opposite spin and momentum are removed from the normal conducting side and injected into the superconducting side as a Cooper pair. In literature the reflected time-reversed electrons are often referred to as “holes” but we will avoid this nomenclature and reserve the term hole to always refer to a state in the valence band of semiconductor materials. From the BCS Hamiltonian the Bogoliubov-de Gennes

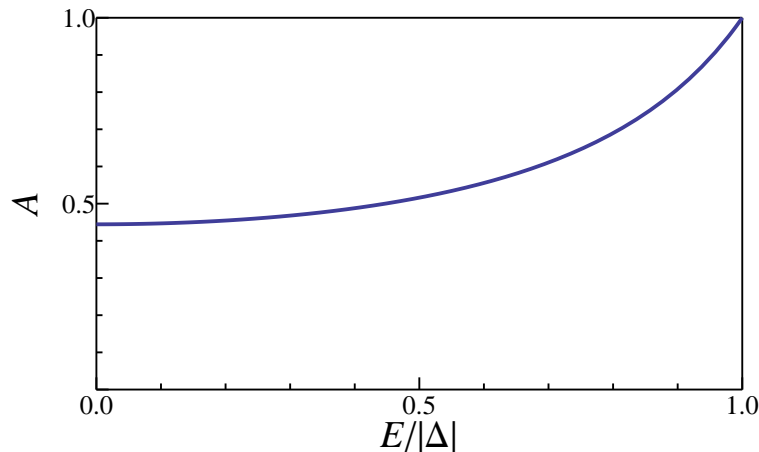


Figure 2.2: Probability of Andreev reflection through a normal metal – superconductor interface with a finite scattering parameter  $Z = |\Delta|/2$ .

equation, which is similar to the Schrödinger equation formulated in Nambu space, has been derived.<sup>36</sup> The Bogoliubov-de Gennes equation reads

$$\begin{pmatrix} H_0 & \Delta \\ \Delta^* & -H_0^* \end{pmatrix} \begin{pmatrix} u(\mathbf{r}) \\ v(\mathbf{r}) \end{pmatrix} = E \begin{pmatrix} u(\mathbf{r}) \\ v(\mathbf{r}) \end{pmatrix}, \quad (2.15)$$

where  $H_0$  is the single-particle Hamiltonian and  $u(\mathbf{r})$  and  $v(\mathbf{r})$  are the Nambu space components of the wave function. In a fundamental work by Blonder *et al.*<sup>35,48</sup> scattering amplitudes of normal-superconductor junctions with a barrier height of  $Z$  have been investigated. From the Bogoliubov-de Gennes equation the probabilities for an injected particle with energy  $E < \Delta$  to be Andreev reflected  $A$  and to be normal reflected  $B$  have been determined to

$$A = \frac{\Delta^2}{E^2 + (\Delta^2 - E^2)(1 + 2Z^2)^2}, \quad (2.16)$$

$$B = 1 - A. \quad (2.17)$$

A vanishing barrier, which corresponds to a perfectly clean interface without a mismatch of Fermi wave vectors, causes the probability for Andreev reflection to be one. For finite barrier strengths the probability for Andreev reflection starts for  $E = 0$  at  $1/(1 + 2Z^2)^2$  and approaches one for  $E \rightarrow \Delta$ , see Fig. 2.2.

## 2.2 Quantum dots

Similar to electrons in single atoms, where the electrons are distributed on quantized energy levels, in quantum dots the occupying electrons are confined in all three spatial dimensions resulting in a quantized energy spectrum. The great advantage of quantum dots is the possibility to control their properties such as the level positions or

## 2 Hybrid systems containing quantum dots and superconductors

---

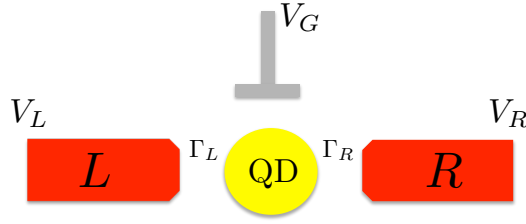


Figure 2.3: Two normal metals are tunnel coupled to a quantum dot. The quantum dot's energy levels can be controlled by the chemical potential of the gate electrode.

the couplings to external electrodes. Due to their small size the Coulomb repulsion between electrons located on the dot can become the dominating energy scale. Therefore, quantum dots have proved to be an ideal device to explore interaction effects in experiments. In order to study the influence of these interaction effects on the transport properties in various situations quantum dots have been tunnel coupled to different kinds of conducting materials such as semiconductors, metallic reservoirs or superconductors.

### 2.2.1 Basic concepts

Exemplary, we focus on a quantum dot tunnel coupled to two normal electrodes, see Fig. 2.3. The voltages  $V_L$  and  $V_R$  determine the chemical potential of the left and right electrode, respectively, and the energy levels of the dot can be tuned by the gate voltage  $V_G$ . Then the capacitance of the quantum dot can be assumed to be the sum of the single capacitances induced by the proximity of the electrodes, i.e.  $C = C_L + C_R + C_G$ . Here  $C_L$  ( $C_R$ ) is the capacitance arising from the tunnel couplings to the left (right) reservoir and  $C_G$  is the capacitance evoked by the gate electrode. The applied voltages induce an external charge  $Q_0 = eN_0 = C_L V_L + C_R V_R + C_G V_G$  on the quantum dot. Changing the dot occupation by one electron requires the energy  $E = e^2/2C$  and, thus, the charging energy for the dot being occupied by  $N$  electrons is given by

$$E_{ch}(N, N_0) = \frac{e^2}{2C}(N - N_0)^2. \quad (2.18)$$

In Fig. 2.4(a) we show a graphical representation of the charging energy of the quantum dot. The charging energy for  $N$  electrons occupying the quantum dot that results from an external charge  $Q_0$  is indicated by the dotted lines. The lowest energies correspond to the ground state and are displayed as straight lines. At integer values of the number of external charges  $N_0$  a maximal amount of energy is required to change the number of electrons occupying the dot by one. In this case electronic transport through the quantum dot is *Coulomb blocked*. But in contrast, at the degeneracy points of half-integer values of  $N_0$  no energy is required to change the dot occupation by one electron. The latter situation is favorable for transport situations because tunneling of electrons onto and off the dot is required in order to drive a current through a quantum dot. This statement is illustrated by the conductance<sup>49</sup> shown in Fig. 2.4(b): at half-integer

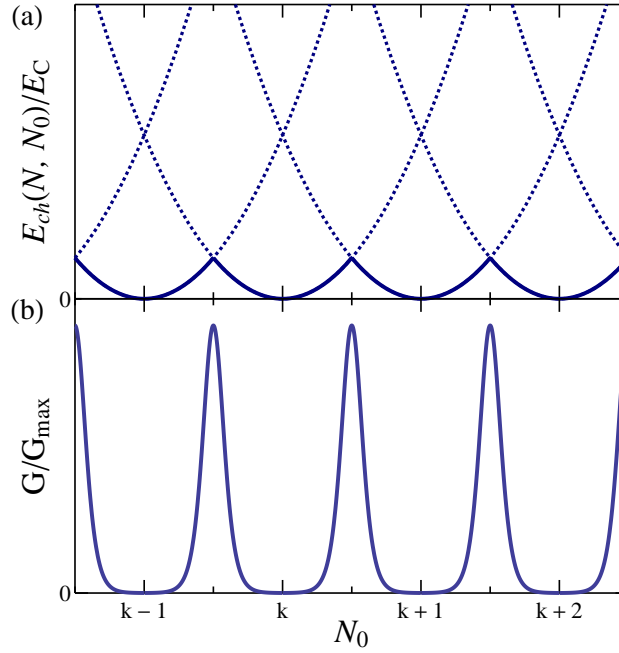


Figure 2.4: Plot of (a) the charging energy of the quantum dot for occupations of  $N$  electrons and (b) the normalized conductance of the quantum dot according to Ref. 49 as a function of the number  $N_0$  of external induced electrons on the dot.

values of the external number of electrons electrons can tunnel onto and from the dot giving rise to a large conductance while at integer values the number of electrons on the dot is fixed and the conductance through the quantum dot is suppressed. The resulting conductance shows oscillations, which are named *Coulomb oscillations*. It implies that a current flowing through the quantum dot can be switched on and off just by varying the external charge by the gate voltage. Such a geometry is called *single-electron transistor*.

### 2.2.2 Transport through single-level quantum dots

A quantum dot in which the splitting of energy levels is so large that only a single energy level can be accessed in transport situations is called *single-level quantum dot*. Theoretically, the single-level quantum dot can be modeled by the Anderson Hamiltonian<sup>50</sup>

$$H_{\text{dot}} = \sum_{\sigma} \epsilon d_{\sigma}^{\dagger} d_{\sigma} + U n_{\uparrow} n_{\downarrow}, \quad (2.19)$$

where  $\epsilon$  is the spin-degenerate single-particle energy and  $U$  is the on-site Coulomb repulsion arising at double occupancy. Electrons of spin  $\sigma$  are being annihilated (created) by the dot's operators  $d_{\sigma}^{(\dagger)}$ , and  $n_{\sigma} = d_{\sigma}^{\dagger} d_{\sigma}$  is the corresponding number operator. The single-level quantum dot has the four eigenstates  $|\chi\rangle \in \{|0\rangle, |\uparrow\rangle, |\downarrow\rangle, |d\rangle \equiv d_{\uparrow}^{\dagger} d_{\downarrow}^{\dagger} |0\rangle\}$  corresponding to an empty dot, to the dot being singly occupied by an electron of

## 2 Hybrid systems containing quantum dots and superconductors

---

$$\begin{array}{cccc}
 |0\rangle & |\uparrow\rangle & |\downarrow\rangle & |d\rangle \\
 \text{---} & \uparrow\text{---} & \text{---}\downarrow & \uparrow\downarrow \\
 E = & 0 & \epsilon & \epsilon & 2\epsilon + U
 \end{array}$$

Figure 2.5: Eigenstates and eigenenergies of an interacting single-level quantum dot. The dot can either be empty with eigenenergy  $E_0 = 0$ , singly occupied with a spin-up electron or a spin-down electron with eigenenergy  $E_\uparrow = E_\downarrow = \epsilon$  or it can be doubly occupied with eigenenergy  $E_d = 2\epsilon + U$ .

spin  $\sigma$ , and a doubly occupied dot, respectively. The corresponding eigenenergies are  $E_0 = 0$ ,  $E_\uparrow = E_\downarrow = \epsilon$ , and  $E_d = 2\epsilon + U$ , see Fig. 2.5.

In order to drive an electrical current through the dot, external electrodes are being tunnel coupled to the dot and the system's total Hamiltonian is then given by

$$H = H_{\text{dot}} + \sum_{\eta} H_{\eta} + H_{\text{tunn},\eta}. \quad (2.20)$$

Here, the contacted electrodes can be treated as non-interacting reservoirs

$$H_{\eta} = \sum_{k\sigma} \epsilon_{\eta k} c_{\eta k\sigma}^{\dagger} c_{\eta k\sigma}, \quad (2.21)$$

with the single-particle energies  $\epsilon_{\eta k}$  and the annihilation (creation) operators  $c_{\eta k\sigma}^{(\dagger)}$  for electrons with momentum  $k$  and spin  $\sigma$  in lead  $\eta$ . Tunneling between the dot and the leads is modeled by the spin-conserving tunneling Hamiltonian

$$H_{\text{tunn},\eta} = V_{\eta} \sum_{k\sigma} \left( c_{\eta k\sigma}^{\dagger} d_{\sigma} + \text{H.c.} \right), \quad (2.22)$$

where the tunnel-matrix elements  $V_{\eta}$  are assumed to be spin- and energy independent. With the tunnel-matrix elements and the density of states  $\rho_{\eta}$  in lead  $\eta$ , that we assume to be energy independent, we define the tunnel-coupling strengths as  $\Gamma_{\eta} = 2\pi|V_{\eta}|^2\rho_{\eta}$ . In this work we will perform a perturbation expansion in the tunnel-coupling strengths which allows us to treat the on-site Coulomb repulsion exactly.

Though the quantum dot under consideration has only a single level contributing to transport, different tunneling processes can arise. The most fundamental transport process is *sequential tunneling*. Here a single electron tunnels from one of the electrodes onto the dot or vice versa, see Fig. 2.6(a). Since energy needs to be conserved an electronic state with energy  $\epsilon$  is initially required to be occupied or, respectively, to be available in the electrode. Sequential tunneling is of first order in the tunnel coupling strength  $\Gamma_{\eta}$  and is usually the dominating transport process in systems where a quantum dot is weakly tunnel coupled to the electrodes. If no excitation energy lies inside the transport window sequential tunneling is exponentially suppressed.

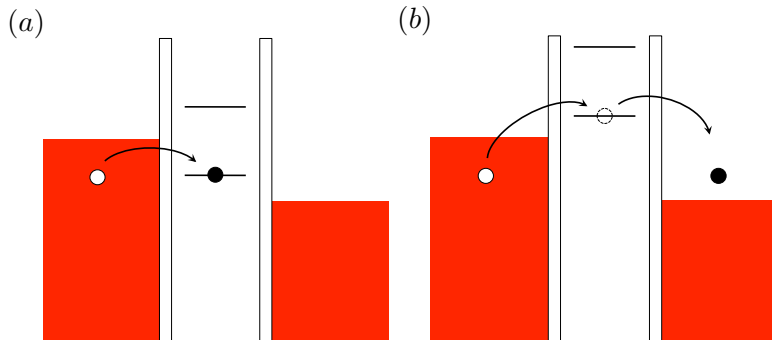


*Figure 2.6:* Tunneling processes of a single-level quantum dot. In (a) a sequential-tunneling process is depicted, where an electron tunnels from the left lead onto the quantum dot, and (b) shows an elastic-cotunneling process, where an electron from the left lead tunnels through the dot via a virtual intermediate state into the right lead.

In contrast, higher order tunneling is only suppressed algebraically so that *cotunneling*, which arises from second-order perturbation theory, can dominate over sequential tunneling. Cotunneling causes a level broadening as well as a renormalization of the excitation energies. One distinguishes between *elastic cotunneling* and *inelastic cotunneling*. In an elastic cotunneling process the initial and final dot states have the same energy while in an inelastic cotunneling process the energies of initial and final dot states differ. Inelastic cotunneling may occur e.g. in multi-level quantum dots and gives rise to an additional resonance at the energy difference of initial and final state.<sup>51</sup> Fig. 2.6(b) shows an example of an elastic cotunneling process: an initial electron in the left lead tunnels via an intermediate virtual state on the dot into the right lead.

For temperatures below the Kondo temperature  $T_K$  the *Kondo effect*<sup>52</sup> may arise. If the dot is occupied with a single electron then this electron can form a singlet state<sup>53,54</sup> with electrons at the Fermi energy of the leads causing the zero-bias conductance to increase.<sup>55</sup> In the present thesis we consider sequential-tunneling processes as well as higher-order tunneling processes but we always assume the temperature to be higher than the Kondo temperature so that the Kondo effect does not play a role.

## 2.3 Quantum dots coupled to superconductors

By coupling superconducting reservoirs to a quantum dot the correlation of electrons, that leads to the formation of Cooper pairs, can be induced on quantum dots giving rise to a variety of interesting effects.<sup>2</sup> Since the present thesis mainly deals with quantum dots coupled to superconductors we demonstrate the relevance of such systems in this section. During recent years experimental groups succeeded in coupling quantum dots to superconductors,<sup>5-7,9,10,56-68</sup> and some prominent examples shall be presented in the next subsections. After that, we give an introduction into the theoretical investigation of quantum dots attached to superconducting leads in the limit of infinitely-large superconducting gaps which defines the starting point for most of the

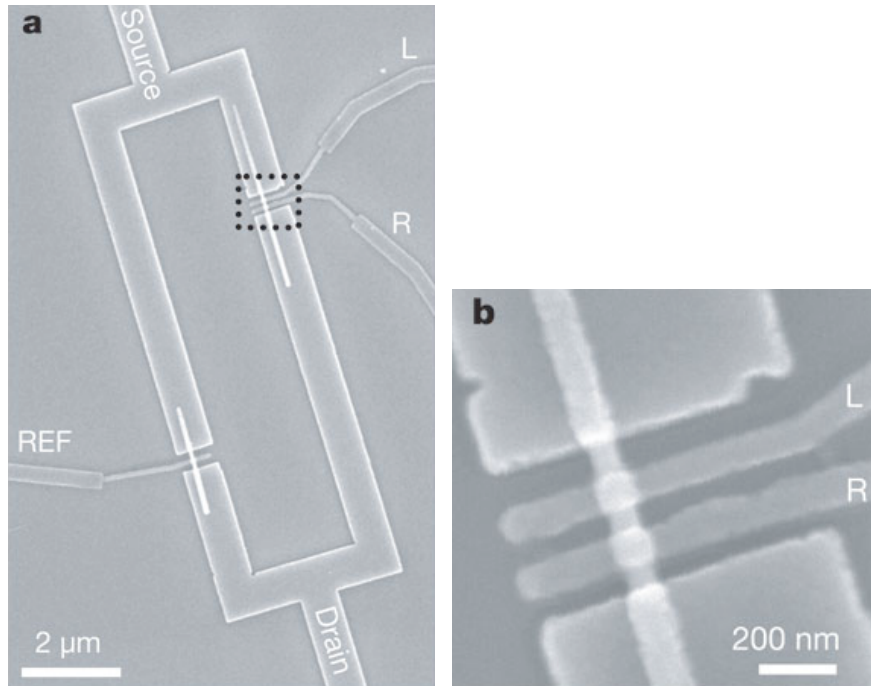


Figure 2.7: Scanning tunneling microscope image of a quantum dot coupled to two superconducting leads. The two superconductors enclose a magnetic flux to form a SQUID. Reprinted by permission from Macmillan Publishers Ltd: Nature **442**, 667, copyright 2006.

calculations appearing in this thesis.

### 2.3.1 Experiments on quantum dots coupled to superconductors

#### Supercurrent reversal in quantum dots

In 2006 van Dam *et al.*<sup>68</sup> explored the Josephson current flowing from one superconductor through an interacting quantum dot into another superconductor. The quantum dot was defined by two gate electrodes in an InAs nanowire that connected the two superconductors, see Fig. 2.7. At the other ends the two superconductors were connected via another nanowire so that a superconducting quantum interference device (SQUID) was obtained. The phase difference of the macroscopic superconducting phases between the two superconductors can be controlled by the magnetic flux enclosed in the SQUID. It has been found that the sign of the Josephson current depends on the dot occupation, see Fig. 2.8. For even occupations the Josephson current has a positive sign, while for odd dot occupations the Josephson current has a negative sign. This behavior is called  $0 - \pi$  transition. It can be explained by looking at the cotunneling processes of Cooper pairs from one superconductor to the other. Cooper pairs consist of two electrons forming a spin-singlet state. If the dot is occupied by an even number of electrons the spin singlet can be transferred through the quantum

## 2.3 Quantum dots coupled to superconductors

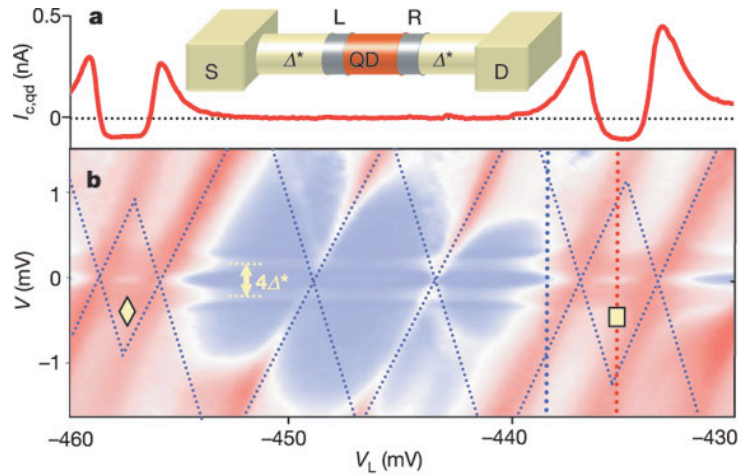


Figure 2.8: In (a) a plot of the critical super current through the quantum dot as a function of the gate voltage is shown and (b) is a density plot of the differential conductance  $dI/dV$  as a function of the gate voltage  $V_L$  and the bias voltage  $V$ . Reprinted by permission from Macmillan Publishers Ltd: Nature **442**, 667, copyright 2006.

dot without changing its phase. However, for an odd number of electrons on the dot a spin singlet gets transferred through the dot by gathering a phase factor of  $\pi$  resulting in a sign change of the Josephson current.

### Cooper pair beam splitter

Three experiments on splitting of Cooper pairs<sup>5-7</sup> show the importance of the on-site Coulomb repulsion on a quantum dot. The idea is to couple a superconducting lead via two quantum dots with strong on-site Coulomb repulsion to two normal leads. In a non-equilibrium situation an Andreev current is driven from the superconductor through the quantum dots into the two normal conductors. Due to the on-site Coulomb repulsion it is energetically favorable for the Cooper pairs to split up onto the two dots rather than tunneling onto the same. The splitting causes a pair of entangled electrons to tunnel non-locally into the two normal leads. Splitting efficiencies of nearly 50% have been reported,<sup>6</sup> but still the nonlocal entanglement of the electrons needs to be measured.

### Observation of Andreev-bound states in quantum dots

A normal conducting region enclosed by two superconductors can show the occurrence of *Andreev-bound states* (ABS). If the normal conducting region is a quantum dot the formation of ABS modifies the physical properties of the quantum dot and one way to detect the presence of ABS is a measurement of the proximized quantum-dot spectrum.<sup>9,10</sup> In the first experiment<sup>9</sup> a quantum has been realized in a carbon nanotube coupled to two superconducting leads and a normal lead, see Fig. 2.9(a) and in the

## 2 Hybrid systems containing quantum dots and superconductors

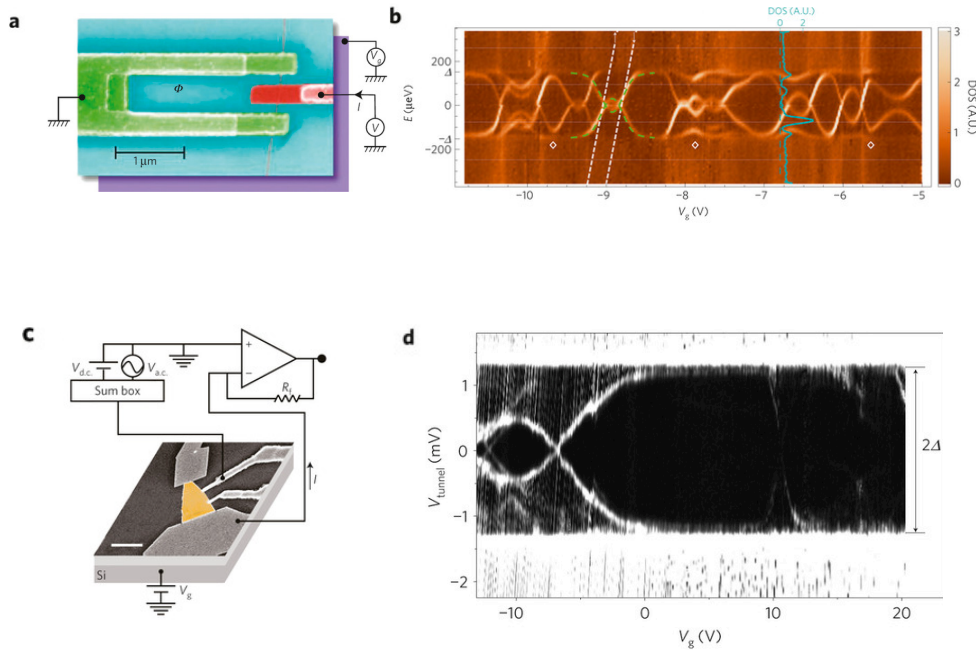


*Figure 2.9:* Observation of ABS in quantum dots. The quantum dot has been realized (a) in a carbon nanotube<sup>9</sup> and (c) in graphene.<sup>10</sup> The density plot in (b) depicts a measurement of the density of states in the carbon-nanotube quantum dot and (d) shows the measured differential conductance of the graphene quantum dot. (a)-(b) Reprinted by permission from Macmillan Publishers Ltd: Nature Phys. **6**, 965, copyright 2010. (c)-(d) Reprinted by permission from Macmillan Publishers Ltd: Nature Phys. **7**, 386, copyright 2011.

second experiment a graphene quantum dot<sup>10</sup> has been coupled to two superconducting leads, see Fig. 2.9(c). In both experiments it has been found that the excitation energies of the proximized dot are greatly different from the normal dot's spectrum. Instead of showing the Coulomb diamonds<sup>3</sup> expected in the normal conducting case the excitation energies exhibit an avoided crossing with the additional property that all excitation energies are bound on the interval  $[-\Delta, \Delta]$ .

This short presentation of experiments is not supposed to be a complete review but it shall illustrate that quantum dots coupled to superconductors are an interesting topic which is investigated frequently.

### 2.3.2 Interacting quantum dots in the infinite-gap limit

Also from the theoretical point of view transport through quantum dots tunnel coupled to superconducting leads is a promising field.<sup>2</sup> In these setups effects like Josephson transport,<sup>19,69–71</sup> Andreev transport<sup>16,17,21,57,72–77</sup> including multiple Andreev reflection<sup>57,76,77</sup> as well as the Kondo effect in superconducting systems<sup>18,20,24,78–81</sup> have

## 2.3 Quantum dots coupled to superconductors

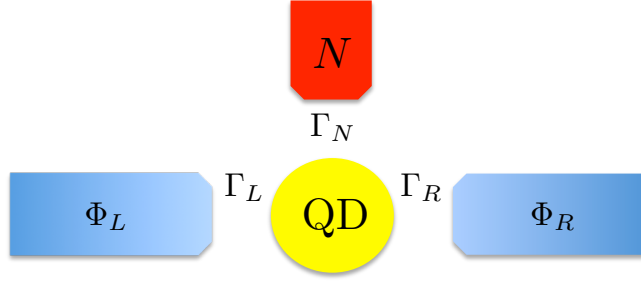


Figure 2.10: Setup of a quantum dot tunnel coupled to two superconductors and one normal conducting lead.

been studied. The limit of vanishing Coulomb repulsion on the dot can be solved exactly, e.g. by means of a scattering approach. However, this is no longer possible for systems that contain interacting quantum dots. A possible alternative is to treat the Coulomb repulsion<sup>16,17,19–21,74</sup> or the tunnel coupling strength<sup>22</sup> perturbatively.

Another important approach is the infinite-gap limit,<sup>22–32</sup> where quasiparticle tunneling is suppressed so that only Cooper pairs contribute to transport. In this limit the Coulomb interaction and the tunnel-coupling strengths to the superconductors can be treated exactly. In the present subsection we want to introduce to this infinite-gap limit for an exemplary system composed of a quantum dot tunnel coupled to one normal lead and two superconducting leads following Ref. 23. This work is of particular interest for the present thesis because it is its fundament and starting point.

### Model

The system considered contains an interacting single-level quantum dot tunnel coupled to a normal lead and two superconducting leads, see Fig. 2.10. The Hamiltonians are the ones given in Sec. 2.2.2 except that the leads are described by the BCS Hamiltonian

$$H = \sum_{k,\sigma} \epsilon_k c_{\eta k\sigma}^\dagger c_{\eta k\sigma} - g_\eta \sum_{k,k'} c_{\eta k'\uparrow}^\dagger c_{\eta -k'\downarrow}^\dagger c_{\eta -k,\downarrow} c_{\eta k\uparrow}, \quad (2.23)$$

where  $\epsilon_k$  are the single-particle energies,  $c_{\eta k\sigma}^{(\dagger)}$  denote the annihilation (creation) operators for electrons in lead  $\eta$  with momentum  $k$  and spin  $\sigma$ , and  $g_\eta$  describes the superconducting pairing which vanishes for the normal lead, i.e.  $g_N = 0$ . Since we are only interested in stationary currents here, we assume that the two superconductors are on the same chemical potential which we choose as the reference for the occurring energies, i.e.  $\mu_L = \mu_R = 0$ . The BCS Hamiltonian can be diagonalized after applying mean-field theory and carrying out the Bogoliubov transformation to

$$H_\eta = \sum_{k\sigma} E_{\eta k} \gamma_{\eta k\sigma}^\dagger \gamma_{\eta k\sigma}, \quad (2.24)$$

## 2 Hybrid systems containing quantum dots and superconductors

---

where the operators  $\gamma_{\eta k\sigma}^{(\dagger)}$  describe the quasiparticles. The quasiparticle energy  $E_{\eta k} = \sqrt{\epsilon_k^2 + |\Delta_\eta|^2}$  shows the expected superconducting gap and  $\Delta_\eta \equiv |\Delta_\eta|e^{i\Phi_\eta}$  is the superconducting pair potential in lead  $\eta$  and  $e^{i\Phi_\eta}$  its phase. For the two superconductors we assume a symmetric situation, where  $\Gamma_L = \Gamma_R \equiv \Gamma_S$  and  $\Phi_L = -\Phi_R \equiv \Phi/2$ .

### Reduced density matrix and current formula

The fermionic degrees of freedom of the leads can be integrated out by means of a diagrammatic technique<sup>82–84</sup> that has been extended to account also for superconducting leads.<sup>22,23</sup> It results in an effective description of a reduced system that is determined by the *reduced density matrix*  $\rho_{\text{red}}$  of the single-level quantum dot. The Hilbert space of the reduced system is spanned by the four eigenstates of the dot  $|\chi\rangle \in \{|0\rangle, |\uparrow\rangle, |\downarrow\rangle, |d\rangle \equiv d_\uparrow^\dagger d_\downarrow^\dagger |0\rangle\}$  with eigenenergies  $E_0 = 0, E_\uparrow = E_\downarrow = \epsilon$ , and  $E_d = 2\epsilon + U$ . With the dot states the elements of the reduced density matrix can be expressed as  $P_{\chi_2}^{\chi_1} \equiv \langle \chi_1 | \rho_{\text{red}} | \chi_2 \rangle$ . In the limit of infinitely-large superconducting gaps ( $|\Delta_\eta| \rightarrow \infty$ ) quasiparticles are not accessible so that only Cooper pairs contribute to transport. In this limit the current in the superconducting leads simplifies<sup>23</sup> to

$$J_\eta = -\frac{2e}{\hbar} \Gamma_\eta |\langle d_\downarrow d_\uparrow \rangle| \sin(\Phi_\chi - \Phi_\eta), \quad (2.25)$$

where  $\langle d_\downarrow d_\uparrow \rangle = |\langle d_\downarrow d_\uparrow \rangle| \exp(i\Phi_\chi)$  is the dot pair amplitude and  $\Phi_\chi$  its phase. This current formula already contains contributions of the Josephson current as well as Andreev current.

### Isospin

The dot pair amplitude is given by<sup>23</sup>  $\langle d_\downarrow d_\uparrow \rangle = P_d^0$ . Since the full current in the superconductors is only determined by the dot pair amplitude we introduce the isospin which is particularly useful to differentiate between the Josephson current and the Andreev current. We define the dot isospin as<sup>22</sup>

$$I_x = \frac{P_0^d + P_d^0}{2}, \quad I_y = i \frac{P_0^d - P_d^0}{2}, \quad I_z = \frac{P_d - P_0}{2}. \quad (2.26)$$

With the isospin the master equation can be brought into a Bloch equation

$$0 = \frac{d\mathbf{I}}{dt} = \mathbf{A} - \mathbf{R} \cdot \mathbf{I} + \mathbf{I} \times \mathbf{B}. \quad (2.27)$$

Here,  $\mathbf{A}$  represents the accumulation term,  $\mathbf{R} \cdot \mathbf{I}$  the relaxation term, and  $\mathbf{I} \times \mathbf{B}$  the rotation term. Then, the isospin components can be determined by solving the Bloch equation.

In the isospin notation the current formula of Eq. (2.25) reads

$$J_{R,L} = \frac{2e}{\hbar} \Gamma_S \left( I_y \cos \frac{\Phi}{2} \pm I_x \sin \frac{\Phi}{2} \right). \quad (2.28)$$

## 2.3 Quantum dots coupled to superconductors

---

Due to the fact that for a vanishing phase difference  $\Phi$  the Josephson current vanishes, in Eq. (2.28) we can identify the Andreev current with the isospin's  $y$ -component and the Josephson current with its  $x$ -component:

$$J_{\text{jos}} = \frac{2e}{\hbar} \Gamma_S I_x \sin \frac{\Phi}{2}, \quad (2.29)$$

$$J_{\text{and}} = -\frac{4e}{\hbar} \Gamma_S I_y \cos \frac{\Phi}{2}. \quad (2.30)$$

The Josephson current is a pure supercurrent and it starts already in zeroth order in the coupling to the normal lead  $\Gamma_N$ , while the Andreev current involves both a normal lead and a superconducting lead so that the Andreev current starts in first order  $\Gamma_N$ . From the definition of the  $z$ -component and from probability conservation  $1 = P_0 + P_\uparrow + P_\downarrow + P_d$  follows

$$Q = -e(1 + 2I_z) \quad (2.31)$$

for the average charge located on the quantum dot.

### Andreev bound states

In the limit of infinitely-large superconducting gaps  $|\Delta| \rightarrow \infty$  the coupling to the superconducting lead can be resummed exactly.<sup>23</sup> It turns out that the excitation energies of the proximized dot differ greatly from the excitation energies of a quantum dot that is only coupled to normal leads. In the normal case the dot has two excitation energies located at  $\epsilon$  and  $\epsilon + U$ . The proximity of a superconductor leads to a splitting of these excitation energies into the infinite-gap Andreev bound states<sup>1</sup> that are located at

$$E_{A\gamma'\gamma} = \gamma' \frac{U}{2} + \gamma \sqrt{\left(\frac{\delta}{2}\right)^2 + \Gamma_S^2 \cos^2 \frac{\Phi}{2}}, \quad (2.32)$$

with  $\gamma, \gamma' \in \{\pm 1\}$  and the detuning  $\delta = 2\epsilon + U$ . A plot of the Andreev bound states as a function of the level position  $\epsilon$  is shown in Fig. 2.11. In contrast to the normal excitation energies that are straight lines as a function of  $\epsilon$ , the Andreev bound states kink at the symmetry point of  $\epsilon = -U/2$ . There are several ways to map out the Andreev bound states, for example the Josephson current, the Andreev current, or the average charge located on the quantum dot, see Fig. 2.12. The plots presented here can be calculated with the diagrammatic technique given in Ref. 23, though, as we will show in the following Chapter 3 the calculations simplify tremendously. As expected from Eq. (2.32) the positions of the excitation energies of the proximized dot depend on the tunnel coupling strengths to the superconducting leads. In particular, in Figs. 2.12 (a) and (b) the Josephson current is depicted. For small detuning  $\delta$  and small chemical potential of the normal lead  $\mu_N$  the dot is in the Coulomb-blockade regime and, thus, the Josephson current is suppressed in this limit. The Coulomb blockade can be overcome to enable a Josephson current by either bringing the dot

---

<sup>1</sup>A slightly more precise denotation would be *Andreev excitation energies*. For simplicity, however, we use the term *Andreev bound state energy* throughout the paper.

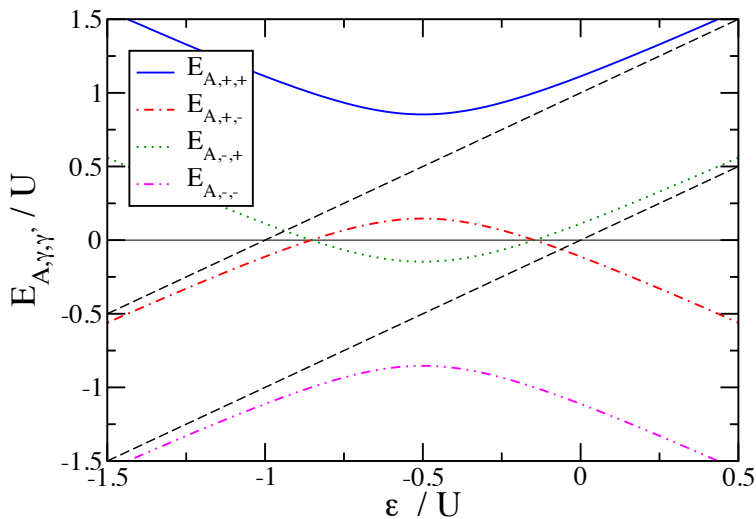


Figure 2.11: Plot of the normal excitation energies (black lines) and of the Andreev bound states (colored lines) as a function of the level position  $\epsilon$ .

out of equilibrium by means of the voltage applied to the normal lead or by changing the level position  $\epsilon$ . A  $0 - \pi$  transition can be driven in two different ways. First, for a fixed detuning  $\delta \neq 0$  the chemical potential of the normal lead  $\mu_N$  can be varied to result in a  $\pi$  transition. The second way to drive a  $\pi$  transition is to control the level position while the chemical potential of the normal lead is kept above or below all Andreev bound states, i.e.  $\mu_N > E_{A,+,+}$  or  $\mu_N < E_{A,-,-}$ . In the second case the  $\pi$  transition occurs at zero detuning.

Figs. 2.12 (c) and (d) show the Andreev current. Similar to the Josephson current also the Andreev current is suppressed for small detuning and small chemical potential of the normal lead due to the Coulomb blockade. The Andreev current requires finite transport voltages because here a normal conductor is involved into transport. The Andreev current is largest for small detunings because there the superconductors are in resonance with the dot, i.e. the energies of zero occupation and double occupation match so that Cooper pair tunneling between dot and superconductors is energetically favorable.

The average charge on the dot is presented in Figs. 2.12 (e) and (f). In the Coulomb blockade regime the average dot charge is equal to one as expected. Increasing the level position and reducing the chemical potential of the normal lead lowers the average charge down to values of zero occupation while reducing the level position and increasing the chemical potential of the normal lead leaves the dot being doubly occupied. The situation of zero detuning forms an exception. As stated in the previous paragraph superconductors and dot are in resonance at zero detuning. This causes the

## 2.3 Quantum dots coupled to superconductors

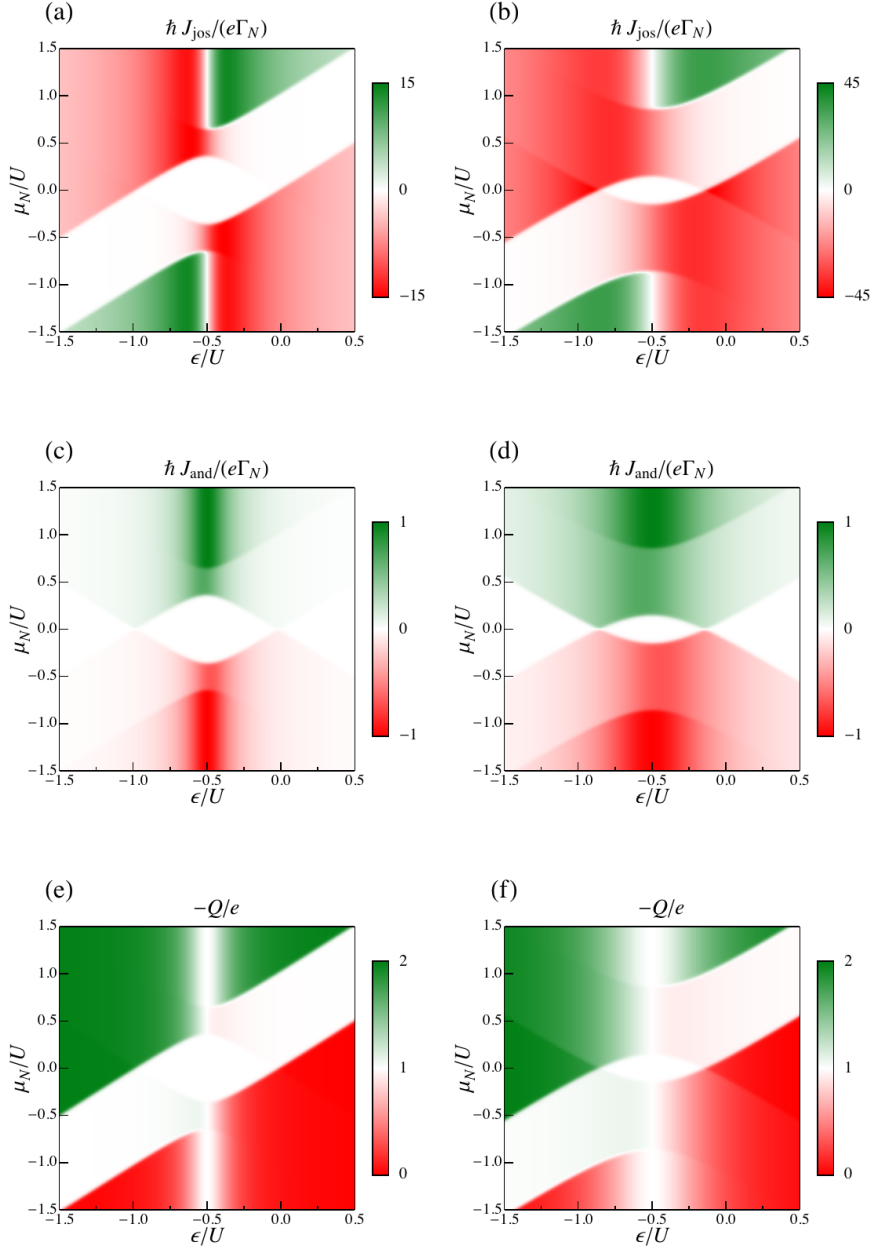


Figure 2.12: Density plot of (a)-(b) the Josephson current, (c)-(d) the Andreev current, and (e)-(f) the average charge on the quantum dot as a function of the level position  $\epsilon$  and the chemical potential of the normal lead  $\mu_N$ . The coupling to the superconductor  $\Gamma_S = 0.2U$  for (a), (c), and (e) is chosen smaller than for (b), (d), and (f), which is  $\Gamma_S = 0.5U$ . The other parameters are  $k_B T = 0.01U$ ,  $\Gamma_N = 0.005U$ , and  $\Phi = \pi/2$ .

## 2 Hybrid systems containing quantum dots and superconductors

---

dot to be in an equally balanced superposition of the states  $|0\rangle$  and  $|d\rangle$  resulting in an average dot charge of one.

### 3 Diagrammatic technique

In this thesis we consider different setups of interacting single-level quantum dots coupled to external leads. It is our objective to treat the on-site Coulomb repulsion exactly and to allow for arbitrary couplings to the superconducting leads while we assume a weak coupling between the dot and the normal conducting leads. Here, we present a diagrammatic real-time technique that accounts for an arbitrary number of normal leads, ferromagnetic leads, and superconducting leads. To this end we combine the theories of Ref. 23 and Ref. 85 to formulate a comprehensive theory in a basis which we will introduce as  $\pm$ -basis. We will demonstrate that the great advantage of the  $\pm$ -basis is that it already contains the couplings to the superconductors in the limit of infinitely-large superconducting gaps.

#### 3.1 Model

We consider an interacting single-level quantum dot that is coupled to an arbitrary number of normal leads, ferromagnetic leads, and superconducting leads. The system's total Hamiltonian is given by

$$H = H_{\text{dot}} + \sum_{\eta} H_{\eta} + H_{\text{tunn},\eta}, \quad (3.1)$$

where  $\eta \in \{N, F, S\}$  and  $N$ ,  $F$ , and  $S$  are the sets of normal, ferromagnetic, and superconducting leads, respectively. The quantum dot is modeled by the Anderson Hamiltonian

$$H_{\text{dot}} = \sum_{\sigma} \epsilon d_{\sigma}^{\dagger} d_{\sigma} + U n_{\uparrow} n_{\downarrow}, \quad (3.2)$$

with the annihilation (creation) operators  $d_{\sigma}^{(\dagger)}$  for electrons on the dot with spin  $\sigma$ , the Coulomb repulsion  $U$ , and the number operators for dot electrons  $n_{\sigma} = d_{\sigma}^{\dagger} d_{\sigma}$ . We treat the leads as reservoirs of non-interacting electrons and include BCS-pairing terms for the superconducting leads

$$H_{\eta} = \sum_{k\sigma} \epsilon_{\eta k\sigma} c_{\eta k\sigma}^{\dagger} c_{\eta k\sigma} - \delta_{\eta,S} \sum_k (\Delta_{\eta} c_{\eta-k\downarrow} c_{\eta k\uparrow} + \text{H.c.}), \quad (3.3)$$

where the single-particle energies  $\epsilon_{\eta k\sigma}$  are spin dependent only for ferromagnets,  $c_{\eta k\sigma}^{(\dagger)}$  are the annihilation (creation) operators for electrons in lead  $\eta$ , and  $\Delta_{\eta} = |\Delta_{\eta}| e^{i\Phi_{\eta}}$  is the superconducting pair potential of lead  $\eta$ , and  $\Phi_{\eta}$  is the related macroscopic phase. The BCS-pairing term is non-vanishing only for superconducting leads, i.e.  $\eta \in S$ . Throughout the entire thesis we will choose the Fermi level of the superconductors as

### 3 Diagrammatic technique

---

reference for the energies, i.e.  $\mu_\eta = 0$  for  $\eta \in S$ . Tunneling between dot and leads is modeled by the tunneling Hamiltonian

$$H_{\text{tunn},\eta} = V_\eta \sum_{k\sigma} \left( c_{\eta k\sigma}^\dagger d_\sigma + \text{H.c.} \right), \quad (3.4)$$

with  $V_\eta$  being the (real) spin- and momentum independent tunnel-matrix elements. We define the tunnel-coupling strengths which we assume to be energy independent as  $\Gamma_{\eta\sigma} = 2\pi|V_\eta|^2\rho_{\eta\sigma}$ , where  $\rho_{\eta\sigma}$  is the density of states of electrons with spin  $\sigma$  in lead  $\eta$ . We then introduce the mean-level broadening as  $\Gamma_\eta = \frac{1}{2}\sum_\sigma \Gamma_{\eta\sigma}$ . Furthermore, we describe the ferromagnets by the Stoner model and define the degree of spin polarization at the Fermi energy as  $p = (\rho_{F\uparrow} - \rho_{F\downarrow}) / (\rho_{F\uparrow} + \rho_{F\downarrow})$ .

### 3.2 Effective Hamiltonian

We start by rewriting the total Hamiltonian which will turn out to be very convenient later on:

$$H = H_{\text{dot}} + \sum_{\eta} (H_{\eta} + H_{\text{tunn},\eta}) + H_p - H_p, \quad (3.5)$$

where  $H_p = \chi^* d_\downarrow d_\uparrow + \chi d_\uparrow^\dagger d_\downarrow^\dagger$  and  $\chi = \frac{1}{2}\sum_{\eta \in S} \Gamma_\eta e^{i\Phi_\eta}$ . With the definition of the effective Hamiltonian

$$H_{\text{eff}} = H_{\text{dot}} - H_p \quad (3.6)$$

$$= \sum_{\sigma} \epsilon d_{\sigma}^\dagger d_{\sigma} + U n_{\uparrow} n_{\downarrow} - \chi^* d_{\downarrow} d_{\uparrow} - \chi d_{\uparrow}^\dagger d_{\downarrow}^\dagger \quad (3.7)$$

the total Hamiltonian can be written as

$$H = H_{\text{eff}} + \sum_{\eta} (H_{\eta} + H_{\text{tunn},\eta}) + H_p. \quad (3.8)$$

In comparison to the Anderson Hamiltonian the effective Hamiltonian has very different properties. Its new set of eigenstates is given by

$$\begin{aligned} & |\uparrow\rangle \\ & |\downarrow\rangle \\ |+\rangle &= \frac{1}{\sqrt{2}} \left[ -e^{-i\Phi_\chi/2} \sqrt{1 - \frac{\delta}{2\epsilon_A}} |0\rangle + e^{i\Phi_\chi/2} \sqrt{1 + \frac{\delta}{2\epsilon_A}} |d\rangle \right] \\ |-\rangle &= \frac{1}{\sqrt{2}} \left[ e^{-i\Phi_\chi/2} \sqrt{1 + \frac{\delta}{2\epsilon_A}} |0\rangle + e^{i\Phi_\chi/2} \sqrt{1 - \frac{\delta}{2\epsilon_A}} |d\rangle \right], \end{aligned}$$

where  $\Phi_\chi = \arg(\chi)$  and  $\epsilon_A = \sqrt{(\frac{\delta}{2})^2 + |\chi|^2}$ , with eigenenergies  $\{\epsilon, \epsilon, E_+ = \frac{\delta}{2} + \sqrt{(\frac{\delta}{2})^2 + |\chi|^2}, E_- = \frac{\delta}{2} - \sqrt{(\frac{\delta}{2})^2 + |\chi|^2}\}$ . Here, we have used the detuning  $\delta = 2\epsilon + U$ .

Along with new eigenenergies and eigenstates the effective Hamiltonian has also a different set of excitation energies  $\pm(E_{\pm} - \epsilon)$ , the Andreev-bound states

$$E_{A,\gamma',\gamma}^{\Delta \rightarrow \infty} = \gamma' \frac{U}{2} + \gamma \epsilon_A, \quad (3.9)$$

with  $\gamma', \gamma = \pm$ . Note that the tunneling Hamiltonian  $H_{\text{tunn},\eta}$  couples only the states of odd occupation  $|\sigma\rangle$  to the states of even occupation  $|\pm\rangle$ , while the artificially added Hamiltonian  $H_p$  only couples the states of even occupation  $|\pm\rangle$  with each other.

### 3.3 Reduced density matrix

The quantum mechanical expectation value of an observable  $A$  can be expressed in terms of the density matrix  $\rho$  as

$$\langle A \rangle(t) = \text{Tr}[\rho(t)A]. \quad (3.10)$$

The density matrix is defined as

$$\rho(t) \equiv \sum_i p_i |\alpha_i(t)\rangle \langle \alpha_i(t)|, \quad (3.11)$$

with  $p_i$  being the probability of the system to be in state  $|\alpha_i(t)\rangle$ . For the unperturbed system at time  $t_0$ , i.e. tunnel coupling is switched off, the system's total density matrix factorizes

$$\rho(t_0) = \rho_{\text{leads}}(t_0) \otimes \rho_{\text{red}}(t_0), \quad (3.12)$$

where  $\rho_{\text{leads}} = \Pi_{\eta} Z_{\eta}^{-1} \exp[-(H_{\eta} - \mu_{\eta} N_{\eta})/(k_B T)]$  is the density matrix of the reservoirs with the partition function  $Z_{\eta}$  and  $\rho_{\text{red}}$  is the reduced density matrix describing the degrees of freedom of the quantum dot. The idea is to obtain a reduced system given by the reduced density matrix which is defined as

$$\rho_{\text{red}} = \text{Tr}_{\text{leads}}(\rho), \quad (3.13)$$

where  $\text{Tr}_{\text{leads}}(x)$  describes the trace only over the states of the leads. The elements  $P_{\chi}^{\chi'}$  of the reduced density matrix are given by  $P_{\chi}^{\chi'} = \langle \chi' | \rho_{\text{red}} | \chi \rangle$ . The diagonal elements of the reduced density matrix  $P_{\chi} \equiv P_{\chi}^{\chi}$  are the probability to find the system in state  $\chi$ . Thus,  $\sum_{\chi} P_{\chi} = 1$  holds due to probability conservation. Introducing a coupling of the dot to the external reservoirs in terms of the tunneling Hamiltonian may result in off-diagonal elements of the reduced density matrix. For instance, the coupling to a superconductor may give rise to the formation of a finite dot pair amplitude  $P_d^0$ .

### 3.4 Interaction picture and Keldysh time

Since the quantum dot is a strongly interacting system we cannot calculate transport through the setup exactly. Therefore, we switch into the interaction picture and perform a perturbation expansion in the tunnel-coupling strengths formulated in Keldysh

### 3 Diagrammatic technique

time. The choice of employing Keldysh time is motivated by the problem that in a non-equilibrium situation the final state of the whole system is unknown because a large number of electrons has been transferred between the leads. Therefore, it makes sense to consider Keldysh time, which starts at time  $t_0 = -\infty$  and evolves up to time  $t$  and from time  $t$  back again to time  $t_0$ . Thus, the concept of Keldysh time avoids the problem of the unknown final state. In the interaction picture the time evolution of the elements of the reduced density matrix is determined by

$$P_\chi^{\chi'} = \text{Tr} \left[ \rho_0 T_K \left[ \exp \left( -\frac{i}{\hbar} \int_K dt_1 V_I(t_1) \right) |\chi\rangle \langle \chi'| (t) \right] \right], \quad (3.14)$$

with  $T_K$  being the time-ordering operator along Keldysh time.  $V_I$  is the part of the Hamiltonian that introduces the interaction into the system. In our case  $V_I$  is given by  $V_I = \sum_\eta H_{\text{tunn},\eta} + H_p$ . Expanding Eq. (3.14) in a power series yields

$$P_\chi^{\chi'}(t) = \sum_{n=0}^{\infty} \left( -\frac{i}{\hbar} \right)^n \int_K dt_1 \dots \int_K dt_n \text{Tr} \left[ \rho_0 T_K [V_I(t_1) \dots V_I(t_n) |\chi\rangle \langle \chi'| (t)] \right], \quad (3.15)$$

where the times  $t_1 > \dots > t_n$  are ordered with respect to the Keldysh time. The lead operators arising from  $V_I$  can be contracted pairwise by means of Wick's theorem.<sup>86</sup> For normal and ferromagnetic leads it yields

$$\begin{aligned} \langle c_{\eta k \sigma}^\dagger(t) c_{\eta' k' \sigma'}(t') \rangle &= \delta_{\eta \eta'} \delta_{k k'} \delta_{\sigma \sigma'} e^{\frac{i}{\hbar} \epsilon_{\eta k \sigma} (t-t')} f_\eta^+(\epsilon_{\eta k \sigma}) \\ \langle c_{\eta k \sigma}(t') c_{\eta' k' \sigma'}^\dagger(t) \rangle &= \delta_{\eta \eta'} \delta_{k k'} \delta_{\sigma \sigma'} e^{\frac{i}{\hbar} \epsilon_{\eta k \sigma} (t-t')} f_\eta^-(\epsilon_{\eta k \sigma}), \end{aligned}$$

with  $f_\eta^+(x) = [\exp(\frac{x - \mu_\eta}{k_B T}) + 1]^{-1}$  being the Fermi function in lead  $\eta$  and  $f_\eta^-(x) = 1 - f_\eta^+(x)$ . In superconductors the density of states exhibits an energy gap around the Fermi energy and, additionally, contractions between two creation operators or two annihilation operators are possible. The contractions can be calculated by performing the Bogoliubov transformation of Eqs. (2.7) and (2.8). For superconductors they are given by

$$\begin{aligned} \langle c_{\eta k \sigma}^\dagger(t) c_{\eta' k' \sigma'}(t') \rangle &= \delta_{\eta \eta'} \delta_{k k'} \delta_{\sigma \sigma'} e^{\frac{i}{\hbar} E_{\eta k} (t-t')} f_\eta^+(E_{\eta k}) \\ \langle c_{\eta k \sigma}(t') c_{\eta' k' \sigma'}^\dagger(t) \rangle &= \delta_{\eta \eta'} \delta_{k k'} \delta_{\sigma \sigma'} e^{\frac{i}{\hbar} E_{\eta k} (t-t')} f_\eta^-(E_{\eta k}) \\ \langle c_{\eta k \sigma}^\dagger(t) c_{\eta' k' \sigma'}^\dagger(t') \rangle &= \delta_{\eta \eta'} \delta_{\bar{k} \bar{k}'} \delta_{\sigma \bar{\sigma}'} u_k v_{k'}^* (-1)^{\delta_{\sigma \downarrow}} \left[ e^{-\frac{i}{\hbar} E_{\eta k} (t-t')} f_\eta^-(E_{\eta k}) - e^{\frac{i}{\hbar} E_{\eta k} (t-t')} f_\eta^+(E_{\eta k}) \right] \\ \langle c_{\eta k \sigma}(t) c_{\eta' k' \sigma'}(t') \rangle &= \delta_{\eta \eta'} \delta_{\bar{k} \bar{k}'} \delta_{\sigma \bar{\sigma}'} u_k^* v_{k'} (-1)^{\delta_{\sigma \uparrow}} \left[ e^{-\frac{i}{\hbar} E_{\eta k} (t-t')} f_\eta^-(E_{\eta k}) - e^{\frac{i}{\hbar} E_{\eta k} (t-t')} f_\eta^+(E_{\eta k}) \right]. \end{aligned}$$

Here,  $E_{\eta k}$  is the quasiparticle energy of Eq. (2.24),  $u_k$  and  $v_k$  are the coefficients of the Bogoliubov transformation, and  $\bar{k} \equiv -k$  as well as  $\bar{\sigma} \equiv -\sigma$ .

To allow for a systematic and consistent expansion in  $V_I$  we formulate a diagrammatic language that is capable of describing the dynamics of the reduced density matrix. The unperturbed time evolution along Keldysh time that starts at time  $t_0 = -\infty$  is symbolized by a Keldysh contour, i.e. an upper and a lower branch, corresponding to a forward and backward propagation in time, respectively, that are connected at

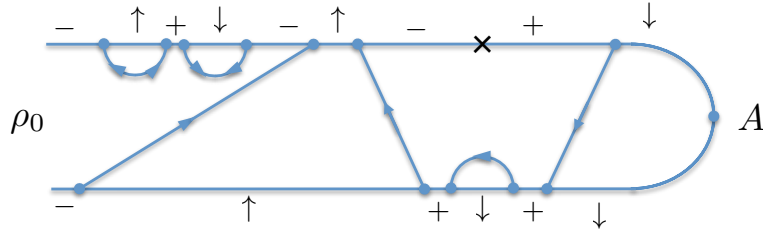


Figure 3.1: Example of the visualization of tunneling processes on the Keldysh contour.

time  $t$ . The perturbations arising from  $V_I$  are symbolized by vertices. Whenever the perturbation arises from  $H_p$  we choose the vertex to be a cross and when it arises from  $H_{\text{tunn},\eta}$  we choose it to be a bullet. A bullet vertex may be an *incoming vertex* symbolizing a term  $V_\eta d_\sigma^\dagger c_{\eta k\sigma}$  or it may be an *outgoing vertex* representing a term  $V_\eta c_{\eta k\sigma}^\dagger d_\sigma$ . Each two bullet vertices are connected by a tunneling line containing arrows pointing towards incoming vertices and away from outgoing ones (Two arrows on a single line pointing in the same direction can be abbreviated by a single arrow). These tunneling lines illustrate the respective contractions arising from Wick's theorem. We will refer to lines containing a single arrow as *normal lines* and lines containing two arrows (pointing into different directions) as *anomalous lines*.<sup>23</sup> In Fig. 3.1 we show an example of tunneling processes containing normal lines as well as anomalous lines and a cross vertex.

### 3.5 Generalized master equation

We define the free propagator  $\Pi^{(0)}(t, t')$  as a section of the Keldysh contour that contains no vertices

$$\Pi_{\chi_2}^{\chi_1(0)}(t, t') = \frac{\chi_1}{\mathbf{\Pi}^{(0)}} \frac{t'}{\chi_2} t \quad (3.16)$$

as well as irreducible sections  $W_{\chi_2\chi_2'}^{\chi_1\chi_1'}(t, t')$  that cannot be “cut” by any vertical cut into two sections without cutting a tunneling line

$$W_{\chi_2\chi_2'}^{\chi_1\chi_1'}(t, t') = \begin{array}{c} \chi_1' \\ \square \\ \chi_2'_{t'} \end{array} \begin{array}{c} \chi_1 \\ t \\ \chi_2 \end{array} = \begin{array}{c} \chi_1' \\ \triangle \\ \chi_2'_{t'} \end{array} \begin{array}{c} \chi_1 \\ t \\ \chi_2 \end{array} + \begin{array}{c} \chi_1' \\ \triangle \\ \chi_2'_{t'} \end{array} \begin{array}{c} \chi_1 \\ t \\ \chi_2 \end{array} + \begin{array}{c} \chi_1' \\ \cap \\ \chi_2'_{t'} \end{array} \begin{array}{c} \chi_1 \\ t \\ \chi_2 \end{array} + \dots \quad (3.17)$$

The full propagator is determined by the sum over all possible combinations of the free propagator and all irreducible sections. It can be written in terms of a diagrammatic

### 3 Diagrammatic technique

---

Dyson equation

$$\begin{array}{|c|} \hline \mathbf{\Pi} \\ \hline \end{array} = \begin{array}{|c|} \hline \mathbf{\Pi}^{(0)} \\ \hline \end{array} + \begin{array}{|c|c|c|} \hline \mathbf{\Pi} & \mathbf{W} & \mathbf{\Pi}^{(0)} \\ \hline \end{array} . \quad (3.18)$$

From the Dyson equation a generalized master equation that determines the elements of the reduced density matrix can be derived. In the stationary limit  $\frac{d}{dt}P_{\chi_2}^{\chi_1}(t) = 0$  it reads

$$i(E_{\chi_1} - E_{\chi_2})P_{\chi_2}^{\chi_1} = \sum_{\chi'_1\chi'_2} W_{\chi_2\chi'_2}^{\chi_1\chi'_1} P_{\chi'_2}^{\chi'_1}, \quad (3.19)$$

where we have used the generalized rates  $W_{\chi_2\chi'_2}^{\chi_1\chi'_1} = \int_{-\infty}^0 dt W_{\chi_2\chi'_2}^{\chi_1\chi'_1}$ .

### 3.6 Current formula

In this thesis we are mainly interested in calculating electrical currents through interacting quantum dots. The current flowing out of lead  $\eta$  is given by the change of the number of particles

$$J_\eta(t) = e \frac{d}{dt} n_\eta(t) = e \frac{i}{\hbar} [H, n_\eta](t) = -e \frac{i}{\hbar} \sum_{k\sigma} V_\eta \left[ c_{\eta k\sigma}^\dagger d_\sigma - d_\sigma^\dagger c_{\eta k\sigma} \right], \quad (3.20)$$

where  $n_\eta$  is the number operator for electrons in lead  $\eta$ . The current operator is very similar to the tunneling Hamiltonian. It differs merely by the prefactors and a relative minus sign from the latter. In addition to the diagrams that contribute to general rates also diagrams occur in which the rightmost vertex is caused by the current operator. These current diagrams contribute to the generalized current rates  $W_{\chi\chi'_2}^{\chi\chi'_1} I_\eta$ . The stationary current flowing out of lead  $\eta$  can then be expressed as

$$J_\eta = -\frac{e}{\hbar} \sum_{\chi\chi'_1\chi'_2} W_{\chi\chi'_2}^{\chi\chi'_1} I_\eta P_{\chi'_2}^{\chi'_1}. \quad (3.21)$$

### 3.7 Diagrammatic rules

From Eq. (3.19) follows that in order to determine the elements of the reduced density matrix one needs to calculate the generalized rates  $W_{\chi_2\chi'_2}^{\chi_1\chi'_1}$ . In this section we give the diagrammatic rules<sup>87</sup> required to evaluate the generalized rates. We have started from the diagrammatic rules of Ref. 85 and Refs. 23,29 and formulated them in the  $\pm$ -basis introduced in Sec. 3.2. Additionally, we added a paragraph that describes how to deal with the perturbation arising from the additional Hamiltonian  $H_p$ .

(1) Draw all topologically different diagrams with fixed ordering of the vertices in

### 3.7 Diagrammatic rules

the real axis. The vertices may be bullets or crosses. The bullets are connected in pairs by tunneling lines carrying energy  $\omega_i$  while crosses are not connected by tunneling lines. The tunneling lines can be normal or anomalous. For each anomalous line, choose the direction (forward or backward with respect to the Keldysh contour) arbitrarily.

(2) For each vertical cut between two vertices, assign a factor  $1/(\Delta E + i0^+)$ , where  $\Delta E$  is the difference between the left-going and the right-going energies, including the energy of the dot states  $E_\chi$  and the tunneling lines  $\omega_i$ .

(3) For each tunneling line, assign a factor  $\frac{1}{2\pi}\Gamma_{\eta\sigma}D_\eta(\omega_i)f_\eta^\pm(\omega_i)$ , where  $f_\eta^+(\omega) = f_\eta(\omega) = \{1 + \exp[(\omega - \mu_\eta)/k_B T]\}^{-1}$  and  $f_\eta^-(\omega) = 1 - f_\eta(\omega)$ , and  $D_\eta(\omega) = \frac{|\omega|}{\sqrt{\omega^2 - |\Delta_\eta|^2}}\Theta(|\omega| - |\Delta_\eta|)$ .

The upper (lower) sign applies for lines going backward (forward) with respect to the Keldysh contour. For anomalous lines, multiply an additional factor  $\pm \text{sign}(\omega_i) \frac{|\Delta_\eta|}{|\omega_i|}$ . Moreover, assign a factor  $e^{i\Phi_\chi} e^{-i\Phi_\eta}$  for an outgoing and  $e^{-i\Phi_\chi} e^{i\Phi_\eta}$  for an incoming anomalous line, where  $\Phi_\chi = \arg(\chi)$  and  $\chi = \frac{1}{2} \sum_{\eta \in S} \Gamma_\eta e^{i\Phi_\eta}$ . [For normal leads, only normal lines with  $D_\eta(\omega_i) \equiv 1$  appear.]

(4) Every bullet vertex connects a dot state  $|\alpha\rangle$ , with  $\alpha \in \{+, -\}$ , to another dot state  $|\sigma\rangle$ , with  $\sigma \in \{\uparrow, \downarrow\}$ , and to a tunneling line describing a tunneling electron of spin  $\sigma' \in \{\uparrow, \downarrow\}$ . For each bullet vertex assign a factor  $\sqrt{1 - S_\alpha S_\sigma S_{\sigma'} \frac{\delta}{2\epsilon_A}} / \sqrt{2}$ , where  $S_{\alpha=+} = S_{\sigma=\uparrow} = S_{\sigma'=\uparrow} = 1$  and  $S_{\alpha=-} = S_{\sigma=\downarrow} = S_{\sigma'=\downarrow} = -1$ .

(5) Each cross vertex connects a state  $|\alpha\rangle$  with  $\alpha \in \{+, -\}$  to a state  $|\alpha'\rangle$  with  $\alpha' \in \{+, -\}$ . For each cross vertex with  $\alpha = \alpha'$  assign a factor  $(-1)S_\alpha \sqrt{1 - \frac{\delta^2}{4\epsilon_A^2}} |\chi|$  and for  $\alpha \neq \alpha'$  assign a factor  $\frac{\delta}{2\epsilon_A} |\chi|$ .

(6) Assign an overall prefactor  $-i$ .

Furthermore, assign a factor  $-1$  for each

- (a) vertex on the lower propagator;
  - (b) crossing of tunneling lines;
  - (c) outgoing (incoming) bullet vertex ending (starting) in the state  $|+\rangle$  or  $|\uparrow\rangle$ ;
  - (d) outgoing (incoming) anomalous tunneling line, in which the earlier (later) tunnel vertex with respect to the Keldysh contour is connected to a tunneling spin-up electron.
- (7) For each tunneling line, integrate over the energy  $\omega_i$ . Sum over all diagrams.

The generalized current rates  $W_{\chi\chi_2}^{\chi\chi_1} I_\eta$  are evaluated in the following way:

(8) Multiply each diagram that contributes to the corresponding generalized rate  $W_{\chi\chi_2}^{\chi\chi_1}$  and where the rightmost line is associated with lead  $\eta$  with a factor:

- (a) for the rightmost line being a normal line: 1 if the line is going from the lower to the upper propagator, -1 if it is going from the upper to the lower propagator, and 0 otherwise;
- (b) for the rightmost line being an anomalous line: 1 for incoming lines within the upper and outgoing lines within the lower propagator, -1 for outgoing lines within the upper and incoming lines within the lower propagator, and 0 otherwise.

### 3.8 Large-gap limit

In this section we demonstrate that the effective Hamiltonian of Eq. (3.7) is particularly useful in the limit of infinitely-large superconducting gaps, i.e.  $|\Delta| \rightarrow \infty$ . In this limit quasiparticles are inaccessible and only Cooper pairs contribute to transport. In Ref. 23 it has been shown that for large gaps only anomalous lines with the superconductors exist. Both vertices of these anomalous lines are required to be in the same propagator and no other vertex can be between them. Now we compare the effect of superconducting tunneling lines with that of the cross vertices. Tunneling lines associated with the superconductors as well as cross vertices connect a dot state  $\chi' \in \{|+\rangle, |-\rangle\}$  to a dot state  $\chi \in \{|+\rangle, |-\rangle\}$ . Since the calculations are very similar even for different starting and ending states and for different propagating energies we exemplarily present two calculations for each, tunneling lines associated with the superconductor and cross vertices. The first calculation regards the connection of equal states  $\chi' = \chi$  while the second regards the connection of different states  $\chi' \neq \chi$ . We find

$$\begin{aligned}
 & \begin{array}{c} \text{---} \sigma \text{---} \\ \omega' \text{---} \text{---} \\ \text{---} \omega \text{---} \\ \text{---} \\ + \end{array} = \sum_{\sigma} \int_{\Delta}^{\infty} \frac{d\omega'}{2\pi} \frac{|\chi|}{E_+ - \epsilon - \omega - \omega'} \frac{|\Delta|}{\sqrt{\omega'^2 - |\Delta|^2}} \sqrt{1 + \frac{\delta^2}{4\epsilon_A^2}} \\
 & \qquad \qquad \qquad = -\frac{|\chi|}{2} \sqrt{1 + \frac{\delta^2}{4\epsilon_A^2}}, \\
 & \begin{array}{c} \text{---} \sigma \text{---} \\ \omega' \text{---} \text{---} \\ \text{---} \omega \text{---} \\ \text{---} \\ + \end{array} = -\frac{|\chi|}{2} \sqrt{1 + \frac{\delta^2}{4\epsilon_A^2}}, \\
 & \begin{array}{c} \text{---} \times \text{---} \\ \text{---} \omega \text{---} \\ \text{---} \\ + \end{array} = |\chi| \sqrt{1 + \frac{\delta^2}{4\epsilon_A^2}},
 \end{aligned}$$

so that

$$\begin{array}{c} \text{---} \sigma \text{---} \\ \omega' \text{---} \text{---} \\ \text{---} \omega \text{---} \\ \text{---} \\ + \end{array} + \begin{array}{c} \text{---} \sigma \text{---} \\ \omega' \text{---} \text{---} \\ \text{---} \omega \text{---} \\ \text{---} \\ + \end{array} + \begin{array}{c} \text{---} \times \text{---} \\ \text{---} \omega \text{---} \\ \text{---} \\ + \end{array} = 0. \quad (3.22)$$

Analogously we find for the connection of different states

$$\begin{aligned}
 & \begin{array}{c} + \\ \omega' \\ \sigma \\ \omega \\ - \\ \hline \end{array} = \frac{|\chi|}{2} \left( 1 - \frac{\delta}{2\epsilon_A} \right), \\
 & \begin{array}{c} + \\ \omega' \\ \sigma \\ \omega \\ - \\ \hline \end{array} = -\frac{|\chi|}{2} \left( 1 + \frac{\delta}{2\epsilon_A} \right), \\
 & \begin{array}{c} + \\ \omega \\ \times \\ \omega \\ - \\ \hline \end{array} = \frac{\delta}{2\epsilon_A} |\chi|,
 \end{aligned}$$

so that again

$$\begin{array}{c} + \\ \omega' \\ \sigma \\ \omega \\ - \\ \hline \end{array} + \begin{array}{c} + \\ \omega' \\ \sigma \\ \omega \\ - \\ \hline \end{array} + \begin{array}{c} + \\ \omega \\ \times \\ \omega \\ - \\ \hline \end{array} = 0. \quad (3.23)$$

By means of similar calculations Eqs. (3.22) and (3.23) can be generalized for all different starting and ending states and propagating energies. For the forward propagator and the backward propagator we obtain

$$\begin{array}{c} \chi'_1 \\ \omega' \\ \sigma \\ \omega \\ \chi_1 \\ \hline \chi_2 \end{array} + \begin{array}{c} \chi'_1 \\ \omega' \\ \sigma \\ \omega \\ \chi_1 \\ \hline \chi_2 \end{array} + \begin{array}{c} \chi'_1 \\ \omega \\ \times \\ \omega \\ \chi_1 \\ \hline \chi_2 \end{array} = 0, \quad (3.24)$$

$$\begin{array}{c} \chi_1 \\ \omega \\ \hline \chi_2 \\ \omega' \\ \sigma \\ \chi'_2 \end{array} + \begin{array}{c} \chi_1 \\ \omega \\ \hline \chi_2 \\ \omega' \\ \sigma \\ \chi'_2 \end{array} + \begin{array}{c} \chi_1 \\ \omega \\ \hline \chi_2 \\ \omega \\ \times \\ \chi'_2 \end{array} = 0, \quad (3.25)$$

### 3 Diagrammatic technique

---

respectively. Note that Eqs. (3.24) and (3.25) are valid for an arbitrary number of normal lines with arbitrary directions. Since these incoming- and outgoing anomalous lines are the only possible tunneling lines involving superconductors in the limit of infinitely-large gaps the effect of all occurring tunneling lines associated with superconducting leads is cancelled by the effect of the cross vertices in this limit. This argument holds in every order so that the coupling to the superconducting leads is treated exactly. The consequence is that the effective Hamiltonian  $H_{\text{eff}}$  already contains the tunneling dynamics of the superconductors so that only transition rates involving the normal conducting leads need to be evaluated in the large-gap limit. Nevertheless, in order to calculate the current in a superconducting lead current rates that include tunneling lines associated with this lead still need to be accounted for. For example, the rather lavishly resummation of diagrams according to Ref. 23 could be skipped and the same results could be obtained just by calculating the first-order rates in the  $\pm$ -basis. If there is only one superconductor in the setup, the large-gap currents can be calculated by Fermi's golden rule allowing a quick access to the results.

## 4 Generation of pure spin currents by superconducting proximity effect in quantum dots

In this chapter we focus on a three-terminal hybrid system, composed of an interacting quantum dot tunnel coupled to one superconducting, one ferromagnetic, and one normal lead in the infinite-gap limit in order to find pure spin currents.

Hybrid systems containing ferromagnetic materials are of interest for the possibilities they open up to generate and control spin currents. The current between two tunnel-coupled ferromagnets depends strongly on the relative magnetization direction of the two ferromagnets. For parallel alignments the tunneling current is enhanced, while for antiparallel alignments the current is suppressed. This effect is known as the tunneling magneto resistance (TMR).<sup>88</sup>

In quantum dots connected to ferromagnets, spin accumulation in the dot plays an important role. Theoretically, for such systems complex transport properties as negative differential conductance<sup>89,90</sup> and spin precession<sup>85,91</sup> have been predicted. Experimentally, quantum dots realized in carbon nanotubes have already been coupled to ferromagnets.<sup>11-14</sup>

Cooper pairs in a BCS superconductor are made up of a spin up and spin down electron in a singlet state. Hence the combination of superconducting and ferromagnetic materials in a nano-structure is expected to give rise to rich spin physics and to non-local effects due to the entanglement intrinsic to the Cooper pairs. A good example is crossed Andreev reflection in three terminal setups consisting of a superconductor and two ferromagnets.<sup>92-96</sup>

Recently, S. Das *et al.* have proposed a scheme for pure spin currents in a three-terminal setup, where a ferromagnet, a superconductor, and a normal conductor are connected via quantum wires.<sup>97</sup> In the present work, we consider a similar setup, however involving a quantum dot. In particular, we consider an interacting, single-level quantum dot tunnel coupled to a superconducting, a ferromagnetic, and a normal lead, see Fig. 4.1. We exploit the tunability of the quantum-dot spectrum and non-equilibrium to generate a pure spin current in the normal lead, i.e. a spin current with no charge current.

The contents of this chapter have been published in Ref. 98.

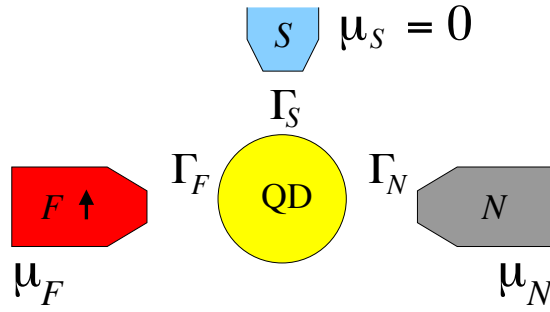


Figure 4.1: Setup: a quantum dot is tunnel coupled to one superconducting, one ferromagnetic, and one normal lead.

### 4.1 Model and method

In the limit of an infinite-large superconducting gap, i.e.  $|\Delta| \rightarrow \infty$ , the Hamiltonian of Eq. (3.8) simplifies for the three-terminal system depicted in Fig. 4.1 to

$$H = H_{\text{eff}} + \sum_{\eta=N,F} (H_{\eta} + H_{\text{tunn},\eta}), \quad (4.1)$$

with  $\chi = \Gamma_S/2$ , where  $\Delta$  has been chosen to be real. Since this system only contains a single superconductor all occurring currents be calculated without the current rates for the superconductor so that the complete dynamics of the superconductor is already contained in the effective Hamiltonian. In this chapter we consider the regime  $|\delta| < \sqrt{U^2 - \Gamma_S^2}$ , for which the inequality  $E_{A,-,-} < E_{A,-,+} < 0 < E_{A,+,-} < E_{A,+,+}$  holds. We consider only the case of weak coupling to the non-superconducting leads,  $\Gamma_N, \Gamma_F \lesssim k_B T$  and we compute results up to first order in these couplings. We also assume that  $\Gamma_N, \Gamma_F \ll \epsilon_A$ . When these conditions are fulfilled, we need to retain only the diagonal elements of the density matrix in the  $\pm$  basis introduced in Sec. 3.2. The generalized rates required to determine elements of the reduced density matrix can be calculated either with the diagrammatic technique presented in Chapter 3 or by means of Fermi's golden rule.

The current of electrons with spin  $\sigma$  out of lead  $\eta$  can be expressed as

$$J_{\eta\sigma} = \frac{1}{\hbar} \sum_{\chi\chi'} W_{\chi'\chi}^{\eta\sigma} P_{\chi}, \quad (4.2)$$

where  $W_{\chi'\chi}^{\eta\sigma} \equiv \sum_s s W_{\chi'\chi}^{\eta\sigma}$ , and  $W_{\chi'\chi}^{\eta\sigma}$  is the sum of all rates that describe transitions from  $\chi$  to  $\chi'$  in which in total  $s$  electrons of spin  $\sigma$  are removed from lead  $\eta$ . The charge current and the spin current out of lead  $\eta$  are given, respectively, by

$$J_{\eta}^Q \equiv c_Q (J_{\eta\uparrow} + J_{\eta\downarrow}), \quad (4.3)$$

$$J_{\eta}^S \equiv c_S (J_{\eta\uparrow} - J_{\eta\downarrow}), \quad (4.4)$$

where  $c_Q = e$  and  $c_S = \hbar/2$ .

## 4.2 Results

We discuss the case of equal tunnel-coupling strengths to the normal and ferromagnetic leads,  $\Gamma_N = \Gamma_F \equiv \Gamma \lesssim k_B T$ , and focus on the regime of positive bias,  $\mu_N > 0$ . The case  $\mu_N < 0$  is obtained from the symmetry transformation  $\mu_N \rightarrow -\mu_N$ ,  $\mu_F \rightarrow -\mu_F$ ,  $\delta \rightarrow -\delta$ , and  $J_N \rightarrow -J_N$ .

The spin current in the normal lead

$$J_N^S = -S_z \Gamma_N \left[ [f_N^-(E_{A,-,+}) + f_N^+(E_{A,+,+})] \left(1 + \frac{\delta}{2\epsilon_A}\right) + [f_N^+(E_{A,+,-}) + f_N^-(E_{A,-,-})] \left(1 - \frac{\delta}{2\epsilon_A}\right) \right], \quad (4.5)$$

is proportional to the spin accumulation  $S_z \equiv (P_\uparrow - P_\downarrow)/2$ , where  $f_N^+(\omega) = f_N(\omega) = [1 + \exp(\frac{\omega - \mu_N}{k_B T})]^{-1}$  is the Fermi function of the normal lead and  $f_N^-(\omega) = 1 - f_N(\omega)$ . In Eq. (4.5), the effect of the voltage bias applied to the ferromagnetic lead,  $\mu_F$ , is contained in the spin accumulation  $S_z$ . For small chemical potentials applied to the normal lead,  $E_{A,-,+} < \mu_N < E_{A,+,-}$ , the spin current is exponentially suppressed. For intermediate chemical potentials of the normal lead,  $E_{A,+,-} < \mu_N < E_{A,+,+}$ , and arbitrary  $\mu_F$ , the spin current simplifies to

$$J_N^S \approx -S_z \Gamma \left(1 - \frac{\delta}{2\epsilon_A}\right). \quad (4.6)$$

In the same bias regime, the charge current is given by the expression

$$J_N^Q \approx \Gamma \left[ \frac{1}{2} \left(1 - \frac{\delta}{2\epsilon_A}\right) P_1 + \left(1 + \frac{\delta}{2\epsilon_A}\right) P_- - \frac{\delta}{\epsilon_A} P_+ \right], \quad (4.7)$$

where  $P_1 = P_\uparrow + P_\downarrow$  is the probability for the dot to be singly occupied. We note that the charge current in intermediate bias regime can be tuned to zero by means of the dot-level position  $\epsilon$ .

On the other hand, in the large-bias regime for the normal lead,  $E_{A,+,+} < \mu_N$ , where processes with electrons entering the normal conductor are exponentially suppressed, there will always be a finite Andreev charge current flowing out of the normal lead into the superconductor, i.e., the charge current will be finite for any value of the level position.

In conclusion, a pure spin current is only possible in the intermediate-bias regime, which we will focus on in the following.

How to tune the system parameters to obtain a pure spin current is illustrated in Fig. 4.2, where the charge and spin currents are plotted as a function of the level position (tunable by the gate voltage) and of the chemical potential of the ferromagnetic lead  $\mu_F$  (tunable by the bias voltage). For the value of the level position corresponding to the thin line, the charge current vanishes for  $E_{A,+,+} < \mu_F$ , while the spin current remains finite. The level position  $\epsilon_0$  that tunes the charge current in the normal lead to zero, is a function of the charging energy  $U$ , the polarization  $p$ , and the tunnel-coupling

## 4 Generation of pure spin currents

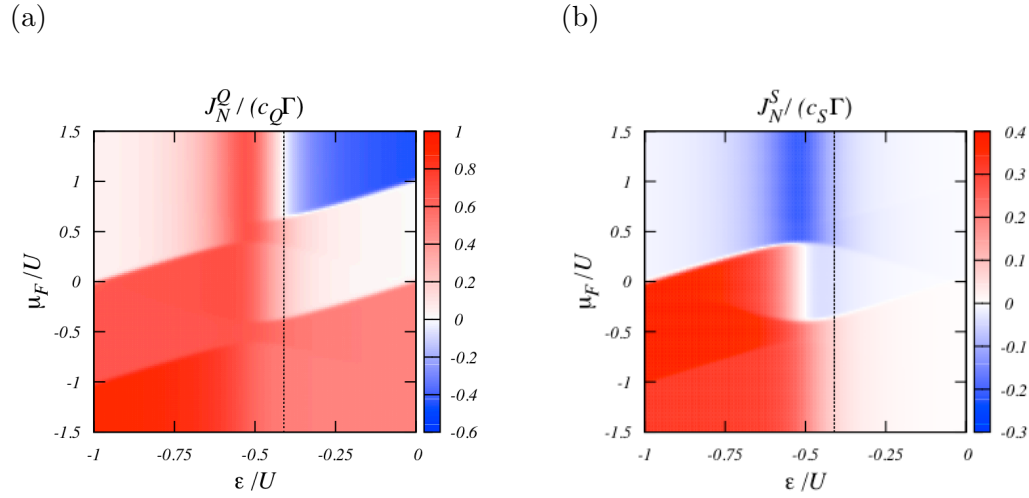


Figure 4.2: Density plot of (a) the charge current and (b) the spin current in the normal lead as a function of the level position  $\epsilon$  and the chemical potential of the ferromagnetic lead  $\mu_F$ . The thin line indicates the value of the level position for which the charge current vanishes in the high-bias regime for the ferromagnetic lead. The other parameters are  $\mu_N = 0.5U$ ,  $\Gamma_S = 0.2U$ ,  $\Gamma = 0.001U$ ,  $p = 0.6$ , and  $k_B T = 0.01U$ .

strength to the superconductor  $\Gamma_S$ :

$$\epsilon_0 = -\frac{U}{2} + \frac{\Gamma_S}{16} \sqrt{\frac{-p^4 + 27p^2 - 18 + (9 - p^2) \sqrt{p^4 - 36p^2 + 36}}{1 - p^2}}. \quad (4.8)$$

The equation is valid for the normal lead being in the intermediate-bias regime,  $E_{A,-,-}, E_{A,-,+}, E_{A,+,-} < \mu_N < E_{A,+,+}$ , and the ferromagnetic lead being in the large-bias regime,  $E_{A,+,+} < \mu_F$ . For its derivation we have assumed that all occurring Fermi functions can be approximated to either zero or one, i.e. that  $|\mu_N - E_{A,\gamma',\gamma}|, |\mu_F - E_{A,\gamma',\gamma}| \gg k_B T$  for all possible values of  $\gamma$  and  $\gamma'$ .

Increasing the polarization  $p$  increases the spin accumulation on the dot and reduces the proximization of the dot by the superconductor. Thus the probability for the dot to be singly occupied,  $P_1$ , is increased, while the probability for the dot to be in state  $|+\rangle$ ,  $P_+$ , is reduced. In order to keep the charge current in the normal lead tuned to zero for increased polarizations the prefactor of  $P_1$ , i.e.  $(1 - \delta/2\epsilon_A)$ , in Eq. (4.7) has to be reduced by increasing  $\epsilon = \epsilon_0$ .

For moderate values of the polarization  $p$  the monotonically increasing function  $\epsilon_0(p)$  grows slowly. Only for large polarizations  $\epsilon_0(p)$  grows fast.

When  $\epsilon_0$  becomes of the same order of the single-particle level spacing in the quantum dot, the single-level model for the dot ceases to be valid. However, for the system under consideration this situation is not realized for realistic polarizations of the ferromagnetic lead. In fact, for  $\Gamma_S = 0.2U$  and  $p = 0.995$  we find that the level position

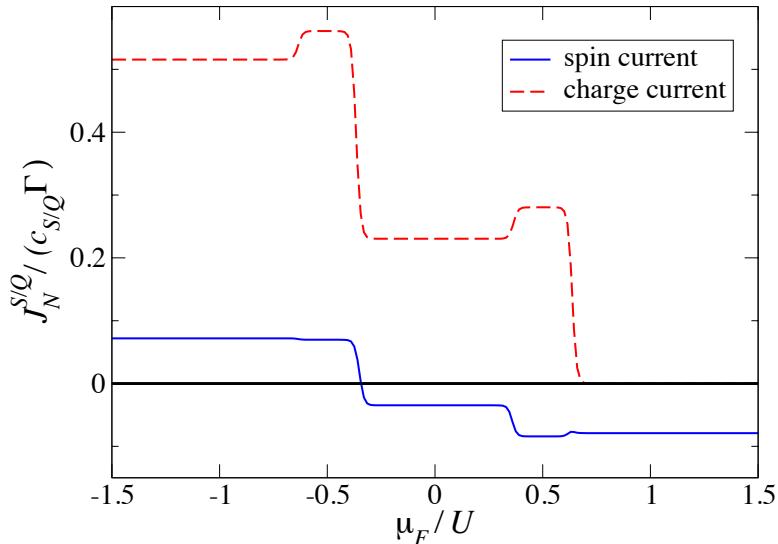


Figure 4.3: Spin current  $J_N^S$  and charge current  $J_N^Q$  as a function of the chemical potential of the ferromagnetic lead  $\mu_F$  for  $\epsilon = \epsilon_0$ ,  $\mu_N = 0.5U$ ,  $\Gamma_S = 0.2U$ ,  $\Gamma = 0.001U$ ,  $p = 0.6$ , and  $k_B T = 0.01U$ .

that tunes the charge current in the normal lead to zero only reaches  $\epsilon_0 \approx 0$ .

The pure spin current for  $\epsilon = \epsilon_0$  is independent of the tunnel-coupling strength to the superconductor  $\Gamma_S$  (though a finite  $\Gamma_S$  is required to establish the spin current and the Andreev current tuning the charge current to zero).

Figure 4.3 shows the spin and charge currents in the normal lead for  $\epsilon = \epsilon_0$ , as a function of the chemical potential of the ferromagnetic lead  $\mu_F$ . The dependence of the pure spin current on the polarization of the ferromagnet is shown in Fig. 4.4. With increasing polarization the spin current increases until a maximum is reached. For stronger polarizations, the charge current flowing out of the ferromagnet is reduced due to the spin accumulation, leading to reduction of the spin current in the normal lead.

The occurrence of a pure spin current can be understood examining the transport processes between dot and ferromagnetic / normal lead. Since the ferromagnetic and normal leads are only weakly coupled to the quantum dot, corresponding currents are carried by sequential electron tunneling.

The possible transport processes between dot and ferromagnetic lead in the large bias regime, i.e.  $E_{A,+,+} < \mu_F$ , are illustrated in Figure 4.5 a). The processes involving minority spins, depicted by shorter arrows, are suppressed. In all the processes electrons are transferred from the ferromagnetic lead to the dot. All four dot states can be occupied. Due to the spin polarization of the ferromagnetic lead, an imbalance in

## 4 Generation of pure spin currents

---

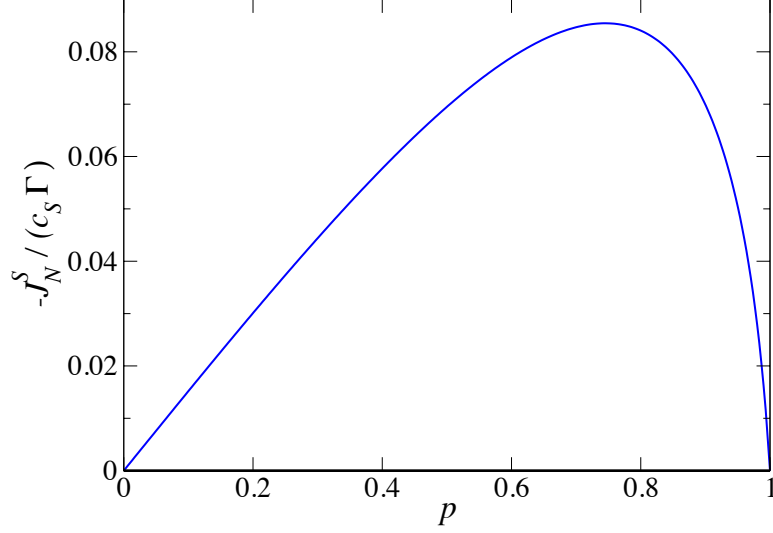


Figure 4.4: Spin current in the normal lead as a function of the polarization of the ferromagnet  $p$  for  $\epsilon = \epsilon_0$ ,  $\mu_N = 0.5U$ ,  $\Gamma_S = 0.2U$ ,  $\Gamma = 0.001U$ , and  $k_B T = 0.01U$ .

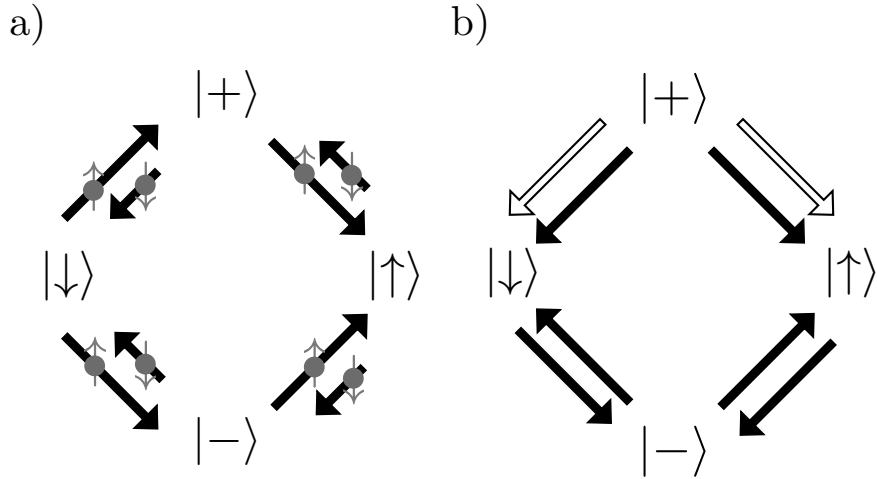


Figure 4.5: Possible tunneling processes between dot and a) ferromagnetic lead with large chemical potential  $E_{A,+} < \mu_F$  and b) normal lead with intermediate chemical potential  $E_{A,+} < \mu_N < E_{A,+}$ : the arrow direction depicts transitions of dot states. With black (white) arrows an electron leaves (enters) the corresponding lead. Tunneling of minority spins (short arrows) is suppressed.

the occupation of the dot states  $|\uparrow\rangle$  and  $|\downarrow\rangle$ , and thus a finite spin accumulation  $S_z$ , is generated.

The possible transport processes between dot and normal lead in the intermediate bias regime, i.e.  $E_{A,+,-} < \mu_N < E_{A,+,+}$ , are shown in Figure 4.5 b). Because of the spin accumulation on the dot, i.e.  $P_\uparrow > P_\downarrow$ , transitions from state  $|\uparrow\rangle$  to state  $|-\rangle$  take place more frequently than transitions from  $|\downarrow\rangle$  to  $|-\rangle$ . This leads to a finite spin current in the normal lead. Black arrows represent processes where an electron flows out of the normal lead, while white arrows indicate processes where electrons enter the normal lead. The latter processes require the dot to be in state  $|+\rangle$ . The occupation of dot state  $|+\rangle$  is provided by the ferromagnet. By controlling the gate voltage, and thus the occupation of the different dot states, the charge current in the normal lead can be tuned to zero yielding a pure spin current. This pure spin current is generated by the interplay of superconductivity, non-equilibrium, and spin-dependent transport: the superconducting lead proximates the quantum dot, leading to the superposition states  $|-\rangle$  and  $|+\rangle$ . The biased ferromagnetic lead first provides occupation of the dot state  $|+\rangle$ , which gives the possibility to tune the charge current in the normal to zero. Second, it causes spins to accumulate on the dot inducing a spin current in the normal lead.

### 4.3 Conclusions

Spin-dependent transport in a three-terminal structure consisting of a quantum dot tunnel coupled to a superconducting, a ferromagnetic and a normal lead has been investigated in the large-superconducting-gap regime, by means of a master-equation approach. It has been established that such a system can be used to generate a pure spin current in the normal lead, exploiting the tunability of the dot's spectrum, non-equilibrium driven by finite bias voltages, spin accumulation due to the ferromagnet, and the Andreev bound states induced by the superconductor.

## 4 Generation of pure spin currents

---

## 5 Renormalization effects in interacting quantum dots coupled to superconducting leads

An exact theoretical treatment of the transport properties of hybrid systems coupled to superconducting leads requires to account for Coulomb interaction, superconducting correlations, and non-equilibrium at the same time. To circumvent this challenge, various approximation schemes have been proposed. In the case of vanishing Coulomb interaction, an exact solution can be obtained within a scattering approach.<sup>15</sup> As a first step beyond, Coulomb interaction has been treated perturbatively,<sup>16–21</sup> which, however, is not justified for the large charging energies that are typical for small quantum dots. An alternative possibility is to allow for strong Coulomb interaction but perform a perturbation expansion in the strength of the tunnel coupling between dot and leads.<sup>22,23</sup> However, in the limit of an infinitely-large superconducting gap, an exact treatment of both the Coulomb interaction and the tunnel coupling between quantum dot and superconducting leads is possible.<sup>23–27</sup> In this case, quasiparticle tunneling is completely suppressed and transport from and to the superconducting leads is fully sustained by Cooper pairs. The formation of Andreev-bound states (ABSs) in the quantum dot indicates that superconducting correlations are induced via the proximity to superconducting leads. The dependence of the ABS energies on the quantum dot's level position is directly reflected in the transport spectrum of the system.

A diagrammatic real-time approach to transport through quantum dots coupled both to normal and superconducting leads has been introduced in Ref. 23. This method has been applied in the limit of an infinitely-large superconducting gap,  $\Delta \rightarrow \infty$ , to study a variety of transport phenomena in different quantum-dot setups,<sup>28–32,98–100</sup> including, for example, pure spin-current generation,<sup>98</sup> shot-noise suppression,<sup>99</sup> Cooper-pair splitting,<sup>30,31</sup> and time dependent driving.<sup>32</sup>

The calculations in the infinite-gap limit neglect quasiparticle contributions to transport. They, furthermore, approximate the ABS energies since the latter are a function of the superconducting gap. In the experiments, the superconducting gap  $\Delta$  is often of the same order of magnitude as other energy scales such as charging energy or tunnel-coupling strength. For this reason, it is quite natural to investigate the quality of the approximation introduced by considering the infinite-gap limit. This is the main goal of this chapter. Furthermore, we analyze the effect of next-to-lowest order corrections in the tunnel coupling to the normal leads.

A finite superconducting gap in the leads affects the Andreev and Josephson transport through quantum dots in two ways. First, it modifies the ABSs. This affects the position of bias or gate voltages at which a new transport channel is opened. Second,

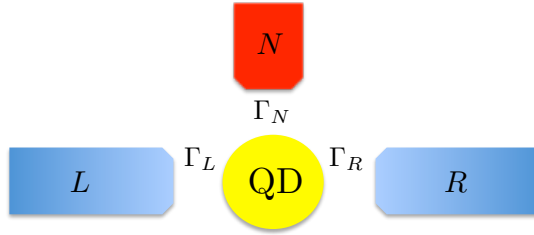


Figure 5.1: (Color online) Setup: a quantum dot is tunnel coupled to one normal and two superconducting leads.

the value of the current away from these threshold voltages is changed. To address the effect of a finite  $\Delta$ , we start by performing a systematic expansion in  $1/\Delta$  around  $\Delta \rightarrow \infty$ . Exemplarily, we will focus on a quantum dot tunnel coupled to one normal and two superconducting reservoirs and compare the currents obtained by the  $1/\Delta$  expansion with the  $\Delta \rightarrow \infty$  limit.<sup>23</sup> We find that away from the threshold voltages, both the Andreev and the Josephson currents are hardly modified, i.e., the  $\Delta \rightarrow \infty$  limit provides quite an accurate description of subgap transport. The  $1/\Delta$  expansion, furthermore, indicates a renormalization of the ABS energies. It can, however, only predict the direction towards which the energies are shifted. To determine the position of the ABS, we go beyond the  $1/\Delta$  expansion and perform a partial resummation of diagrams. The results within this approach are considerably more accurate than those obtained by a simple Hartree-Fock treatment and compare favorably with the numerical renormalization group (NRG) data of Martín-Rodero and Levy Yeyati.<sup>33</sup>

Finally, we present (for the  $\Delta \rightarrow \infty$  limit) results from a systematic perturbation expansion to next-to-lowest order in the tunnel coupling to the normal leads. In this way, we go beyond the regime of weak tunnel coupling but do not cover Kondo correlations.<sup>14,16–19,66,67,101–112</sup> We find that the next-to-leading correction leads to a renormalization of the gate-voltage position at which a  $0 - \pi$  transition occurs in the Josephson current. This renormalization also affects the Andreev current and the average quantum-dot charge. The contents of this chapter have been published in Ref. 87.

## 5.1 Model and Method

### 5.1.1 Hamiltonian

We focus on a three-terminal setup composed of a normal conductor and two superconductors tunnel coupled to an interacting single-level quantum dot, see Fig. 5.1. The system's Hamiltonian is given by  $H = H_{\text{dot}} + \sum_{\eta} H_{\eta} + H_{\text{tunn},\eta}$ , with  $\eta \in \{L, R, N\}$ . We assume the normal lead to be a reservoir of noninteracting electrons and model the superconductors with the mean-field BCS Hamiltonian

$$H_{\eta} = \sum_{k\sigma} \epsilon_{\eta k} c_{\eta k\sigma}^{\dagger} c_{\eta k\sigma} - \delta_{\eta,S} \sum_k (\Delta e^{i\Phi_{\eta}} c_{\eta-k\downarrow} c_{\eta k\uparrow} + \text{H.c.}), \quad (5.1)$$

with  $\epsilon_{\eta k}$  being the single-particle energies and  $c_{\eta k \sigma}^{(\dagger)}$  are the annihilation (creation) operators for electrons in lead  $\eta$  with momentum  $k$  and spin  $\sigma$ . Here,  $\Delta$  is the modulus of the superconducting pair potential, which we assume to be the same in both superconductors, and  $\Phi_\eta$  is the corresponding phase in lead  $\eta = S$  with  $S \in \{L, R\}$ . We measure all occurring energies with respect to the Fermi level of the superconductors, i.e.  $\mu_{L,R} = 0$ . Furthermore, we assume all occurring excitation energies of the dot to lie inside the superconducting gap of the leads so that only subgap transport takes place.

The Anderson Hamiltonian describing the single-level quantum dot reads

$$H_{\text{dot}} = \sum_{\sigma} \epsilon d_{\sigma}^{\dagger} d_{\sigma} + U n_{\uparrow} n_{\downarrow}, \quad (5.2)$$

where  $\epsilon$  is the energy of the spin-degenerate single-particle level, and  $U$  the on-site Coulomb repulsion. The dot's annihilation (creation) operators of spin  $\sigma$  are given by  $d_{\sigma}^{(\dagger)}$ , and  $n_{\sigma} = d_{\sigma}^{\dagger} d_{\sigma}$  is the corresponding number operator. Tunneling between dot and leads is described by the tunneling Hamiltonian

$$H_{\text{tunn},\eta} = V_{\eta} \sum_{k\sigma} \left( c_{\eta k \sigma}^{\dagger} d_{\sigma} + \text{H.c.} \right), \quad (5.3)$$

with the spin and momentum independent tunnel matrix elements  $V_{\eta}$ . We define the tunnel-coupling strengths as  $\Gamma_{\eta} = 2\pi |V_{\eta}|^2 \rho_{\eta}$ , where  $\rho_{\eta}$  is the density of states in lead  $\eta$  that we assume to be independent of spin and energy.

### 5.1.2 Diagrammatic Technique

#### Effective Dot Hamiltonian

The main idea of the diagrammatic real-time technique is to integrate out the leads' degrees of freedom to arrive at a reduced density matrix for the quantum dot. As a basis for the reduced density matrix one may use the eigenstates of the decoupled quantum dot,  $H_{\text{dot}}$ . This is a convenient choice for weak tunnel couplings to the superconductors.<sup>22</sup> In the opposite limit of strong coupling to the superconductor, a resummation of an infinite number of diagrams is required. This resummation can be carried out exactly in the  $\Delta \rightarrow \infty$  limit.<sup>23</sup> For a systematic  $1/\Delta$ -expansion, however, it is more convenient to work in the eigenbasis of  $H_{\text{eff}} = H_{\text{dot}} - H_{\text{p}}$ , with the pairing Hamiltonian  $H_{\text{p}} = \chi^* d_{\downarrow} d_{\uparrow} + \chi d_{\uparrow}^{\dagger} d_{\downarrow}^{\dagger}$  and  $\chi = \frac{1}{2} \sum_{\eta=L,R} \Gamma_{\eta} e^{i\Phi_{\eta}}$ . The remaining part of the Hamiltonian

$$H - H_{\text{eff}} = H_{\text{p}} + \sum_{\eta} H_{\eta} + H_{\text{tunn},\eta}, \quad (5.4)$$

is treated diagrammatically as a perturbation. Thereby,  $H_{\text{p}}$  has been chosen such that in the  $\Delta \rightarrow \infty$  limit the diagrammatic contributions stemming from  $H_{\text{p}}$  exactly cancel those from the tunneling to the superconducting leads, i.e.,  $H_{\text{eff}}$  describes the hybrid system of quantum dot and superconducting leads in the limit of an infinite superconducting gap.

## 5 Renormalization effects in interacting quantum dots

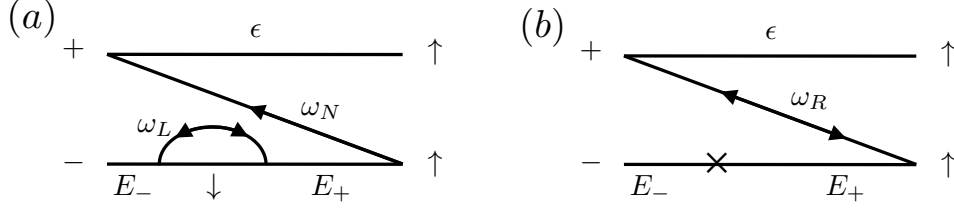


Figure 5.2: Example diagrams contributing to the rate  $W_{+-}^{\uparrow\uparrow}$ .

The eigenstates of  $H_{\text{eff}}$  are  $|\uparrow\rangle$ ,  $|\downarrow\rangle$ , and  $|\pm\rangle = \frac{1}{\sqrt{2}} \left[ \mp e^{-i\Phi_\chi/2} \sqrt{1 \mp \frac{\delta}{2\epsilon_A}} |0\rangle + e^{i\Phi_\chi/2} \sqrt{1 \pm \frac{\delta}{2\epsilon_A}} |d\rangle \right]$ , with eigenenergies  $\epsilon$ ,  $\epsilon$ , and  $E_\pm = \frac{\delta}{2} \pm \epsilon_A$ , respectively. Here,  $\Phi_\chi = \arg(\chi)$ ,  $\epsilon_A = \sqrt{(\frac{\delta}{2})^2 + |\chi|^2}$ , and  $\delta = 2\epsilon + U$  is the detuning between the energies for empty and doubly-occupied quantum dot. The superconducting proximity effect is indicated by the fact that  $|0\rangle$  and  $|d\rangle$  are no longer eigenstates but appear as linear combinations in  $|\pm\rangle$ . The mixing between  $|0\rangle$  and  $|d\rangle$  becomes largest around zero detuning,  $\delta \sim 0$ .

The excitation energies associated with  $H_{\text{eff}}$  are given by the differences of the eigenenergies of states with even and odd dot occupation numbers,

$$E_{A,\gamma',\gamma}^{\Delta \rightarrow \infty} = \gamma' \frac{U}{2} + \gamma \epsilon_A, \quad (5.5)$$

with  $\gamma', \gamma = \pm$ . They are nothing but the Andreev bound state (ABS) energies

### Generalized Master Equation

The system's dynamics is determined by a generalized master equation for the reduced density matrix  $\rho_{\text{red}}$ , which is obtained by integrating out the lead's degrees of freedom. Its matrix elements  $P_{\chi_2}^{\chi_1} = \langle \chi_1 | \rho_{\text{red}} | \chi_2 \rangle$  obey, in the stationary limit, the generalized master equation

$$i(E_{\chi_1} - E_{\chi_2}) P_{\chi_2}^{\chi_1} = \sum_{\chi'_1 \chi'_2} W_{\chi_2 \chi'_2}^{\chi_1 \chi'_1} P_{\chi'_2}^{\chi'_1}, \quad (5.6)$$

where  $W_{\chi_2, \chi'_2}^{\chi_1, \chi'_1}$  are generalized rates that can be computed in a diagrammatic way, see Chapter 3. To illustrate what types of diagrams need to be included we show two exemplary diagrams here. The first example is a diagram containing one line associated with the normal lead and one line associated with the left superconductor, see Fig. 5.2 (a), and it reads

$$\begin{aligned} & -i \int \frac{d\omega_L}{2\pi} \int \frac{d\omega_N}{2\pi} \Gamma_N \Gamma_S e^{i(\Phi_L - \Phi_\chi)} f_N^+(\omega_N) f^-(\omega_L) \\ & \times \frac{1}{\omega_N + E_- - \epsilon + i0^+} \frac{1}{\omega_N + \omega_L + i0^+} \frac{1}{\omega_N + E_+ - \epsilon + i0^+} \\ & \times \text{sign}(\omega_L) \frac{\Delta}{\sqrt{\omega_L^2 - \Delta^2}} \Theta(|\omega_L| - \Delta) \left(1 - \frac{\delta}{2\epsilon_A}\right)^2. \end{aligned}$$

The second example is a diagram, see Fig. 5.2 (b), containing a line associated with the right superconductor and a cross vertex and it yields the following expression

$$\begin{aligned}
 & i \int \frac{d\omega_R}{2\pi} \Gamma_S e^{i(\Phi_R - \Phi_\chi)} f^-(\omega_R) \frac{1}{E_- - \omega_R - \epsilon + i0^+} \\
 & \times \frac{1}{E_+ - \omega_R - \epsilon + i0^+} \text{sign}(\omega_R) \frac{\Delta}{\sqrt{\omega_R^2 - \Delta^2}} \\
 & \times \Theta(|\omega_R| - \Delta) \frac{\delta|\chi|}{2\epsilon_A} \sqrt{1 - \frac{\delta^2}{4\epsilon_A^2}}.
 \end{aligned}$$

As explained in the previous section, we work in the basis  $\{\uparrow, \downarrow, +, -\}$ . This has the consequence that the off-diagonal matrix elements on the right hand side of Eq. (5.6) vanish to lowest order in  $\Gamma_N$  and  $1/\Delta$  as long as  $\epsilon_A \gtrsim \Gamma_N$ . Only their next-order correction remains finite.

Superconducting correlations in the quantum dot are associated with coherent superpositions of an empty and a doubly-occupied dot. This motivates the following definition of an isospin,<sup>22,23</sup>

$$I_x = \frac{P_0^d + P_d^0}{2}, \quad I_y = i \frac{P_0^d - P_d^0}{2}, \quad I_z = \frac{P_d - P_0}{2}, \quad (5.7)$$

formulated in the basis  $\{\uparrow, \downarrow, 0, d\}$  (the transformation to the basis  $\{\uparrow, \downarrow, +, -\}$  is straightforward). A finite value of the isospin components  $I_x$  and/or  $I_y$  indicates the presence of superconducting proximity effect.

It turns out that the generalized master equations for the isospin components do not couple to the probabilities of the quantum dot to be singly occupied with either spin. They can be written in the form of a Bloch-like equation

$$0 = \frac{d\mathbf{I}}{dt} = \mathbf{A} - \mathbf{R} \cdot \mathbf{I} + \mathbf{I} \times \mathbf{B}, \quad (5.8)$$

where the terms with  $\mathbf{A}$ ,  $\mathbf{R}$ , and  $\mathbf{B}$  describe the generation, relaxation, and coherent rotation of the isospin.

### Current formulae

The current in lead  $\eta$  is given by

$$J_\eta = -\frac{e}{\hbar} \sum_{\chi\chi'_1\chi'_2} W_{\chi\chi'_2}^{\chi\chi'_1} I_\eta P_{\chi'_2}^{\chi'_1}, \quad (5.9)$$

with  $W_{\chi\chi'_2}^{\chi\chi'_1} I_\eta$  being the generalized current rates. For a systematic perturbation expansion in powers of  $\Gamma_N$  and  $1/\Delta$  one needs to expand  $P$ ,  $W$ , and  $W^{I_\eta}$  in Eqs. (5.6) and (5.9).

We refer to the current flowing out of the normal lead as the Andreev current and to the difference of the currents between left and right superconductor as the Josephson

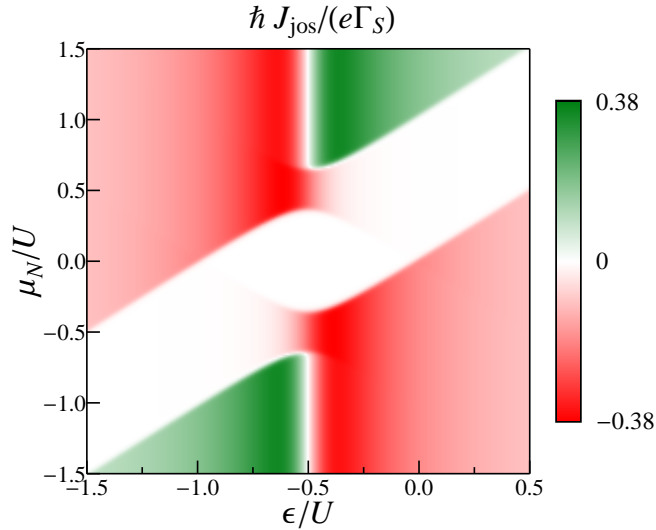


Figure 5.3: (Color online) Density plot of the Josephson current in the limit of  $\Delta \rightarrow \infty$  as a function of the level position  $\epsilon$  and the chemical potential of the normal lead  $\mu_N$ . The other parameters are  $\Gamma_S = 0.2U$ ,  $\Gamma_N = 0.001U$ ,  $\Phi = \pi/2$ , and  $k_B T = 0.01U$ .

current. In the limit  $\Delta \rightarrow \infty$ , the Andreev current and the Josephson current are directly connected to the isospin via<sup>23</sup>

$$J_{\text{jos}}^{\Delta \rightarrow \infty} = \frac{2e}{\hbar} \Gamma_S I_x^{\Delta \rightarrow \infty} \sin \frac{\Phi}{2}, \quad (5.10)$$

$$J_{\text{and}}^{\Delta \rightarrow \infty} = -\frac{4e}{\hbar} \Gamma_S I_y^{\Delta \rightarrow \infty} \cos \frac{\Phi}{2}. \quad (5.11)$$

For the  $1/\Delta$  corrections to the currents, however, one needs to use the more general Eq. (5.9).

## 5.2 Finite-gap effects

### 5.2.1 $1/\Delta$ Expansion

We assume symmetric tunnel couplings to the superconducting leads,  $\Gamma_L = \Gamma_R = \Gamma_S$ . Furthermore, we choose a gauge such that  $\Phi_L = -\Phi_R = \Phi/2$ . For both the Josephson and the Andreev current we calculate the value for the  $\Delta \rightarrow \infty$  limit and the correction to first order in  $1/\Delta$ . The tunnel coupling to the normal lead,  $\Gamma_N$  is accounted for in lowest non-vanishing order, i.e., to zeroth order for the Josephson current and to first order for the Andreev current.

Figures 5.3 and 5.4 show the Josephson current and the Andreev current in the limit of  $\Delta \rightarrow \infty$  as a function of the level position  $\epsilon$  and the chemical potential of the

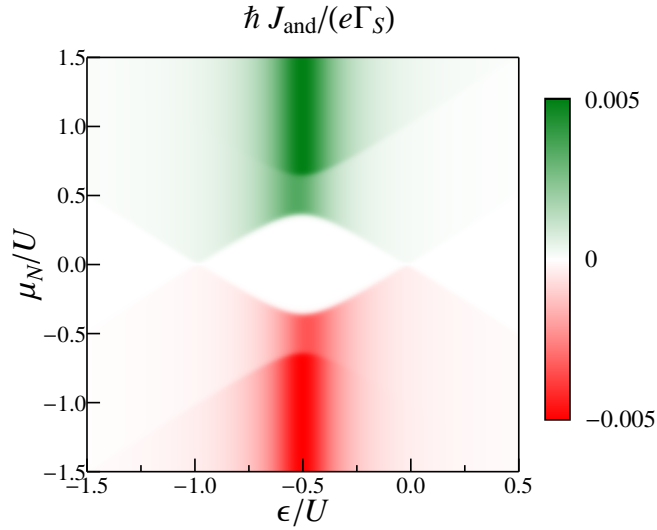


*Figure 5.4:* (Color online) Density plot of the Andreev current in the limit of  $\Delta \rightarrow \infty$  as a function of the level position  $\epsilon$  and the chemical potential of the normal lead  $\mu_N$ . The other parameters are  $\Gamma_S = 0.2U$ ,  $\Gamma_N = 0.001U$ ,  $\Phi = \pi/2$ , and  $k_B T = 0.01U$ .

normal lead  $\mu_N$ . This is the limit considered in Ref. 23 and is used as a reference for the present discussion. A cut through the density plots at a fixed level position  $\epsilon = -0.4U$  is shown in Fig. 5.5 (solid blue line). The currents display a step-like behavior with the position of the steps reflecting the ABS energies. This is compared with the currents expanded up to first order in  $1/\Delta$ , dashed red lines in Fig. 5.5. From this comparison, we can draw two conclusions.

First, away from the ABS, the solid and dashed curves almost coincide, i.e., the  $1/\Delta$  correction to the current is small. This leads to the conclusion that the  $\Delta \rightarrow \infty$  calculations provide a useful and quantitatively accurate description of sub-gap transport also for finite values of the superconducting gap.

Second, we find peaks at the positions of the ABSs in the  $1/\Delta$  correction to the current. While the peaks themselves are artefacts of the  $1/\Delta$  expansion, they carry important physical information about the renormalization of the ABSs as compared to their  $\Delta \rightarrow \infty$  value. This can be understood in the following way. The currents vary stepwise at the position of the ABSs. The latter are renormalized due to finite  $\Delta$ . Therefore, a systematic expansion in the small parameter with which the renormalization scales gives rise to the occurrence of peaks at the original position of the steps. The sign of the peaks relative to the sign of the steps indicates the direction of the renormalization. The ABS is renormalized towards (away from) zero if step and peak have the same (the opposite) sign. In the examples plotted in Fig. 5.5 the curves indicate a renormalization of all four ABSs towards zero.

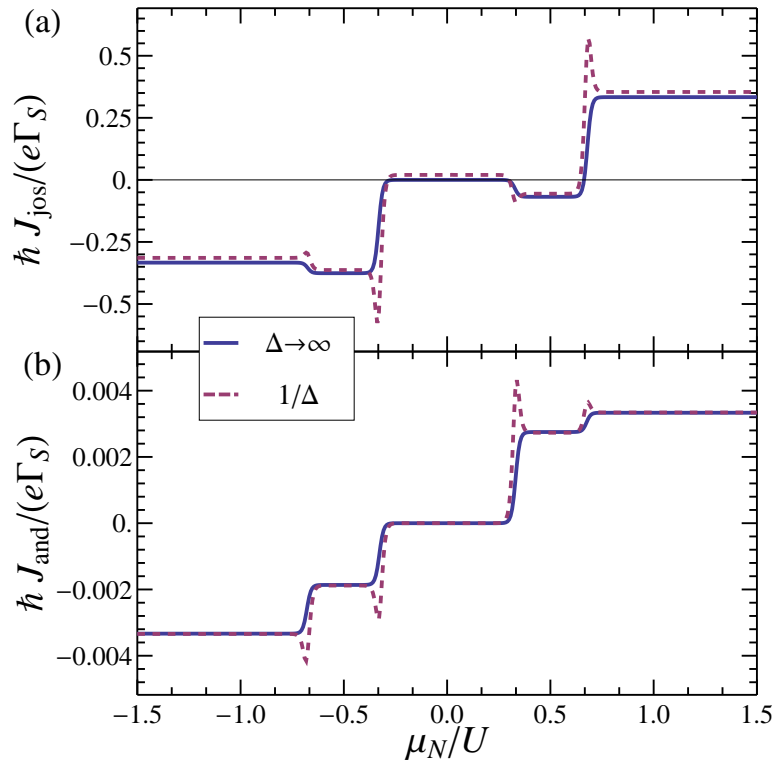


Figure 5.5: (Color online) Plot of (a) the Josephson current and (b) the Andreev current as a function of the chemical potential of the normal lead  $\mu_N$ . The solid (blue) curve shows the  $\Delta \rightarrow \infty$  limit, the dashed (red) curve includes the first  $1/\Delta$  correction. The other parameters are  $\epsilon = -0.4U$ ,  $\Gamma_S = 0.2U$ ,  $\Gamma_N = 0.001U$ ,  $\Delta = 5U$ ,  $\Phi = \pi/2$ , and  $k_B T = 0.01U$ .

### 5.2.2 Renormalization of Andreev Bound States

The  $1/\Delta$  expansion indicates that the ABSs are renormalized as compared to the  $\Delta \rightarrow \infty$  limit. It even predicts the sign of the renormalization. It does, however, not provide a possibility to calculate the ABSs at finite  $\Delta$ . For this task, alternative approaches are required. In the limit of vanishing Coulomb interaction, the problem can be solved exactly.<sup>15,107</sup> A mean-field treatment of the Coulomb interaction provides easily an estimate of the ABSs.<sup>9,33</sup> Numerical renormalization group (NRG) calculations are exact but numerically demanding.<sup>33,113–116</sup> Instead, we propose a resummation approach that is more accurate than mean field but less computationally heavy than NRG.

In the following, we consider the limit of weak tunnel coupling to the normal lead, i.e., we discuss the spectrum to zeroth order in  $\Gamma_N$ . Furthermore, we choose  $\Phi = 0$  without loss of generality (to consider the case of a finite  $\Phi$  one has to replace  $\Gamma_S$  by  $\Gamma_S \cos(\Phi/2)$ ; to model the case of a single superconducting lead,  $\Gamma_S$  needs to be replaced by  $\Gamma_S/2$ ).

#### Exact Green's function for the noninteracting dot

For a noninteracting dot,  $U = 0$ , the exact Green's function for spin  $\sigma$  is given, in Nambu space, by

$$\hat{G}^r = \left( \omega \cdot \mathbf{I}_{2 \times 2} - \hat{h}_\sigma(U = 0) - \hat{\Sigma}_S \right)^{-1}, \quad (5.12)$$

with  $\mathbf{I}_{n \times n}$  being the identity matrix in  $n$  dimensions. The matrix

$$\hat{h}_\sigma(U = 0) = \begin{pmatrix} \epsilon_\sigma & 0 \\ 0 & -\epsilon_{-\sigma} \end{pmatrix} \quad (5.13)$$

accounts for the single-particle energies, and the self-energy due to tunneling reads

$$\hat{\Sigma}_S = \Gamma_S \begin{pmatrix} -\frac{\omega}{\sqrt{\Delta^2 - \omega^2}} & \frac{\Delta}{\sqrt{\Delta^2 - \omega^2}} \\ \frac{\Delta}{\sqrt{\Delta^2 - \omega^2}} & -\frac{\omega}{\sqrt{\Delta^2 - \omega^2}} \end{pmatrix}. \quad (5.14)$$

The ABSs, i.e. the excitation energies, are found as the real part of the poles of the Green's function's determinant. An example is shown in Fig. 5.6. In the noninteracting case, there are only two ABSs. Their energies for finite  $\Delta$  are reduced as compared to the  $\Delta \rightarrow \infty$  limit. In particular, the curvature of the energy as a function of the bare level position  $\epsilon$  changes for large  $|\epsilon|$ , such that the ABSs lie within the window  $[-\Delta, \Delta]$ .

#### Hartree-Fock approximation

A Hartree-Fock (HF) treatment of the Coulomb interaction has been used in Ref. 9 to fit the experimental data. This HF approach corresponds to replace  $\hat{h}_\sigma(U = 0)$  in Eq. (5.12) by

$$\hat{h}_\sigma(U) = \begin{pmatrix} \tilde{\epsilon}_\sigma & 0 \\ 0 & -\tilde{\epsilon}_{-\sigma} \end{pmatrix}, \quad (5.15)$$

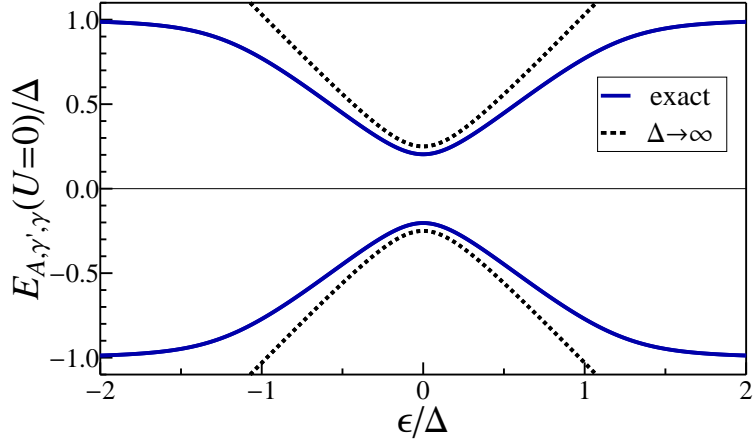


Figure 5.6: (Color online) Plot of the  $U = 0$  Andreev-bound states for a tunnel-coupling strength to the superconducting lead of  $\Gamma_S = 0.25\Delta$  as a function of the level position  $\epsilon$ . All energies are normalized to  $\Delta$ . The solid (blue) line shows the exact result, the dashed (black) line the bound states computed by means of the  $\Delta \rightarrow \infty$  expression, which in the non-interacting case is simply  $\pm\epsilon_A$ .

where  $\tilde{\epsilon}_\downarrow = \tilde{\epsilon}_\uparrow + U$ . For  $U = 0$ , the exact Green's function Eq. (5.12) is recovered. Furthermore, it reproduces the exact ABSs in the  $\Delta \rightarrow \infty$  limit.

An improved version is self-consistent HF, in which the dot occupations are calculated self-consistently.<sup>33</sup> In the following, however, we use the simpler version of HF for comparison with the results from the resummation approach.

### Resummation Approach

An important feature of the diagrammatic technique presented in this paper is that Coulomb interaction can be included beyond the mean-field level. The downside is that for an exact solution one has to sum up infinitely many diagrams. A great simplification is achieved by working in the basis  $\{\uparrow, \downarrow, +, -\}$ . As discussed above, in the  $\Delta \rightarrow \infty$  limit, all diagrams that contain superconducting lines are cancelled by cross vertices. This means that all contributing diagrams contain normal tunnel lines only.

At finite  $\Delta$ , the situation is different. Now, both superconducting lines and cross vertices dress the original normal tunnel lines. We define the propagator  $\Pi(\omega)$  as the diagram part between two vertices that are connected by a normal tunnel line with energy  $\omega$  running from right to left. This propagator obeys a Dyson equation

$$\Pi(\omega) = \Pi^{(0)}(\omega) + \Pi(\omega) \Sigma(\omega) \Pi^{(0)}(\omega), \quad (5.16)$$

where  $\Pi^{(0)}(\omega)$  is the free propagator (without superconducting lines and cross vertices) and  $\Sigma(\omega)$  the self energy.

In the  $\Delta \rightarrow \infty$  limit, the self energy is exactly zero. For an approximative treatment of the case of finite  $\Delta$ , we now include all self energy parts that contain one superconducting tunnel line or one cross vertex. Examples are shown in Fig. 5.7.

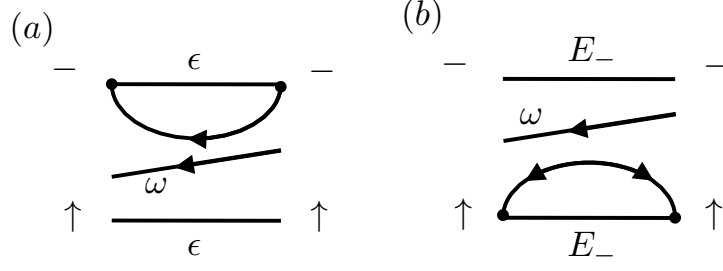


Figure 5.7: Examples for diagrams that contribute to the self-energy.

Since the Hilbert space is four dimensional, the dimension of the corresponding Liouville space and, thus, of the matrices appearing in Eq. (5.16) is, in general, 16. However, as a consequence of spin and charge conservation while tunneling, the Dyson equation decouples into blocks of  $4 \times 4$  matrices. The presence of the normal tunneling line running from right to left which carries a definite charge and spin puts constraints on the possible states at the beginning and end of the upper ( $\chi_1$ ) and lower ( $\chi_2$ ) contour. In the following, we choose, without loss of generality,  $(\chi_1, \chi_2) \in \{(-, \uparrow), (\downarrow, +), (\downarrow, -), (+, \uparrow)\}$ , which is the relevant case when the normal tunneling line carries spin  $\downarrow$ . Then,

$$\left(\Pi^{(0)}(\omega)\right)^{-1} = \omega \cdot \mathbf{I}_{4 \times 4} - \text{diag}(E_{A,+,-}, E_{A,-,-}, E_{A,-,+}, E_{A,+,+}) \quad (5.17)$$

for the inverse free propagator, and the self energy

$$\Sigma(\omega) = \begin{pmatrix} W_{\uparrow\uparrow}^{--}(\omega) & W_{\uparrow\uparrow}^{-\downarrow}(\omega) & W_{\uparrow\uparrow}^{-\downarrow}(\omega) & W_{\uparrow\uparrow}^{-+}(\omega) \\ W_{\uparrow\uparrow}^{\downarrow-}(\omega) & W_{\uparrow\uparrow}^{\downarrow\downarrow}(\omega) & W_{\uparrow\uparrow}^{\downarrow\downarrow}(\omega) & W_{\uparrow\uparrow}^{\downarrow+}(\omega) \\ W_{\uparrow\uparrow}^{\downarrow-}(\omega) & W_{\uparrow\uparrow}^{\downarrow\downarrow}(\omega) & W_{\uparrow\uparrow}^{\downarrow\downarrow}(\omega) & W_{\uparrow\uparrow}^{\downarrow+}(\omega) \\ W_{\uparrow\uparrow}^{+-}(\omega) & W_{\uparrow\uparrow}^{+\downarrow}(\omega) & W_{\uparrow\uparrow}^{+\downarrow}(\omega) & W_{\uparrow\uparrow}^{++}(\omega) \end{pmatrix} \quad (5.18)$$

is given by the generalized rates  $W_{\chi_2\chi_2'}^{\chi_1\chi_1'}(\omega)$  that contain a left-going external line with energy  $\omega$ .

We solve Eq. (5.16) for the full propagator to obtain

$$\Pi(\omega) = \left[ \left(\Pi^{(0)}(\omega)\right)^{-1} - \Sigma(\omega) \right]^{-1}. \quad (5.19)$$

The excitation energies of the proximized dot are probed by the external energy  $\omega$  and they are given by the real poles of the full propagator. As mentioned above, we approximate the self-energy  $\Sigma(\omega)$  by including only diagrams that contain a single superconducting tunneling line or one cross vertex, in addition to the external line of

## 5 Renormalization effects in interacting quantum dots

---

energy  $\omega$ , see Fig. 5.7. In Appendix B we exemplarily show how the rate  $W_{\uparrow\uparrow}^{--}(\omega)$  is calculated.

Although the resummation scheme does not define a controlled approximation, its results are with a few limitations quantitatively accurate, as we discuss in the following. It is clear that, by construction, the  $\Delta \rightarrow \infty$  limit is reproduced exactly. Also for the noninteracting case,  $U = 0$ , the resummation approach yields the exact solution. As an artifact, however, the resummation scheme produces for  $U = 0$  two extra, unphysical, solutions in addition to the two correct ones shown in Fig. 5.6.

The most interesting regime, however, is the case of finite  $U$  and finite  $\Delta$ . Results obtained from the resummation approach for different values of  $\Gamma_S$  and  $U$  are presented in Fig. 5.8 as solid (blue) curves. Depending on the values of the parameters of the model, we find either two or four solutions. The ABSs are renormalized as compared to the  $\Delta \rightarrow \infty$  solution. The sign of the renormalization agrees with the prediction of the  $1/\Delta$  expansion of Sec. 5.2.1. For comparison, we also show the results from HF as dashed (black) lines. While qualitatively similar, there are substantial quantitative deviations. First, HF seems to underestimate the renormalization of the ABSs. Second, the position of the crossing points of the ABS energies in the resummation scheme is shifted as compared to the HF and the  $\Delta \rightarrow \infty$  result, see Fig. 5.8(c).

A reliable quality check of the proposed approximation, however, is only given by the comparison with the full NRG results.<sup>34</sup> We find a remarkably good agreement between NRG data, dotted (red) lines in Fig. 5.8, and resummation approach. The ABS spectrum is quantitatively reproduced in almost the entire parameter space. The main difference is that the resummation scheme sometimes yields four solutions when NRG only predicts two. Furthermore, sometimes the resummation approach produces solutions with finite imaginary part. Since the ABSs in the absence of coupling to a normal reservoir are sharp due to the gap in the quasiparticle spectrum, these solutions are discarded. This gives rise to the small gaps in the solid (blue) line in Fig. 5.8(a) and (b). Both features (extra pair of solutions and poles with finite imaginary part) are artifacts of the approximation employed.

### 5.3 Beyond weak coupling to the normal lead

In the previous section we have discussed how a finite superconducting gap in the leads renormalizes the ABSs of a quantum dot weakly tunnel-coupled to a normal lead. Now, we want to address the influence of the tunnel coupling to the normal lead beyond the weak-coupling limit. For this, we go back to  $\Delta \rightarrow \infty$  but include next-to-leading order corrections in  $\Gamma_N$ . To distinguish the contributions of different order in  $\Gamma_N$ , we introduce in the following an index ( $n$ ) for  $n$ -th order. We study the Josephson and the Andreev current as well as the average charge of the quantum dot. Within a perturbation expansion, they start to zeroth, first, and zeroth order, respectively, i.e., the next-to-leading order corrections are of first, second, and first order, respectively. To evaluate them we have to include diagrams with two tunneling lines from the normal lead. This increases the number of diagrams considerably and we generate and evaluate them by means of a computer code.

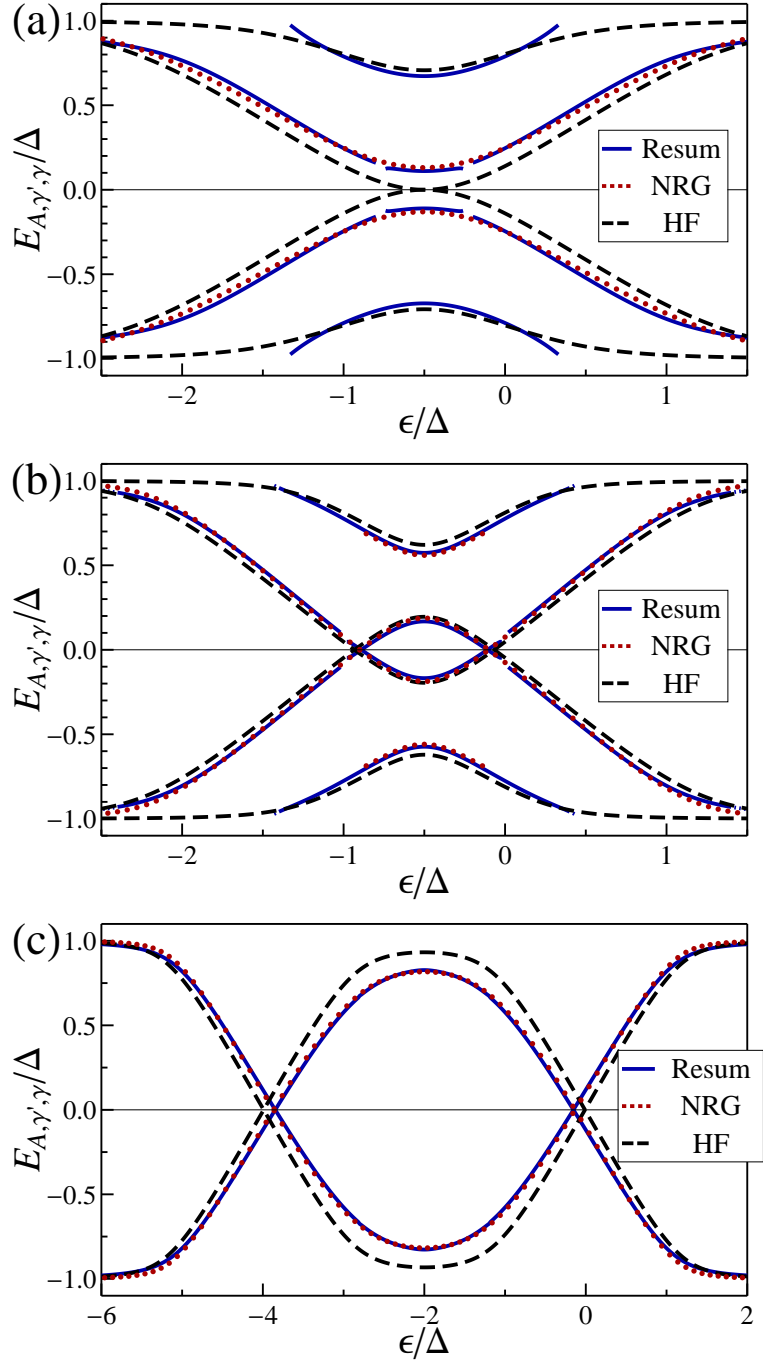


Figure 5.8: (Color online) Plot of the Andreev-bound states from the resummation approach, NRG,<sup>34</sup> and the Hartree-Fock approximation as a function of the level position  $\epsilon$  for (a)  $U = \Delta$  and  $\Gamma_S = 0.5\Delta$ , (b)  $U = \Delta$  and  $\Gamma_S = 0.2\Delta$ , and (c)  $U = 4\Delta$  and  $\Gamma_S = 0.2\Delta$ .

## 5 Renormalization effects in interacting quantum dots

---

It is natural for a systematic perturbation expansion in a small parameter that higher-order corrections are quantitatively small. Therefore, we focus, in the following, on qualitative features that appear in the region close to the point of zero detuning  $\delta = 2\epsilon + U = 0$  when going beyond the weak-coupling limit. Around zero detuning, the weights of the states  $|0\rangle$  and  $|d\rangle$  entering the coherent superpositions  $|\pm\rangle$  become equal, indicating a large proximization of the quantum dot. For bias voltages large enough such that the quantum dot has a finite probability to be either empty or doubly occupied, Josephson and Andreev currents set in.

In the regime of large bias voltage, the Josephson current changes sign as function of the quantum dot's level position  $\epsilon$ . This indicates a transition from a 0- to a  $\pi$ -junction behavior. In the limit  $\Delta \rightarrow \infty$  and weak tunnel coupling to the normal lead,<sup>23</sup> this 0 –  $\pi$  transition happens exactly at zero detuning,  $\epsilon = -U/2$ , and then bends when the bias voltage approaches the highest ABS, see Fig. 5.3. When including the next-order correction in  $\Gamma_N$ , the position of this 0 –  $\pi$  transition becomes renormalized, Fig. 5.9 (a). The origin of this renormalization can be understood in terms of an effective, tunnel-coupling induced field that acts on the isospin introduced in Eq. (5.7). A finite bias voltage leads to the generation of the  $z$ -component of the isospin. The tunnel coupling to the superconductors leads to an effective field along the  $x$ -direction. This causes the isospin to rotate and acquire a finite  $y$ -component. According to Eq. (5.10), however, a finite  $x$ -component of the isospin is needed for a Josephson current. This is accomplished with an additional finite  $z$ -component of the effective field. To lowest order, this component is given by the detuning,  $B_z^{(0)} = \delta$ , which explains the position of the 0 –  $\pi$  transition in Fig. 5.3. The next-order correction,  $B_z^{(1)}$ , renormalizes this position.

We remark that this renormalization of the 0 –  $\pi$  transition has already been predicted in Ref. 22, in which the tunnel couplings to both the superconductors and the normal leads as well as the detuning  $\delta$  have been simultaneously treated as small parameters, i.e., the systematic perturbation expansion included already both  $B_z^{(0)}$  and  $B_z^{(1)}$ . On the other hand, the formation of ABSs could not be treated in that expansion. In Ref. 23, on the other hand, no constraints were put on  $\Gamma_S$  and  $\delta$ , i.e., the ABSs could be described, but the renormalization  $B_z^{(1)}$  did not contribute to lowest order in  $\Gamma_N$ . Only the present calculation, with arbitrary  $\Gamma_S$  and  $\delta$  and next-to-leading order on  $\Gamma_N$  enables us to address both the ABSs and the renormalization of the position of the 0 –  $\pi$  transition.

While the Josephson current changes sign at small detuning, the Andreev current becomes extremal as a function of  $\epsilon$ , see Fig. 5.4. In Fig. 5.9 (b) we show the position of this extremum in the  $\epsilon$ - $\mu_N$ -plane. (We do not show the position of the extremum in the Coulomb-blockade regime). To lowest order and for large bias voltage, the extremum is at zero detuning. The next-order correction, however, leads to a renormalization of this position, for the same reason as the renormalization of the 0 –  $\pi$  transition in the Josephson current.

Finally, we address the average quantum dot charge  $Q$ , which is related to the  $z$ -component of the isospin via  $Q = -e(1 + 2I_z)$ . Again, we focus on the region of small detuning where the proximity effect is most pronounced. In the Coulomb-blockade

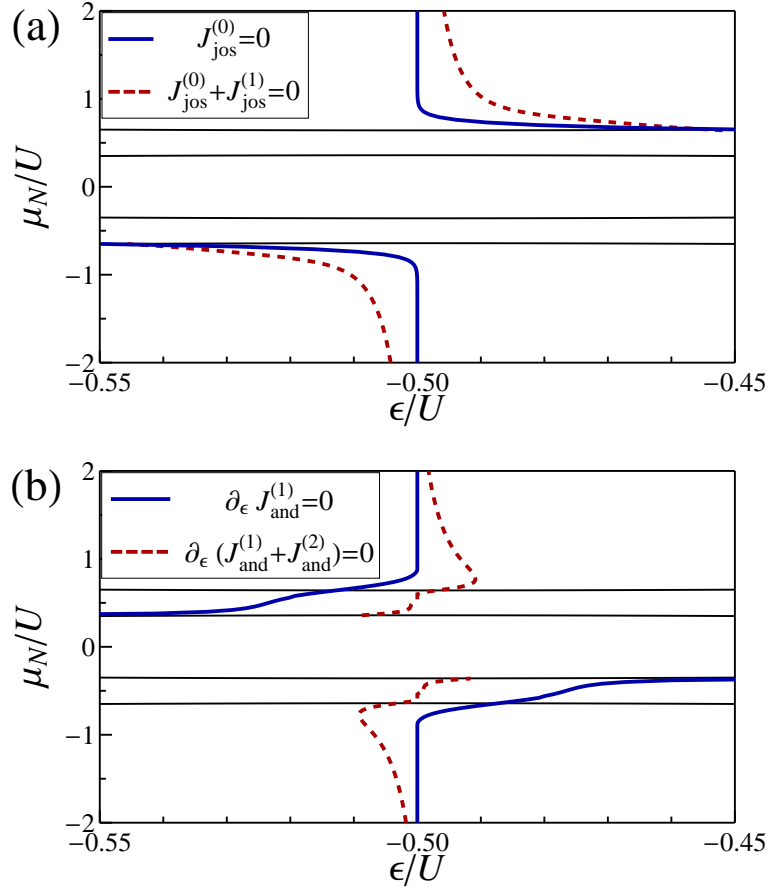


Figure 5.9: (Color online) Plot of (a) the position of the  $0 - \pi$  transition of the Josephson current and (b) the extreme values of the Andreev current. The chosen parameters are  $k_B T/U = 0.05$ ,  $\Gamma_N/U = 0.05$ ,  $\Gamma_S/U = 0.2$ , and  $\Phi = \pi/2$ . The thin black lines show the position of the ABS.

## 5 Renormalization effects in interacting quantum dots

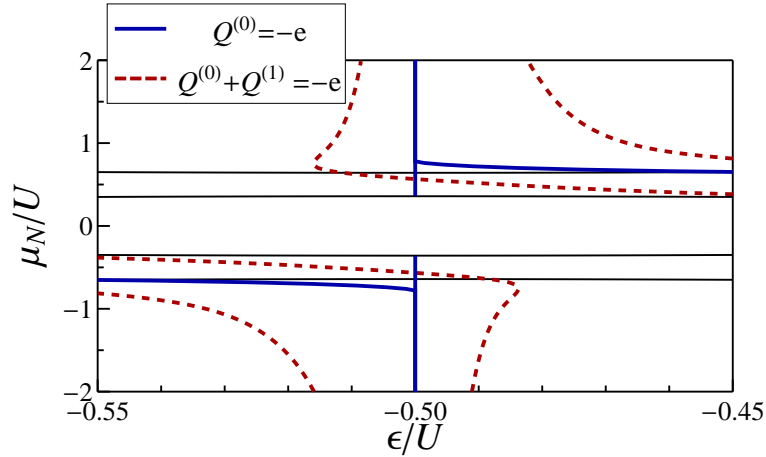


Figure 5.10: (Color online) Plot of the average dot charge. The chosen parameters are  $k_B T/U = 0.05$ ,  $\Gamma_N/U = 0.05$ ,  $\Gamma_S/U = 0.2$ , and  $\Phi = \pi/2$ .

regime (at small bias voltage), the dot is preferably singly occupied,  $Q = -e$ . A larger bias voltage has the tendency to inject a second electron into the quantum dot. Superconducting correlations, however, mix the states of empty and double occupation and, thus, reduce the average number of electrons. For zero detuning  $\delta$  and to zeroth order in  $\Gamma_N$ , the charge  $Q$  remains  $-e$  even for large bias voltage. Only when increasing  $|\delta|$  the number of charges increases above 1. In the intermediate-bias regime for finite detuning values the average charge tends towards 0 or  $-2e$ , depending on the sign of the detuning. This effect can easily be understood by looking at the eigenstates  $|\pm\rangle$ : in the intermediate-bias regime for positive values of  $\mu_N$ , i.e.  $E_{A,+,-} < \mu_N < E_{A,+,+}$ , the state  $|-\rangle$  can already be excited while state  $|+\rangle$  is still inaccessible. From the definition of state  $|-\rangle$  it follows that a positive (negative) detuning causes the weight of the zero component to dominate over (be dominated by) the double component resulting in a decrease (increase) of the average number of electrons.

In Fig. 5.10 we show the position of  $Q/(-e) = 1$ , or equivalently  $I_z = 0$ , for both zeroth and first order. (We do not plot the position in the Coulomb-blockade regime.) As discussed above, the position of  $Q^{(0)}/(-e) = 1$  is at zero detuning in the large-bias regime and splits in the intermediate-bias regime, with  $Q^{(0)}/(-e) < 1$  between and  $Q^{(0)}/(-e) > 1$  outside the two lines. When including the next-order correction, the situation changes. Now, the line of  $[Q^{(0)} + Q^{(1)}]/(-e) = 1$  is split even for the large-bias regime, opening a region with  $[Q^{(0)} + Q^{(1)}]/(-e) < 1$  in between. To understand this, we analyze  $I_z$  at zero detuning,  $\delta = 0$ . Solving the generalized master equation<sup>1</sup> immediately yields<sup>23</sup>  $I_z^{(0)}(\delta = 0) = 0$  and  $I_z^{(1)}(\delta = 0) = -A_y^{(1)}/B_x^{(0)}$ , where  $B_x^{(0)} = 2|\chi|$

<sup>1</sup>Please note that in Ref. 23  $A_y^{(1)}$  has mistakenly been taken to be zero. For Ref. 23 this error has no influence on the results because all investigated quantities have been independent of  $A_y^{(1)}$ .

and

$$\begin{aligned} A_y^{(1)} &= \frac{1}{4} \text{Im} \left[ W_{+-}^{--(1)} + W_{++}^{-+(1)} + W_{--}^{+- (1)} + W_{-+}^{++(1)} \right], \\ &= \frac{\Gamma_N}{4\pi} \sqrt{1 - \frac{\delta^2}{4\epsilon_A^2}} \sum_{\gamma, \gamma' = \pm} \text{Re} \left[ \psi \left( \frac{1}{2} + i \frac{E_{A, \gamma', \gamma} - \mu_N}{2\pi k_B T} \right) \right]. \end{aligned}$$

Here  $W_{\chi_1 \chi_2}^{\chi_1' \chi_2' (1)}$  are generalized rates in first order in  $\Gamma_N$  and  $\psi(x)$  is the digamma function. It is, thus, the isospin generation term  $A_y^{(1)}$ , describing combined Andreev processes that involve both the normal and the superconducting leads, which reduce  $Q/(-e)$  below 1.

## 5.4 Conclusions

The theoretical description of sub-gap (Josephson and Andreev) transport through quantum dots with strong Coulomb interaction coupled to normal and superconducting leads simplifies substantially in the limit of infinitely-large superconducting gap  $\Delta$  and weak tunnel coupling  $\Gamma_N$  to the normal lead. For experimental devices with finite  $\Delta$  and larger  $\Gamma_N$  these calculations may still be used as an approximation. The assessment of the quality of this approximation to describe sub-gap transport has been the focus of this chapter. In particular we came to the following conclusions. The positions of the ABSs strongly depend on  $\Delta$ , i.e., a  $\Delta \rightarrow \infty$  approximation is insufficient. These ABSs define threshold voltages in the current-voltage characteristics at which new transport channels open. The numerical values for the Josephson and Andreev current between these threshold voltages, however, seem to be nicely approximated by the  $\Delta \rightarrow \infty$  limit.

Similarly, we find that the next-to-leading order correction in the tunnel coupling  $\Gamma_N$  to the normal lead mainly yields small quantitative corrections. But there are also qualitative differences: the position of the  $0 - \pi$  transition in the Josephson current and the peak positions in the Andreev current are shifted.

In conclusion, we find that the  $\Delta \rightarrow \infty$  and weak-coupling calculations provide a very good approximation for sub-gap transport with the limitation that the positions of the ABSs for finite  $\Delta$  are not properly described. To address the latter, we proposed a resummation approach that substantially improves over mean-field treatments and favorably compares with more elaborate NRG calculations.



## 6 Band-mixing-mediated Andreev reflection of semiconductor holes

In all previous result chapters we have focused on the case that the normal conducting leads all have metallic character. This allowed us to neglect the influence of the band structure on the investigated transport properties. The aim of this chapter is to explore Andreev reflections in a system where the normal conducting region is a semiconductor so that the band structure cannot be neglected.

Mesoscopic superconductivity has developed strongly over recent years.<sup>117–122</sup> Starting from the early theoretical studies of superconductor–normal-metal (S-N) interfaces,<sup>46,47</sup> the interplay of pair correlations and quantum transport in phase-coherent conductors has attracted a lot of interest.<sup>117–120</sup> As the charge carriers’ mean free path can be much longer in semiconductors than it typically is in metals, hybrid structures of semiconductor materials are ideal for investigating the regime of ballistic transport.<sup>121,123</sup> Most recently, opportunities for realizing quantum-logical circuits and investigating fundamentals of quantum physics in these systems have been explored.<sup>122</sup>

In most previous studies, the band electrons in the normal-conducting part of S-N hybrid systems were simple in the sense that their properties could be modeled using quantum states of free spin-1/2 particles. In the fundamentally interesting and practically relevant<sup>124</sup> situation where the normal carriers are from the valence band, their electronic and spin properties are much richer.<sup>125,126</sup> States in the upper-most valence bands of common semiconductor materials carry a spin-3/2 degree of freedom and also exhibit a strong coupling between this larger spin and their orbital motion. In our work presented here, we address the question how these peculiar features that have been seen to result in interesting mesoscopic-transport effects<sup>127–132</sup> will affect the physical properties of p-type semiconductor–superconductor hybrid systems.

Many of the interesting phenomena exhibited by S-N structures are fundamentally due to the process of Andreev reflection,<sup>46,47</sup> which is the conversion of a charge carrier incident on the interface from the normal side into its charge-conjugated and time-reversed copy. This counter-intuitive effect fundamentally results from the fact that the two electrons forming a Cooper pair in the superconducting condensate are from time-reversed states.<sup>36</sup> A superconductor in close proximity to a normal conductor induces pair correlations between such states also on the normal side of the hybrid system. As a result, a charge carrier with energy below the gap for quasiparticle excitations in the superconductor can, upon incidence on the S-N interface, combine with its appropriate partner to enter the superconducting side as a Cooper pair. In the process, the normal conductor is left with a missing carrier, usually referred to as a “hole”, that has all attributes of the time-reversed partner of the incident particle. As this “hole” is really a quasiparticle excitation of the Fermi sea of nearly-free band

## 6 Band-mixing-mediated Andreev reflection of semiconductor holes

---

electrons in the normal conductor, we avoid this nomenclature here and reserve the term “hole” to always refer to a state in the valence band of the semiconductor material making up the normal-conducting part of the hybrid structure.

Based on the Bogoliubov-de Gennes formalism,<sup>36</sup> a theory for scattering at non-ideal S-N interfaces was developed by Blonder, Tinkham, and Klapwijk<sup>35</sup> (BTK). Later works have generalized this approach to describe oblique incidences of the charge carrier from the normal side<sup>133–135</sup> and to discuss the case of small values of Fermi energies typically realized in semiconductors.<sup>136</sup> It turns out that a finite angle of incidence (measured with respect to the interface normal) reduces the probability of Andreev reflection, and a critical angle exists above which no Andreev reflection is possible in a semiconductor. The BTK model has also been adapted to situations without spin-rotational symmetry, e.g., when the normal-conducting side of the hybrid system is ferromagnetic.<sup>137–142</sup> In the extreme case of a half-metallic ferromagnet where only one spin-polarized band contributes to transport and pairing seems to be impossible, spin-flip processes still enable Andreev reflections.<sup>140,142</sup>

In the present work, we incorporate a  $6 \times 6$  Kane-type Hamiltonian<sup>126</sup> into the Bogoliubov-de Gennes theory to model a hybrid p-type semiconductor/superconductor structure. States in the lowest conduction and uppermost (heavy-hole and light-hole) valence bands are included, as is the coupling between them. We focus on the situation where the chemical potential lies in the valence band of the semiconducting side and calculate the normal and Andreev-reflection probabilities when either light holes or heavy holes are incident at an angle on the interface. In general, states from the superconductor’s conduction band will be incompatible with those from the semiconductor’s valence band due to their different orbital character and no direct coupling will be possible. Nevertheless, we find that the mixing between valence- and conduction-band states in the semiconductor mediates a coupling to the superconducting pair potential and thus enables Andreev reflection of holes. Even the valence-band states with spin projection  $\pm 3/2$  (heavy holes) can have a finite probability to be Andreev-reflected, even though the pair potential in the superconductor is between states having spin projection  $\pm 1/2$ . The wave-vector dependence of band mixing is reflected in the variation of the Andreev-reflection amplitudes as a function of the holes’ angle of incidence onto the S-N interface.

The remainder of this chapter is organized as follows: we introduce our model for a p-type-semiconductor/superconductor hybrid structure and discuss its relevant physical parameters in the following Section 6.1. Results for normal and Andreev-reflection probabilities for different scenarios of incident heavy-hole and light-hole carriers are presented in Sec. 6.2. A summary and conclusions of our work are given in the final Section 6.3.

The contents of this chapter have been published in Ref. 143.

### 6.1 Model

We consider a hybrid p-type semiconductor/superconductor structure with an ideal interface. To calculate the transport properties of the system, we solve the Bogoliubov-

De Gennes equation with the single-particle Hamiltonians on the normal conducting and superconducting side formulated in Nambu space. In order to avoid confusions with valence-band carriers we do not use the term “Nambu-hole”. Instead, we will address the corresponding states as “time-reversed” states, indicated by a “tilde”, so that solely valence-band carriers are referred to as “holes”. The relevant Hamiltonians will be invariant under time reversal,  $\hat{H} = \Theta \hat{H} \Theta^{-1}$ , where  $\Theta$  is the time-reversal operator, thus  $\langle \tilde{\alpha} | \hat{H} | \tilde{\beta} \rangle = \langle \beta | \hat{H} | \alpha \rangle$  holds.

We model the semiconductor using a  $6 \times 6$  Kane-Hamiltonian<sup>126</sup> within the spherical approximation in the basis of the  $k = 0$ -band-edge states  $\{|\frac{1}{2} \frac{1}{2}\rangle_c, |\frac{1}{2} -\frac{1}{2}\rangle_c, |\frac{3}{2} \frac{3}{2}\rangle_v, |\frac{3}{2} \frac{1}{2}\rangle_v, |\frac{3}{2} -\frac{1}{2}\rangle_v, |\frac{3}{2} -\frac{3}{2}\rangle_v\}$ , representing conduction electrons, heavy holes, and light holes, respectively, and the corresponding time-reversed states, so that we get

$$H^N = \begin{pmatrix} H_0^{6c6c} & H_0^{6c8v} & & \mathbf{0} \\ H_0^{8v6c} & H_0^{8v8v} & & \\ & \mathbf{0} & -(H_0^{6c6c})^T & -(H_0^{8v6c})^T \\ & & -(H_0^{6c8v})^T & -(H_0^{8v8v})^T \end{pmatrix}, \quad (6.1)$$

with

$$H_0^{6c6c} = \begin{pmatrix} \frac{\hbar^2 k^2}{2m'} + E_F^N + E_0 & 0 \\ 0 & \frac{\hbar^2 k^2}{2m'} + E_F^N + E_0 \end{pmatrix}, \quad (6.2a)$$



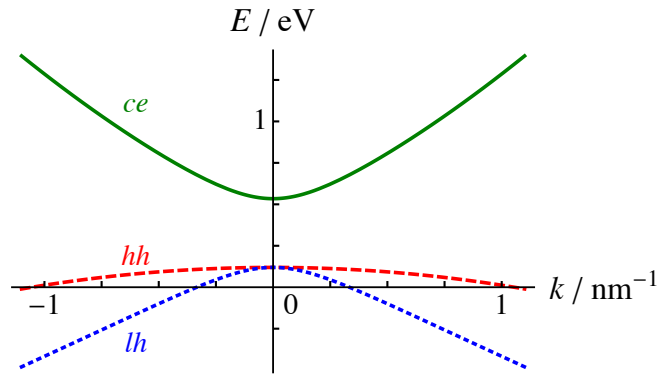


Figure 6.1: (Color online) Schematic dispersions of conduction electrons (*ce*), heavy holes (*hh*) and light holes (*lh*).

$$\begin{aligned}
 H_0^{6c8v} &= (H_0^{8v6c})^\dagger \\
 &= \begin{pmatrix} -\frac{1}{\sqrt{2}}Pk_+ & \sqrt{\frac{2}{3}}Pk_z & \frac{1}{\sqrt{6}}Pk_- & 0 \\ 0 & -\frac{1}{\sqrt{6}}Pk_+ & \sqrt{\frac{2}{3}}Pk_z & \frac{1}{\sqrt{2}}Pk_- \end{pmatrix}, \quad (6.2c)
 \end{aligned}$$

and  $\mathbf{0}$  being the zero matrix of the appropriate dimensions. The spherical approximation implies that the terms arising from bulk inversion asymmetry can be neglected and that  $\gamma'_1 \rightarrow \gamma_1 - \frac{1}{3} \frac{2m_0}{\hbar^2} \frac{P^2}{E_0}$  and  $\gamma'_{2,3} \rightarrow \frac{2\gamma_2 + 3\gamma_3}{5} - \frac{1}{6} \frac{2m_0}{\hbar^2} \frac{P^2}{E_0}$ . We have used the abbreviations  $m' = m_0 \left( \frac{m_0}{m^*} - \frac{2}{3} \frac{2m_0}{\hbar^2} \frac{P^2}{E_0} \right)^{-1}$ , where  $m^*$  is the effective mass of conduction band electrons,  $k^2 = k_x^2 + k_y^2 + k_z^2$ ,  $k_\pm = k_x \pm ik_y$ , and  $\hat{K} = k_x^2 - k_y^2$ . The Fermi energy of the semiconductor is  $E_F^N$ ,  $E_0$  is the energy gap between conduction band and valence bands,  $P$  is the coupling parameter between the conduction band and the valence band and  $\gamma_{1,2,3}$  are parameters generating the effective masses in the valence band. Figure 6.1 schematically shows the dispersion resulting from the  $6 \times 6$  Kane-Hamiltonian, exemplarily calculated with the parameters of InAs, which will be discussed in more detail in Sec. 6.2, and a Fermi energy of  $E_F^N = 110\text{meV}$  corresponding to a carrier concentration  $n$  of  $n = 10^{20}\text{cm}^{-3}$ .

In the superconductor we assume the gap between the conduction band and the valence bands to be very large, so that valence-band states of the superconductor are irrelevant. In order to be able to match the wave function in the superconductor with the wave function in the semiconductor, we write  $H^S$  also in the  $12 \times 12$ -basis of the  $k = 0$ -band-edge states and shift the valence bands in the superconductor to minus infinity. Then the Hamiltonian  $H^S$  of the superconductor is given by

$$H^S = \begin{pmatrix} H_0^S & \mathbf{0} & \Delta \cdot \mathbf{I}_{2 \times 2} & \mathbf{0} \\ \mathbf{0} & -\infty \cdot \mathbf{I}_{4 \times 4} & \mathbf{0} & \mathbf{0} \\ \Delta^* \cdot \mathbf{I}_{2 \times 2} & \mathbf{0} & -(H_0^S)^T & \mathbf{0} \\ \mathbf{0} & \mathbf{0} & \mathbf{0} & -\infty \cdot \mathbf{I}_{4 \times 4} \end{pmatrix}, \quad (6.3)$$

## 6 Band-mixing-mediated Andreev reflection of semiconductor holes

where

$$H_0^S = \begin{pmatrix} \frac{\hbar^2 k^2}{2m_S} - E_F^S & 0 \\ 0 & \frac{\hbar^2 k^2}{2m_S} - E_F^S \end{pmatrix}, \quad (6.4)$$

with  $\mathbf{I}_{n \times n}$  being the identity matrix in  $n$  dimensions,  $m_S$  being the effective mass of the superconductor and  $E_F^S$  its Fermi energy. Without loss of generality, we choose the superconducting order parameter  $\Delta = \Delta_0$  to be real. It follows from Eq. (6.3) that only states of the semiconductor with non-zero  $|\frac{1}{2} \pm \frac{1}{2}\rangle_c$ -component couple to the superconductor. In the following we consider either the injection of a light hole, abbreviated by  $lh$ , or the injection of a heavy hole, abbreviated by  $hh$ , from the semiconducting side. For oblique reflections it is sufficient to consider all particles to move in a plane, which we choose to be the x-y-plane. This choice block-diagonalizes the Kane-Hamiltonian and thus, reduces the full Bogoliubov-de Gennes Hamiltonian from  $12 \times 12$  to  $6 \times 6$ . We assume the N-S interface to be in the y-z-plane at  $x = 0$ . For an injected light hole,  $\xi = lh$ , (heavy hole,  $\xi = hh$ ) in the semiconductor we make the following Ansatz:

$$\begin{aligned} \psi_\xi(\mathbf{x}) = & \frac{1}{\sqrt{|v_\xi(k_\xi^i)|}} \mathbf{u}_\xi(k_\xi^i) e^{ik_{\xi,\perp}^i x_\perp + ik_\parallel x_\parallel} \\ & + \sum_\chi \frac{r_{\chi/\xi}}{\sqrt{|v_\chi(k_\chi^r)|}} \mathbf{u}_\chi(k_\chi^r) e^{ik_{\chi,\perp}^r x_\perp + ik_\parallel x_\parallel}, \end{aligned} \quad (6.5)$$

where  $x_\perp$  ( $x_\parallel$ ) is the component perpendicular (parallel) to the junction,  $\mathbf{u}_\chi(k)$  is the eigenvector corresponding to state  $\chi$  and momentum  $k$  and  $v_\chi(k) = \mathbf{u}_\chi(k)^T \hat{v}_\perp \mathbf{u}_\chi(k)$ , with  $\hat{v}_\perp = \frac{i}{\hbar} [H, \mathbf{x}_\perp]$ , denotes the velocity perpendicular to the junction. The reflection coefficient, describing the reflection amplitude from state  $\xi$  into state  $\chi$  is labeled  $r_{\chi/\xi}$ . The index  $\chi \in \{ce, hh, lh, \tilde{c}\tilde{e}, \tilde{h}\tilde{h}, \tilde{l}\tilde{h}\}$  denotes a combination of the band (conduction band, heavy-holes band, light-holes band) and the Nambu-state (non-time-reversed, time-reversed). Due to the fact that in scattering processes the momentum parallel to the interface needs to be conserved, all parts of the wave function have the same momentum parallel to the scattering interface,  $k_\parallel$ . With  $k_\parallel$  and  $k_{\xi,\perp}^i$  ( $k_{\chi,\perp}^r$ ) the angle  $\theta$  of the injected (reflected) particle is determined, where  $\theta = 0$  corresponds to the case of normal incidence. Note, that we explicitly allow for a conversion between conduction electrons, light holes, and heavy holes, i.e. we allow for light holes to be normal reflected as heavy holes and conduction electrons, and Andreev reflected as heavy holes and conduction electrons and analogously, we allow for heavy holes to be normal reflected as light holes and conduction electrons and Andreev reflected as light holes and conduction electrons. Since the semiconductor's conduction band lies above the Fermi energy, only evanescent conduction-electron modes exist. But nevertheless, these modes are important for matching the wave functions at the boundary.

We restrict ourselves to excitation energies inside the superconducting gap,  $|E| < \Delta_0$ , which implies that only evanescent quasiparticle-wave functions exist in the superconductor. For the wave function in the superconductor we set

$$\psi_S(\mathbf{x}) = \frac{c_{ce}}{\sqrt{\text{Re}[q_{ce}]}} \begin{pmatrix} \gamma^* \\ 0 \\ 0 \\ \gamma \\ 0 \\ 0 \end{pmatrix} e^{iq_{ce,\perp}x_\perp + ik_{\parallel}x_{\parallel}} + \frac{c_{\bar{c}\bar{e}}}{\sqrt{\text{Re}[q_{\bar{c}\bar{e}}]}} \begin{pmatrix} \gamma \\ 0 \\ 0 \\ \gamma^* \\ 0 \\ 0 \end{pmatrix} e^{iq_{\bar{c}\bar{e},\perp}x_\perp + ik_{\parallel}x_{\parallel}}, \quad (6.6)$$

with

$$\gamma = \exp \left[ -\frac{i}{2} \arccos \left( \frac{E}{\Delta_0} \right) \right], \quad (6.7)$$

where  $c_{ce}$  and  $c_{\bar{c}\bar{e}}$  are transmission coefficients and  $q_{ce}$  ( $q_{\bar{c}\bar{e}}$ ) is the complex wave vector of the (time-reversed) evanescent quasiparticle wave function.

At the junction the wave function and the velocity need to be continuous:

$$\psi_N(x_\perp = 0) = \psi_S(x_\perp = 0) \quad (6.8)$$

$$\hat{v}_\perp \psi_N(x_\perp = 0) = \hat{v}_\perp \psi_S(x_\perp = 0), \quad (6.9)$$

with  $\psi_N$  being  $\psi_{lh}$  or  $\psi_{hh}$ , respectively.

## 6.2 Results

The results shown in this section have been calculated for InAs-Al. InAs is a commonly used material that meets the requirements of a large mixing between conduction band and valence bands, described by a large value of  $P$  and a small energy gap  $E_0$  between conduction band and valence bands as well as a large spin-orbit coupling so that the spin split-off band can be neglected and Al is often used by experimentalists as a superconducting material. We use the band structure parameters for InAs given in Ref. 126, which are  $E_0 = 0.418$  eV,  $P = 9.197$  eVÅ,  $m^* = 0.0229 m_0$ ,  $\gamma_1 = 20.40$ ,  $\gamma_2 = 8.30$ , and  $\gamma_3 = 9.10$ . Typical carrier concentrations  $n$  of p-type InAs range from about  $10^{16}$  cm $^{-3}$  up to about  $10^{20}$  cm $^{-3}$ . This corresponds to Fermi energies ranging from about 0.2 meV up to about 120 meV. For Al we set  $m_S = m_0$  and  $E_F^S = 11.63$  eV.

It follows from Eqs. (6.2) that all semiconductor states with  $k = 0$  are orthogonal to each other. This implies that the valence-band states at  $k = 0$  are orthogonal to the ( $k = 0$ ) conduction-band states  $|\frac{1}{2} \pm \frac{1}{2}\rangle_c$ . They are, therefore, decoupled from the superconductor and Andreev reflections are not possible. Only valence-band states with finite momentum  $k$  can have a finite  $|\frac{1}{2} \pm \frac{1}{2}\rangle_c$ -component so that these states can

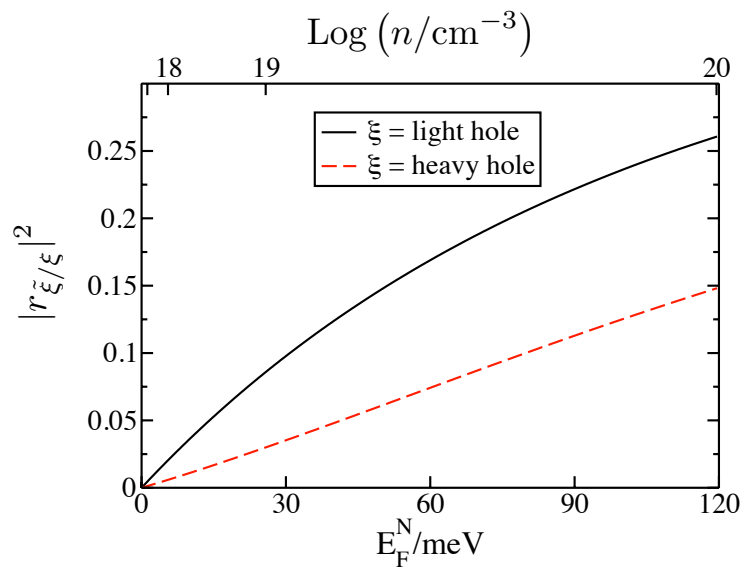


*Figure 6.2:* (Color online) Plot of the conversion-less Andreev-reflection probabilities as a function of the Fermi energy of the semiconductor  $E_F^N$  or the corresponding carrier concentration of the semiconductor. The other parameters are  $\Delta_0 = 0.1$  meV,  $\theta = \pi/8$  and  $E = 0$ .

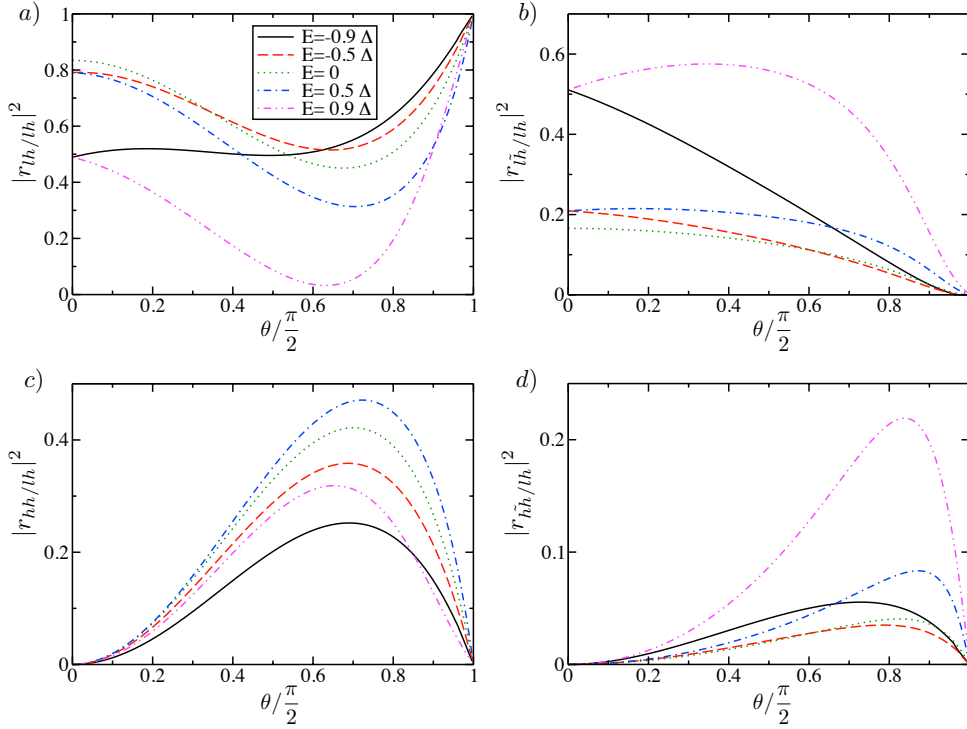


Figure 6.3: (Color online) Plot of the reflection probabilities for an injected light hole as a function of the injection angle  $\theta$  for different excitation energies  $E$ . The other parameters are  $\Delta_0 = 0.1$  meV and  $E_F^N = 53.6$  meV, which corresponds to  $n = 3 \cdot 10^{19} \text{cm}^{-3}$ .

participate in Andreev-reflection processes. At carrier concentrations in the range of  $10^{16} \text{cm}^{-3}$  in the semiconductor the Fermi energy is smaller than 1 meV causing the injected hole to have a small Fermi momentum. In this situation Andreev-reflection probabilities are strongly suppressed, see Fig. 6.2. At larger carrier concentrations the Fermi energy is shifted away from the band edge causing the Fermi momentum to be increased and the probability of Andreev reflection is finite, see Fig. 6.2.

Light holes and heavy holes are distinguished by the projection of their total angular momentum in the direction of motion. If a heavy hole is incident onto a scattering interface at a finite angle with the surface normal, the reflected state would have a different spin-quantization axis and would, therefore, be a mixture of heavy-hole and light-hole components. As a result, it is possible to convert heavy holes into light holes and vice versa in oblique scattering processes. This conversion also occurs in Andreev-reflection processes, so that heavy holes may also be Andreev reflected as light holes and vice versa. For normal incidence, heavy holes are decoupled from light holes and conduction electrons. This can be seen by setting  $k_x$  and  $k_y$  to zero in Eq. (6.1). For

## 6 Band-mixing-mediated Andreev reflection of semiconductor holes

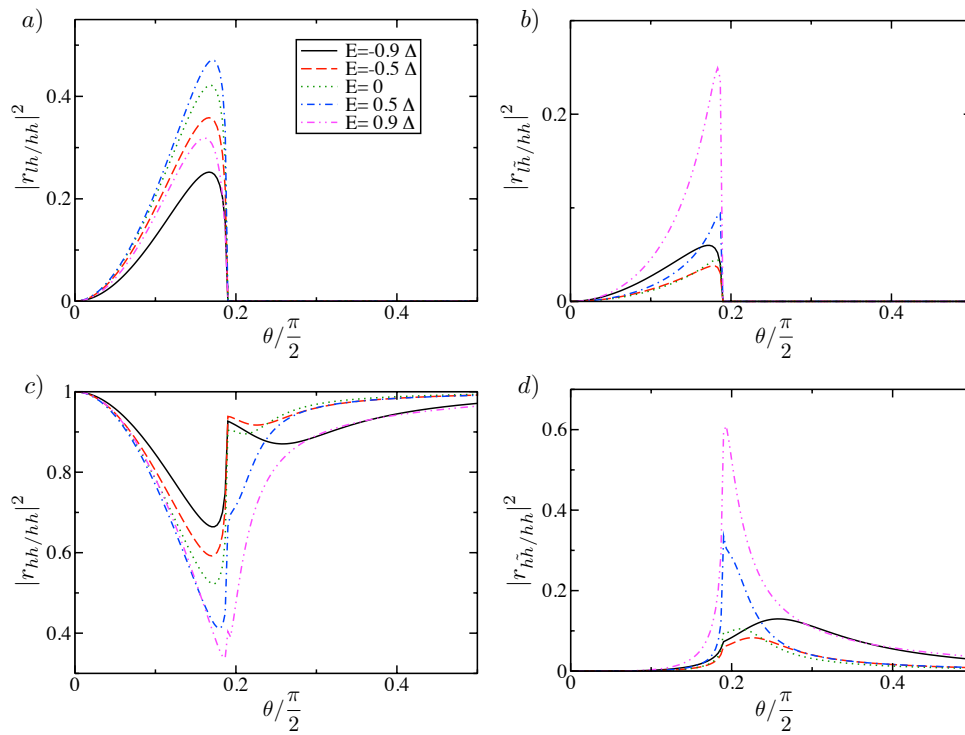


Figure 6.4: (Color online) Plot of the reflection probabilities for an injected heavy hole as a function of the injection angle  $\theta$  for different excitation energies  $E$ . The other parameters are  $\Delta_0 = 0.1$  meV and  $E_F^N = 53.6$  meV, which corresponds to  $n = 3 \cdot 10^{19} \text{cm}^{-3}$ .

perpendicular (and, in principle, also parallel) incidence, the motion of incoming and reflected particles is collinear so that in this case a conversion is not possible and, additionally, for heavy holes it is not possible to be Andreev reflected. This effect is independent of the semiconductor's carrier concentration and independent of the excitation energy of the incident hole. Figures 6.3 and 6.4 show an exemplary sequence of plots of the reflection probabilities of an injected light hole or injected heavy hole, respectively, as a function of the angle of injection for different excitation energies. In general, the conversion between heavy holes and light holes via normal reflection and Andreev reflection is possible but not in the limits of perpendicular incidence ( $\theta = 0$ ) or parallel incidence ( $\theta = \pi/2$ ). For heavy holes also the probability for Andreev reflection without conversion vanishes in these limits, so that we get  $|r_{hh/hh}|^2 = 1$  and  $|r_{\chi/hh}|^2 = 0$ , for  $\chi \neq hh$ . In contrast to Andreev-reflection probabilities of conduction electrons, which in general get reduced by increased angles of injection we find that heavy holes require a non-zero angle of injection to be Andreev reflected.

For perpendicularly incident light holes we are able to derive analytical results in the limit of the Andreev approximation, i.e.  $|E| \ll E_F^{N,S}$  and  $\Delta_0 \ll E_F^{N,S}$ . This is a reasonable assumption as long as the semiconductor is doped such that its Fermi energy is large compared to the pair potential  $\Delta_0$ . The Andreev approximation implies  $q_{ce} \approx -q_{\bar{c}e}$  as well as  $k_{lh}^i \approx -k_{lh}^r \approx k_{lh}^r$  and  $k_{ce}^r \approx k_{\bar{c}e}^r$ . In this limit, we find that the Andreev-reflection probability of light holes is of the BTK form<sup>35</sup>

$$|r_{\bar{l}h/lh}|^2 = \frac{\Delta_0^2}{E^2 + (\Delta_0^2 - E^2)(1 + 2Z^2)^2} \quad , \quad (6.10)$$

with all materials-specific quantities entering into a single interface parameter given by

$$Z = \left[ \frac{\left( \frac{m_S}{m_0} k_{lh}^i - \frac{m'}{m_0} q_{ce} \right)^2 - \left( \frac{m_S}{m_0} + \frac{\hbar^2 k_{lh}^i q_{ce}}{2m_0} \frac{1}{E_F^N + E_0} \right)^2 (k_{ce}^r)^2}{4 \frac{m_S}{m_0} k_{lh}^i q_{ce} \left( \frac{m'}{m_0} + \frac{\hbar^2 (k_{ce}^r)^2}{2m_0} \frac{1}{E_F^N + E_0} \right)} \right]^{\frac{1}{2}}. \quad (6.11)$$

Since no conversion between light holes and heavy holes occurs in the case of normal incidence, we get  $|r_{lh/lh}|^2 = 1 - |r_{\bar{l}h/lh}|^2$ . For energies close to the superconducting gap,  $|E| \rightarrow \Delta_0$ , the probability for Andreev reflection approaches unity,  $|r_{\bar{l}h/lh}|^2 \rightarrow 1$ , i.e. only Andreev reflections take place.

In addition to the above-discussed effects we find two different types of critical angles. On the one hand, a critical angle occurs above which an injected hole cannot be Andreev reflected without conversion, see Fig. 6.5. Furthermore, for an incident heavy hole, there is a critical angle for reflections associated with a conversion to a light hole, see Figs. 6.4 a) and 6.4 b). Both types of critical angle have the same physical origin: the momentum component parallel to a planar interface needs to be conserved in the scattering process. If this parallel component of the incident particle is larger than the total momentum available at a given energy for a particular type of reflected particle, the associated process of reflection is not possible. In contrast to the critical angle of conduction electrons discussed by Mortensen *et al.*,<sup>136</sup> the critical angle for conversion-less Andreev reflection of holes occurs for negative excitation energies (as

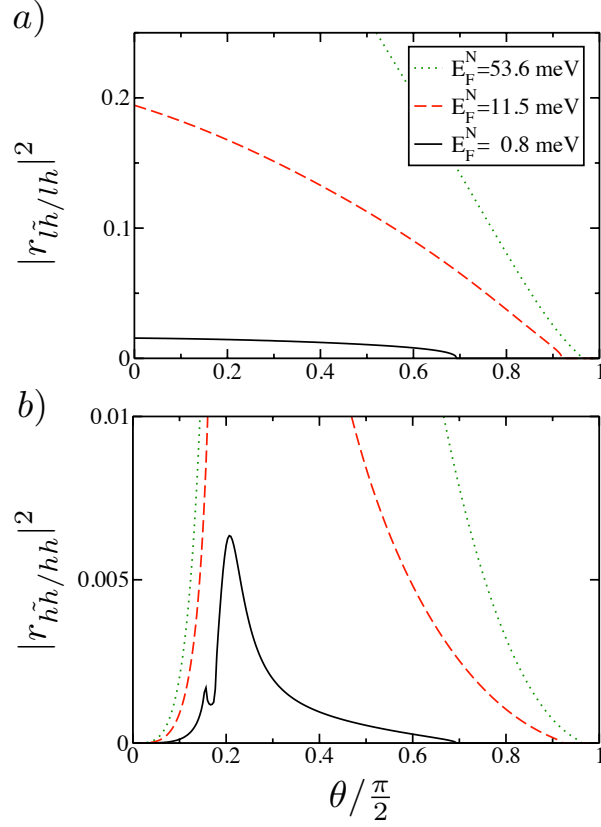


Figure 6.5: (Color online) Plot of the conversion-less Andreev-reflection probabilities as a function of the injection angle  $\theta$  for different Fermi energies of the semiconductor, where  $E_F^N = 53.6$  meV corresponds to  $n = 3 \cdot 10^{19} \text{cm}^{-3}$ ,  $E_F^N = 11.5$  meV corresponds to  $n = 3 \cdot 10^{18} \text{cm}^{-3}$ , and  $E_F^N = 0.8$  meV corresponds to  $n = 5 \cdot 10^{16} \text{cm}^{-3}$ . The other parameters are  $\Delta_0 = 0.1$  meV and  $E = -0.9 \Delta$ .

measured from the Fermi energy of the hole carriers). Due to the shape of the dispersion in the semiconductor, see Fig. 6.1, an injected hole with excitation energy below the Fermi energy has a larger momentum than the corresponding time-reversed hole, thus, a critical angle exists at which the parallel component of the total momentum of the injected light hole (heavy hole) equals the total momentum of the time-reversed light hole (heavy hole):

$$\sin \theta_{cl}^{lh(hh)} = \frac{|k_{\tilde{lh}(\tilde{hh})}|}{|k_{lh(hh)}|}. \quad (6.12)$$

This critical angle requires finite excitation energies (otherwise the injected hole and the reflected time-reversed hole have the same magnitude of the momentum) and is more pronounced for small Fermi energies because then the ratio of  $|k_{\tilde{lh}(\tilde{hh})}|/|k_{lh(hh)}|$  becomes smaller. These considerations are in very good agreement with the plotted results, see Fig. 6.5: the critical angle is visible at negative excitation energies for light holes as well as for heavy holes and has a smaller value for smaller Fermi energies.

The second type of critical angle can also be understood by looking at the semiconductor's dispersion shown in Fig. 6.1. Close to the Fermi energy a heavy hole has a much larger total momentum compared to a light hole of the same energy. Thus, a critical angle exists, at which the parallel component of the total momentum of an injected heavy hole equals the total momentum of the corresponding (time-reversed) light hole:

$$\sin \theta_c^{lh(\tilde{lh})} = \frac{|k_{lh(\tilde{lh})}|}{|k_{hh}|}. \quad (6.13)$$

This critical angle is to a good approximation a constant function of the Fermi energy of the semiconductor and of the excitation energy of the injected hole. In Figures 6.4 a) and 6.4 b) it is clearly seen that the probabilities for a heavy hole to be normal-reflected or Andreev-reflected as light hole vanish nearly independently of the excitation energy at some critical angle.

## 6.3 Conclusions

We have studied reflection of light holes and heavy holes at subgap energies from the interface of a p-type semiconductor with a conventional superconductor. It turns out that Andreev reflection of light holes as well as heavy holes is possible and depends strongly on the angle of incidence and the Fermi energy (i.e., the carrier density) in the semiconductor. In particular, we find that

- (i) light holes as well as heavy holes require a finite coupling to the conduction-band states to experience Andreev reflection and that this coupling can be increased by doping the semiconductor,
- (ii) in the special case of perpendicular incidence, there is no coupling of heavy-hole states to light-hole or conduction-band states. Therefore, heavy holes can only be normal-reflected as heavy holes and the conversion between heavy holes and light holes is impossible, and

## 6 Band-mixing-mediated Andreev reflection of semiconductor holes

---

(iii) critical angles exist for conversion-less Andreev reflection and for the conversion of heavy holes into light holes and time-reversed light holes.

## 7 Conclusions

We have presented a diagrammatic real-time technique that is capable of describing non-equilibrium transport through interacting quantum dots strongly coupled to superconducting leads and weakly coupled to normal and ferromagnetic leads. The hybrid system of a quantum dot strongly coupled to superconducting leads is exactly described by an effective Hamiltonian in the limit of an infinitely-large superconducting gap. The strong proximization of the quantum dot by the superconductors leads to the formation of ABS, which are the excitation energies of the effective Hamiltonian. In contrast to non-proximized dots where only two different biasing schemes are possible (small bias and large bias) for proximized dots additionally the intermediate bias regime occurs, which opens new transport situations.

In a hybrid system composed of an interacting quantum dot coupled to one normal, one ferromagnetic, and one superconducting lead where (1) the superconductor is kept on zero chemical potential, (2) the ferromagnetic lead is in the large bias regime, and (3) the normal lead is in the intermediate bias regime, the possibility of a pure spin current is given. We found that the spin current is proportional to the average spin accumulated on the dot and we gave an analytical expression for the level position required to achieve a pure spin current as a function of both, the tunnel-coupling strength to the superconducting lead and the polarization of the ferromagnetic lead.

Since in real systems the superconducting gap is usually a small parameter we have carried out an expansion of the gap around infinite with the objective of testing the validity of infinite-gap calculations for systems with finite gap. Therefore, we have considered a three terminal setup consisting of a quantum dot coupled to one normal lead and to two superconductors. This setup has the advantage that it allows to study Josephson currents as well as Andreev currents. We calculated the corrections arising from an expansion of the superconducting gap around infinity to these currents and compared the results with the infinite-gap currents. The comparison yielded indications that a finite gap causes a renormalization of the ABS. By means of a resummation approach we estimated the positions of the finite-gap ABS which turned out to be bounded on the interval  $[-\Delta, \Delta]$ . The predicted shape of the finite-gap ABS compares favorably with the NRG data.<sup>33</sup> Despite the renormalization of the ABS the corrected currents and the infinite-gap currents appeared to be very similar. This allowed us to conclude that the infinite-gap calculation is a valuable tool even for calculating finite-gap currents.

In the same three-terminal device we have studied the influence of the normal lead on the proximity effect on the dot. For this purpose we calculated the first corrections arising from the coupling to the normal lead to the leading terms of the Josephson current, the Andreev current, and the average dot charge. We have identified some qualitative changes that occur in the direct vicinity of zero detuning, i.e. a situation

## 7 Conclusions

---

where the superconductors are in resonance with the dot. It turns out that the position of the  $\pi$  transition occurring in the Josephson current and the positions of the extrema of the Andreev current experience a renormalization. In the average dot charge the presence of the normal lead causes an unexpected behavior: for large positive (negative) chemical potentials of the normal lead the average dot charge is reduced (enhanced). This effect is caused by the accumulation term of the isospin's  $y$ -component.

Despite the influence of a finite Coulomb interaction on Andreev transport we have investigated Andreev reflection processes involving valence-band charge carriers. For this purpose we have considered a p-type semiconductor–superconductor interface and calculated the reflection amplitudes of light holes and heavy holes injected at subgap energies under an angle. We found that Andreev reflection of light holes and heavy holes is in general possible and that light holes and heavy holes can be converted into each other in this process. All reflection processes strongly depend on the injection angle. The requirement for holes to be Andreev reflected is a finite mixing with the conduction band, otherwise there would be no coupling to the states in the superconductor. Perpendicularly injected heavy holes decouple from the conduction-band and light-hole states. In this case heavy holes can only be normal reflected as heavy holes. At last, we have identified two different critical angles: first, a critical angle above which conversion-less Andreev reflection is not possible and, second, a critical angle for the conversion from heavy holes into light holes and time-reversed light holes.

# A Calculating diagrams via Mathematica

Since the number of required diagrams for the  $1/\Delta$  expansion ( $> 25.000$ ) and for the corrections arising from the coupling to the normal lead ( $> 2.500$ ) is exceedingly large it is very convenient to calculate these diagrams with the computer. Exemplarily, we give the source code for diagrams containing two tunneling lines associated to the superconducting leads.

The program is divided into several functions. The first function `CreateDiagram` is the core of the program. Its task is to construct the desired diagram from the parameters given to this function like starting- and ending states of the diagram, tunneling lines, position of the vertices, etc. and to return the analytical expression the diagram stands for. However, before constructing the diagram `CreateDiagram` checks via the second function `DiagramPossible` whether the diagram exists or not. An example for `CreateDiagram` is

$$\begin{aligned} & \mathbf{CreateDiagram} [\{\text{plus, plus, plus, plus}\}, \{\text{u, u, u, u}\}, \\ & \{\{\text{incoming, down}\}, \{\text{backward, down}\}\}, 3, \{\text{plus, plus}\}] \\ = & \frac{i2\Gamma_S\Delta\sqrt{1 - \frac{\delta}{2\epsilon_A}} \left(1 + \frac{\delta}{2\epsilon_A}\right)^{3/2} |\chi|\omega_2}{8\pi^2(\omega_1 + \epsilon - E_+)(\omega_2 + \epsilon - E_+)(\omega_1 + \omega_2)\sqrt{\omega_1^2 - \Delta^2}\sqrt{\omega_2^2 - \Delta^2}}. \end{aligned}$$

After the diagram is created, the function `ExpandDiagram` expands the expression in  $1/\Delta$  and the function `IntegrateDiagram` integrates out the energies  $\omega_1$  and  $\omega_2$ . The final function `CalculateRates` sums over all diagrams contributing to a rate.

## A Calculating diagrams via Mathematica

---

### Function CreateDiagram

```
Clear[CreateDiagram]
(* Remark: CreateDiagram works for two tunneling lines associated
to the superconductors. The gaps are so large that the Fermi
functions can be assumed to be 0 or 1,
respectively. We have chosen all directions of the occurring
tunneling lines as 'forward' so that the integrals run from  $+\Delta$  to  $\infty$ 
*)

(* SYNTAX *)
(*  $\chi$ : Vector containing the four states assigned to the diagram
along the Keldysh contour [e.g.: {minus,up,plus,down}] *)
(* v: vector containing the four vertices which are either
located on the top propagator (o) or on the bottom propagator
(u) [e.g.: {u,o,u,o}] *)
(* L: a two-dimensional vector whose components contain each a two-
dim vector, the first component containing the type of line
and the second the spin tunneling at the line's leftmost
vertex [e.g.: {{forward,up},{incomig,down}}] *)
(* v1c: Vertex 1 is connected to Vertex 3 or 4 [e.g.: 3] *)
(* Epm: two-dim vector. Determines which state is connected to vertex
when it can be either 'plus' or 'minus'. The first component
determines the first choice occurring along the Keldysh contour
[e.g.: {plus,minus}]
*)
CreateDiagram[ $\chi$ _, v_, L_, v1c_, Epm_] :=
Module[{Leftgoing, Rightgoing, E, Vertices, TransitionVorwaerts,
TransitionRueckwaerts, aktuellerZustand, v2c, sigma1, sigma2,
sigma1Quer, sigma2Quer, uebrigeObereVertices, uebrigeUntereVertices,
CounterVonEpm,  $\omega$ , vconnected, propagierendeEnergien, lineFactors,
vertexFactors, vertexFactorsSign, GlobalSigns, Ergebnis},

(* diagram will be calculated only in case DiagramPossible
returns True *)
If[DiagramPossible[ $\chi$ , v, L, v1c, Epm] == True,

(* initialising the result variable 'Ergebnis' *)
Ergebnis = 1;

 $\omega$  = { $\omega$ 1,  $\omega$ 2};

(* Leftgoing[[i]]/Rightgoing[[i]] contains the i-
th segment from the left of the propagating energies *)
Leftgoing = ConstantArray[0, 3];
Rightgoing = ConstantArray[0, 3];

(* 'Vertices' contains four vectors of four dimensions
each. Each of the vectors describes one vertex. The first
```

---

```

    component contains the starting state,
the second contains the ending state the third gives the
    direction of tunneling and the fourth gives the spin of
    the tunneling electron *)
Vertices = ConstantArray[1, {4, 4}];

CounterVonEpm = 0;
uebrigeObereVertices = 0;
For[i = 1, i < 5, i++,
    If[v[[i]] == 0, uebrigeObereVertices = uebrigeObereVertices + 1,
        uebrigeObereVertices = uebrigeObereVertices]];
uebrigeUntereVertices = 4 - uebrigeObereVertices;
(* The function TransitionVorwaerts determines the state
following a vertex *)
TransitionVorwaerts[χ1_, direction_, spin_, vertexIndex_] :=
Switch[v[[vertexIndex]],
    0, uebrigeObereVertices = uebrigeObereVertices - 1;
    Vertices[[vertexIndex, 2]] = If[uebrigeObereVertices == 0,
        χ[[2]],
        Switch[χ1, plus, Switch[direction, incoming, spin,
            outgoing, Switch[spin, up, down, down, up], _],
            Print[
                "direction in transtion function is not properly chosen"]],
        minus, Switch[direction, incoming, spin, outgoing,
            Switch[spin, up, down, down, up], _],
            Print[
                "direction in transtion function is not properly chosen"]],
        up, CounterVonEpm = CounterVonEpm + 1; Epm[[CounterVonEpm]],
        down, CounterVonEpm = CounterVonEpm + 1; Epm[[CounterVonEpm]],
        _, Print["χ in transtion function is not an allowed state"]
    ],
u, uebrigeUntereVertices = uebrigeUntereVertices - 1;
Vertices[[vertexIndex, 2]] = If[uebrigeUntereVertices == 0,
    χ[[4]],
    Switch[χ1, plus, Switch[direction, incoming, spin,
        outgoing, Switch[spin, up, down, down, up], _],
        Print[
            "direction in transtion function is not properly chosen"]],
        minus, Switch[direction, incoming, spin, outgoing,
            Switch[spin, up, down, down, up], _],
            Print[
                "direction in transtion function is not properly chosen"]],
        up, CounterVonEpm = CounterVonEpm + 1; Epm[[CounterVonEpm]],
        down, CounterVonEpm = CounterVonEpm + 1; Epm[[CounterVonEpm]],
        _, Print["χ in transtion function is not an allowed state"]
    ],
_, Print["v[[vertexIndex]] is not correct"]];

E[minus] := Em; E[plus] := Ep; E[up] := e; E[down] := e;

```

## A Calculating diagrams via Mathematica

---

```
(* Determining, wheter the vertices 1 and v1c are incoming
or outgoing and determining the spin of the tunneling electron *)
Vertices[[1, 4]] = L[[1, 2]];
sigma1 = L[[1, 2]];
sigma1Quer = Switch[L[[1, 2]], up, down, down, up, _,
Print["Spin of first line not correct"]];
Switch[v[[1]],
o, Switch[L[[1, 1]], backward,
{Vertices[[1, 3]] = incoming, Vertices[[v1c, 3]] = outgoing,
Vertices[[v1c, 4]] = sigma1}, incoming,
{Vertices[[1, 3]] = incoming, Vertices[[v1c, 3]] = incoming,
Vertices[[v1c, 4]] = sigma1Quer}, forward,
{Vertices[[1, 3]] = outgoing, Vertices[[v1c, 3]] = incoming,
Vertices[[v1c, 4]] = sigma1}, outgoing,
{Vertices[[1, 3]] = outgoing, Vertices[[v1c, 3]] = outgoing,
Vertices[[v1c, 4]] = sigma1Quer},
_, Print["Line 1 not well defined"]],
u, Switch[L[[1, 1]], backward,
{Vertices[[1, 3]] = outgoing, Vertices[[v1c, 3]] = incoming,
Vertices[[v1c, 4]] = sigma1}, incoming,
{Vertices[[1, 3]] = incoming, Vertices[[v1c, 3]] = incoming,
Vertices[[v1c, 4]] = sigma1Quer}, forward,
{Vertices[[1, 3]] = incoming, Vertices[[v1c, 3]] = outgoing,
Vertices[[v1c, 4]] = sigma1}, outgoing,
{Vertices[[1, 3]] = outgoing, Vertices[[v1c, 3]] = outgoing,
Vertices[[v1c, 4]] = sigma1Quer}]
, _, Print["v[[1]] not well defined"]
];
(* Determining, wheter the vertices 2 and v2c are incoming
or outgoing and determining the spin of the tunneling electron *)
Vertices[[2, 4]] = L[[2, 2]];
sigma2 = L[[2, 2]];
sigma2Quer = Switch[L[[2, 2]], up, down, down, up, _,
Print["Spin of second line not correct"]];
v2c = Switch[v1c, 3, 4, 4, 3, _, Print["v1c not correct"]];
Switch[v[[2]],
o, Switch[L[[2, 1]], backward,
{Vertices[[2, 3]] = incoming, Vertices[[v2c, 3]] = outgoing,
Vertices[[v2c, 4]] = sigma2}, incoming,
{Vertices[[2, 3]] = incoming, Vertices[[v2c, 3]] = incoming,
Vertices[[v2c, 4]] = sigma2Quer}, forward,
{Vertices[[2, 3]] = outgoing, Vertices[[v2c, 3]] = incoming,
Vertices[[v2c, 4]] = sigma2}, outgoing,
{Vertices[[2, 3]] = outgoing, Vertices[[v2c, 3]] = outgoing,
Vertices[[v2c, 4]] = sigma2Quer},
_, Print["Line 2 not well defined"]],
u, Switch[L[[2, 1]], backward,
{Vertices[[2, 3]] = outgoing, Vertices[[v2c, 3]] = incoming,
Vertices[[v2c, 4]] = sigma2}, incoming,
{Vertices[[2, 3]] = incoming, Vertices[[v2c, 3]] = incoming,
Vertices[[v2c, 4]] = sigma2Quer}, forward,
```

---

```

    {Vertices[[2, 3] = incoming, Vertices[[v2c, 3] = outgoing,
      Vertices[[v2c, 4] = sigma2}, outgoing,
    {Vertices[[2, 3] = outgoing, Vertices[[v2c, 3] = outgoing,
      Vertices[[v2c, 4] = sigma2Quer}}
  , _, Print["v[[2]] not well defined"]
];

(* determining the propagating  $\omega$ 's *)
vconnected = {v1c, v2c};
Switch[v[[1]],
  o, Rightgoing[[1]] = Rightgoing[[1]] +  $\omega$ 1;
  Rightgoing[[2]] = Rightgoing[[2]] +  $\omega$ 1;
  If[v1c == 4, Rightgoing[[3]] = Rightgoing[[3]] +  $\omega$ 1;],
  u, Leftgoing[[1]] = Leftgoing[[1]] +  $\omega$ 1; Leftgoing[[2]] = Leftgoing[[2]] +  $\omega$ 1;
  If[v1c == 4, Leftgoing[[3]] = Leftgoing[[3]] +  $\omega$ 1;],
  _, Print["Problem at determining propagating  $\omega$ 1"];
Switch[v[[2]],
  o, Rightgoing[[2]] = Rightgoing[[2]] +  $\omega$ 2;
  If[v2c == 4, Rightgoing[[3]] = Rightgoing[[3]] +  $\omega$ 2;],
  u, Leftgoing[[2]] = Leftgoing[[2]] +  $\omega$ 2;
  If[v2c == 4, Leftgoing[[3]] = Leftgoing[[3]] +  $\omega$ 2;],
  _, Print["Problem at determining propagating  $\omega$ 2"];

(* Determining the states connected to a vertex and the
  propagating dot energies *)
aktuellerZustand =  $\chi$ [[1]];
For[i = 1, i < 5, i++,
  If[v[[i]] == o, {Vertices[[i, 1] = aktuellerZustand,
    TransitionVorwaerts[aktuellerZustand, Vertices[[i, 3],
      Vertices[[i, 4], i], aktuellerZustand = Vertices[[i, 2]]}}];
  If[i < 4, Rightgoing[[i]] = Rightgoing[[i]] + E[aktuellerZustand];]
];
aktuellerZustand =  $\chi$ [[3]];
For[i = 4, i > 0, i--,
  If[v[[i]] == u, {Vertices[[i, 1] = aktuellerZustand,
    TransitionVorwaerts[aktuellerZustand, Vertices[[i, 3],
      Vertices[[i, 4], i], aktuellerZustand = Vertices[[i, 2]]}}];
  If[i > 1, Leftgoing[[i - 1]] = Leftgoing[[i - 1]] + E[aktuellerZustand];]
];

propagierendeEnergien = 
$$\frac{1}{\frac{1}{\text{Leftgoing}[[2]] - \text{Rightgoing}[[2]} \frac{1}{\text{Leftgoing}[[3]] - \text{Rightgoing}[[3]}}}$$
;

(* Setting the factors for the tunneling lines *)

```

## A Calculating diagrams via Mathematica

---

```

lineFactors =  $\frac{1}{4 \pi^2} \frac{1}{\sqrt{\omega_1^2 - \Delta^2}} \frac{1}{\sqrt{\omega_2^2 - \Delta^2}}$ ;
For[i = 1, i < 3, i++, Switch[L[[i, 1]], backward,
  lineFactors = lineFactors  $\omega[[i]]$  SumFS, forward,
  lineFactors = lineFactors  $\omega[[i]]$  SumFS, incoming,
  lineFactors = lineFactors (-1)  $\Delta^2 \chi_{\text{Betrag}}$ , outgoing,
  lineFactors = lineFactors (-1)  $\Delta^2 \chi_{\text{Betrag}}$ , _,
  Print["Problem at setting the lineFactors"]]];

(* Setting the factors for the Vertices *)
vertexFactors = 1;
vertexFactorsSign = ConstantArray[1, 4];
For[i = 1, i < 5, i++, vertexFactorsSign[[i]] = (
  Switch[Vertices[[i, 1]], plus, 1, minus, -1, up, 1, down, -1,
  _, Print["Problem at setting the vertexFactors"]]
  Switch[Vertices[[i, 2]], plus, 1, minus, -1, up, 1, down,
  -1, _, Print["Problem at setting the vertexFactors"]]
  Switch[Vertices[[i, 4]], up, 1, down, -1, _,
  Print["Problem at setting the vertexFactors"]])
];
For[i = 1, i < 5, i++,
  vertexFactors = vertexFactors  $\frac{1}{\sqrt{2}} \sqrt{1 - \text{vertexFactorsSign}[[i]] \frac{\delta}{2 \epsilon A}}$  ];

(* Determining the signs *)
GlobalSigns = 1;
(* rule: (-1) for each vertex on the lower propagator *)
For[i = 1, i < 5, i++,
  GlobalSigns = GlobalSigns Switch[v[[i]], o, 1, u, -1, _,
  Print[
    "Problem at setting signs for Vertices on the
    lower propagator"]
];
(* rule: (-1) for each crossing of tunneling lines *)
(* If vertex 1 is connected to vertex 3 then a crossing
exists whenever vertex 2 and vertex 3 are located on the
same propagator *)
(* If vertex 1 is connect to vertex 4 then a crossing
existes whenever vertex 2 and vertex 3 are located on
different propagators *)
GlobalSigns = GlobalSigns
Switch[v1c,
  3,
  Switch[v[[2]], o, Switch[v[[3]], o, -1, u, 1], u,
  Switch[v[[3]], o, 1, u, -1], _,
  Print["Problem with signs for crossing of tunneling lines"]],
  4,
  Switch[v[[2]], o, Switch[v[[3]], o, 1, u, -1], u,

```

---

```

Switch[v[[3]], o, -1, u, 1], _,
Print["Problem with signs for crossing of tunneling-lines"]];

(* rule: signs for Vertices *)
For[i = 1, i < 5, i++, GlobalSigns = GlobalSigns
Switch[Vertices[[i, 3]],
outgoing,
Switch[Vertices[[i, 2]], plus, -1, minus, 1, up, -1, down, 1],
incoming,
Switch[Vertices[[i, 1]], plus, -1, minus, 1, up, -1, down, 1],
_
Print["Problem at signs for Vertices"]]
];
(* rule: outgoing (incoming) anomalous line,
where earlier (later) tunneling electron is of spin up *)
For[i = 1, i < 3, i++, GlobalSigns = GlobalSigns
Switch[L[[i, 1]],
incoming,
Switch[v[[i]], o (* i.e. v[[i]] is the earlier vertex *),
Switch[Vertices[[i, 4]], up, 1, down, -1], u
(* i.e. v[[i]] is the later vertex *),
Switch[Vertices[[i, 4]], up, -1, down, 1]],
outgoing,
Switch[v[[i]], o, Switch[Vertices[[i, 4]], up, -1, down, 1],
u, Switch[Vertices[[i, 4]], up, 1, down, -1]],
forward, 1,
backward, 1,
_, Print["Problem with signs for anomalous lines"]]
];

Ergebnis = -i GlobalSigns propagierendeEnergien lineFactors
vertexFactors;
Ergebnis
+ (* this term solves the  $\delta$ -fcts *)

$$\left( \left( -i \text{GlobalSigns} \frac{1}{\text{Leftgoing}[[1]] - \text{Rightgoing}[[1]]} \right. \right.$$


$$\left. \frac{1}{\text{Leftgoing}[[3]] - \text{Rightgoing}[[3]]} \text{lineFactors vertexFactors} \right.$$


$$\left. \frac{1}{\Delta} \left( \text{Switch}[v[[1]], o, \text{Switch}[v[[2]], u, -i \pi, o, 0], u, \right. \right.$$


$$\left. \left. \text{Switch}[v[[2]], o, -i \pi, u, 0] \right) \right) / . \text{Solve}[\text{Leftgoing}[[2]] - \text{Rightgoing}[[2]] == 0, \omega 1][[1]]$$


```

## A Calculating diagrams via Mathematica

---

```

, 0] (* End If[DiagramPossible] *)
];

```

*Function DiagramPossible*

```

Clear[DiagramPossible]
(* DiagramPossible checks,
whether a diagram is required and whether it is possible
regarding spin conservation, particle conservation etc. *)
*)
DiagramPossible[χ_, v_, L_, v1c_, Epm_] :=
Module[{CounterVonEpm, uebrigeObereVertices, uebrigeUntereVertices,
AnzahlObererVertices, TransitionVorwaerts, Vertices, sigma1,
sigma1Quer, sigma2, sigma2Quer, v2c, aktuellerZustand, χNumber,
VerticesNumber, ZwischenUrteil, Urteil},

(* BEGIN of initializing the vertices *)
Vertices = ConstantArray[1, {4, 4}];
CounterVonEpm = 0;
uebrigeObereVertices = 0;
For[i = 1, i < 5, i++,
If[v[[i]] == 0, uebrigeObereVertices = uebrigeObereVertices + 1,
uebrigeObereVertices = uebrigeObereVertices]];
uebrigeUntereVertices = 4 - uebrigeObereVertices;
(* The function TransitionVorwaerts determines the state
following a vertex *)
TransitionVorwaerts[χ1_, direction_, spin_, vertexIndex_] :=
Switch[v[[vertexIndex]],
0, uebrigeObereVertices = uebrigeObereVertices - 1;
Vertices[[vertexIndex, 2]] = If[uebrigeObereVertices == 0,
χ[[2]],
Switch[χ1, plus, Switch[direction, incoming, spin, outgoing,
Switch[spin, up, down, down, up], _],
Print[
"direction in transtion function is not properly chosen"]],
minus, Switch[direction, incoming, spin, outgoing,
Switch[spin, up, down, down, up], _],
Print[
"direction in transtion function is not properly chosen"]],
up, CounterVonEpm = CounterVonEpm + 1; Epm[[CounterVonEpm]],
down, CounterVonEpm = CounterVonEpm + 1; Epm[[CounterVonEpm]],
_, Print["χ in transtion function is not an allowed state"]]
],
u, uebrigeUntereVertices = uebrigeUntereVertices - 1;
Vertices[[vertexIndex, 2]] = If[uebrigeUntereVertices == 0,
χ[[4]],
Switch[χ1, plus, Switch[direction, incoming, spin, outgoing,
Switch[spin, up, down, down, up], _],
Print[
"direction in transtion function is not properly chosen"]],

```

---

```

        minus, Switch[direction, incoming, spin, outgoing,
            Switch[spin, up, down, down, up], _,
            Print[
                "direction in transtion function is not properly chosen"]],
        up, CounterVonEpm = CounterVonEpm + 1; Epm[CounterVonEpm],
        down, CounterVonEpm = CounterVonEpm + 1; Epm[CounterVonEpm],
        _, Print["χ in transition function is not an allowed state"]
    ],
    _, Print["v[vertexIndex] is not correct"]];
(* Determining, wheter the vertices 1 and v1c are incoming
or outgoing and determining the spin of the tunneling electron *)
Vertices[[1, 4]] = L[[1, 2]];
signal = L[[1, 2]];
signalQuer = Switch[L[[1, 2]], up, down, down, up, _,
    Print["Spin of first line not correct"]];
Switch[v[[1]],
    o, Switch[L[[1, 1]], backward,
        {Vertices[[1, 3]] = incoming, Vertices[v1c, 3]] = outgoing,
        Vertices[v1c, 4]] = signal}, incoming,
        {Vertices[[1, 3]] = incoming, Vertices[v1c, 3]] = incoming,
        Vertices[v1c, 4]] = signalQuer}, forward,
        {Vertices[[1, 3]] = outgoing, Vertices[v1c, 3]] = incoming,
        Vertices[v1c, 4]] = signal}, outgoing,
        {Vertices[[1, 3]] = outgoing, Vertices[v1c, 3]] = outgoing,
        Vertices[v1c, 4]] = signalQuer},
    _, Print["Line 1 is not well defined"]],
    u, Switch[L[[1, 1]], backward,
        {Vertices[[1, 3]] = outgoing, Vertices[v1c, 3]] = incoming,
        Vertices[v1c, 4]] = signal}, incoming,
        {Vertices[[1, 3]] = incoming, Vertices[v1c, 3]] = incoming,
        Vertices[v1c, 4]] = signalQuer}, forward,
        {Vertices[[1, 3]] = incoming, Vertices[v1c, 3]] = outgoing,
        Vertices[v1c, 4]] = signal}, outgoing,
        {Vertices[[1, 3]] = outgoing, Vertices[v1c, 3]] = outgoing,
        Vertices[v1c, 4]] = signalQuer}]
    , _, Print["v[[1]] ist not correct"]
];
(* Determining, wheter the vertices 2 and v2c are incoming
or outgoing and determining the spin of the tunneling electron *)
Vertices[[2, 4]] = L[[2, 2]];
sigma2 = L[[2, 2]];
sigma2Quer = Switch[L[[2, 2]], up, down, down, up, _,
    Print["Spin of second line not correct"]];
v2c = Switch[v1c, 3, 4, 4, 3, _, Print["v1c is not correct"]];
Switch[v[[2]],
    o, Switch[L[[2, 1]], backward,
        {Vertices[[2, 3]] = incoming, Vertices[v2c, 3]] = outgoing,
        Vertices[v2c, 4]] = sigma2}, incoming,
        {Vertices[[2, 3]] = incoming, Vertices[v2c, 3]] = incoming,
        Vertices[v2c, 4]] = sigma2Quer}, forward,
        {Vertices[[2, 3]] = outgoing, Vertices[v2c, 3]] = incoming,

```

```

    Vertices[[v2c, 4] = sigma2}, outgoing,
    {Vertices[[2, 3] = outgoing, Vertices[[v2c, 3] = outgoing,
    Vertices[[v2c, 4] = sigma2Quer},
    _, Print["Line 2 is not well defined"]],
u, Switch[L[[2, 1], backward,
    {Vertices[[2, 3] = outgoing, Vertices[[v2c, 3] = incoming,
    Vertices[[v2c, 4] = sigma2}, incoming,
    {Vertices[[2, 3] = incoming, Vertices[[v2c, 3] = incoming,
    Vertices[[v2c, 4] = sigma2Quer}, forward,
    {Vertices[[2, 3] = incoming, Vertices[[v2c, 3] = outgoing,
    Vertices[[v2c, 4] = sigma2}, outgoing,
    {Vertices[[2, 3] = outgoing, Vertices[[v2c, 3] = outgoing,
    Vertices[[v2c, 4] = sigma2Quer}}]
    , _, Print["v[[2]] ist not correct"]
];
(* Determining the states connected to a vertex *)
aktuellerZustand = x[[1];
For[i = 1, i < 5, i++,
    If[v[[i]] == o, {Vertices[[i, 1] = aktuellerZustand,
    TransitionVorwaerts[aktuellerZustand, Vertices[[i, 3],
    Vertices[[i, 4], i], aktuellerZustand = Vertices[[i, 2]]}]]
];
aktuellerZustand = x[[3];
For[i = 4, i > 0, i--,
    If[v[[i]] == u, {Vertices[[i, 1] = aktuellerZustand,
    TransitionVorwaerts[aktuellerZustand, Vertices[[i, 3],
    Vertices[[i, 4], i], aktuellerZustand = Vertices[[i, 2]]}]]
];
(* END of initializing the vertices *)

(* testing, whether the diagram is required *)
ZwischenUrteil = True;

(* preventing diagrams to occur twice caused by the variable Epm:
Whenever Epm[[i]] does not affect the diagram only Epm[[i]=
plus will be created
*)
Switch[CounterVonEpm,
0, Switch[Epm[[1],
    plus, Switch[Epm[[2], plus, ZwischenUrteil = True, minus,
    ZwischenUrteil = False, _,
    Print["Problem with Epm decision in DiagramPossible"]],
    minus, ZwischenUrteil = False, _,
    Print["Problem with Epm decision in DiagramPossible"]],
1, Switch[Epm[[2], plus, ZwischenUrteil = True, minus,
    ZwischenUrteil = False, _,
    Print["Problem with Epm decision in DiagramPossible"]],
2, ZwischenUrteil = True, _,
    Print["Problem with Epm decision in DiagramPossible"]];

(* excluding diagrams that contain a superposition of states '

```

---

```

up' and 'down' with other states *)
While[ZwischenUrteil == True,
  χNumber = ConstantArray[0, 4];
  For[i = 1, i < 5, i++, χNumber[[i]] =
    Switch[χ[[i]], up, 1, down, 2, plus, 3, minus, 4, _,
    Print[
      "Problem at testing, wheter
      diagram contains forbidden superpositions"]]
];
For[i = 1, i < 3, i++, If[χNumber[[1]] == i && χNumber[[4]] ≠ i,
  ZwischenUrteil = False; Break[]]];
For[i = 1, i < 3, i++, If[χNumber[[4]] == i && χNumber[[1]] ≠ i,
  ZwischenUrteil = False; Break[]]];
For[i = 1, i < 3, i++, If[χNumber[[2]] == i && χNumber[[3]] ≠ i,
  ZwischenUrteil = False; Break[]]];
For[i = 1, i < 3, i++, If[χNumber[[3]] == i && χNumber[[2]] ≠ i,
  ZwischenUrteil = False; Break[]]];

(* excluding diagrams with all vertices in one propagator
while on the other propagator the states are changed.
E.g.: CreateDiagram[{plus, minus, minus, plus}, {0, 0, 0, 0},
{{incoming, up}, {outgoing, up}}, 3, {plus, plus} *)
AnzahlObererVertices = 0;
For[i = 1, i < 5, i++,
  If[v[[i]] == 0, AnzahlObererVertices = AnzahlObererVertices + 1,
  AnzahlObererVertices = AnzahlObererVertices]];
If[AnzahlObererVertices == 4,
  If[χNumber[[3]] ≠ χNumber[[4]], ZwischenUrteil = False; Break[]]];
If[AnzahlObererVertices == 0,
  If[χNumber[[1]] ≠ χNumber[[2]], ZwischenUrteil = False; Break[]]];
Break[]
];
(* end of while *)

(* Introducing VerticesNumber for easier handling *)
VerticesNumber = Vertices;
For[i = 1, i < 5, i++, VerticesNumber[[i, 1]] =
  Switch[Vertices[[i, 1]], up, 1, down, 2, plus, 3, minus, 4, _,
  Print[
    "Problem at initialising VerticesNumber in DiagramPossible"]]
];
For[i = 1, i < 5, i++, VerticesNumber[[i, 2]] =
  Switch[Vertices[[i, 2]], up, 1, down, 2, plus, 3, minus, 4, _,
  Print[
    "Problem at initialising VerticesNumber in DiagramPossible"]]
];
For[i = 1, i < 5, i++, VerticesNumber[[i, 4]] =
  Switch[Vertices[[i, 4]], up, 1, down, 2, _,
  Print[
    "Problem at initialising VerticesNumber in DiagramPossible"]]
];

```

## A Calculating diagrams via Mathematica

---

```
(* testing, whether diagramm is possible *)
While[ZwischenUrteil == True,
  (* testing, whether starting state and ending state of a
  vertex have different parity *)
  For[i = 1, i < 5, i++,
    Switch[VerticesNumber[[i, 1]],
      1,
      If[VerticesNumber[[i, 2]] == 1 || VerticesNumber[[i, 2]] == 2,
        ZwischenUrteil = False; Break[]],
      2,
      If[VerticesNumber[[i, 2]] == 1 || VerticesNumber[[i, 2]] == 2,
        ZwischenUrteil = False; Break[]],
      3,
      If[VerticesNumber[[i, 2]] == 3 || VerticesNumber[[i, 2]] == 4,
        ZwischenUrteil = False; Break[]],
      4,
      If[VerticesNumber[[i, 2]] == 3 || VerticesNumber[[i, 2]] == 4,
        ZwischenUrteil = False; Break[]],
      _/,
      Print[
        "Problem at testing the parity of starting- and ending states"
      ]
    ];

  (* testing, whether the vertices conserve spin *)
  For[i = 1, i < 5, i++,
    Switch[VerticesNumber[[i, 3]],
      incoming,
      If[VerticesNumber[[i, 1]] == VerticesNumber[[i, 4]],
        ZwischenUrteil = False; Break[]];
      Switch[VerticesNumber[[i, 4]],
        1, If[VerticesNumber[[i, 2]] == 2, ZwischenUrteil = False; Break[]],
        2, If[VerticesNumber[[i, 2]] == 1, ZwischenUrteil = False; Break[]],
        _, Print["Problem at testing the spin conservation"]
      ],
      outgoing,
      If[VerticesNumber[[i, 2]] == VerticesNumber[[i, 4]],
        ZwischenUrteil = False; Break[]];
      Switch[VerticesNumber[[i, 4]],
        1, If[VerticesNumber[[i, 1]] == 2, ZwischenUrteil = False; Break[]],
        2, If[VerticesNumber[[i, 1]] == 1, ZwischenUrteil = False; Break[]],
        _, Print["Problem at testing the spin conservation"]],
      _, Print["Problem at testing the spin conservation"]
    ];
  Break[]
  (* end of while*)
];

Urteil = ZwischenUrteil;
Urteil
];
```

*Function ExpandDiagram*

```

Clear[ExpandDiagram]
(* Remark: ExpandDiagram creates the Diagramm with CreateDiagram
und subtracts, if necessary CreateDoubleDiagram
(in order to prevent double counting,
in case the inner diagram is of 0th order in  $\frac{1}{\Delta}$ ).
The resulting expression will be expanded up to 1st order in  $\frac{1}{\Delta}$ . *)

```

```

ExpandDiagram[χ_, v_, L_, vlc_, Epm_] := Module[{Ergebnis},
  Ergebnis =
  Normal[
    Series[[( $\frac{1}{z^2}$  CreateDiagram[χ, v, L, vlc, Epm] /.
      {Δ →  $\frac{1}{z}$ , ω1 →  $\frac{x}{z}$ , ω2 →  $\frac{y}{z}$ }), {z, 0, 1}]];
  If[vlc == 4,
    Ergebnis = Ergebnis -
    Normal[
      Series[
        Normal[Series[( $\frac{1}{z1} \frac{1}{z2}$  CreateDoubleDiagram[χ, v, L, vlc, Epm] /.
          {Δ1 →  $\frac{1}{z1}$ , Δ2 →  $\frac{1}{z2}$ , ω1 →  $\frac{x}{z1}$ , ω2 →  $\frac{y}{z2}$ }), {z2, 0, 0}]],
        {z1, 0, 1}]] /. {z1 → z}
      , 0];
  Ergebnis
];

```

*Function IntegrateDiagram*

```

(* IntegrateDiagram performs solves all integrals *)
Clear[IntegrateDiagram]
IntegrateDiagram[Integrand_] := Module[{Ergebnis},
  Ergebnis = Integrate[Integrand, {x, 1, ∞}, Assumptions → {y > 0}];
  Ergebnis = Integrate[Ergebnis, {y, 1, ∞}];
  Ergebnis
];

```

## A Calculating diagrams via Mathematica

---

### *Function CalculateRate*

```
(* Here, the arguments of CreateDiagram get assign numbers so
that summations can be performed *)
Clear[χ, χAusgabe]
χ[j_] := (χAusgabe = ConstantArray[1, 4];
  For[i = 1, i < 5, i++,
    χAusgabe[[i]] = Switch[j[[i]], 1, up, 2, down, 3, plus, 4, minus,
      _, Print["Problem in summing over χ"]]; χAusgabe);
Clear[v, vAusgabe]
v[j_] := (vAusgabe = ConstantArray[1, 4];
  For[i = 1, i < 5, i++,
    vAusgabe[[i]] = Switch[j[[i]], 1, o, 2, u, _,
      Print["Problem in summing over v"]]; vAusgabe);
Clear[L, LAusgabe]
L[j_] := (LAusgabe = ConstantArray[1, {2, 2}];
  For[i = 1, i < 3, i++,
    LAusgabe[[i, 1]] = Switch[j[[i, 1]], 1, backward, 2, forward, 3,
      incoming, 4, outgoing, _,
      Print["Problem in summing over the line types"]];
  For[i = 1, i < 3, i++,
    LAusgabe[[i, 2]] = Switch[j[[i, 2]], 1, up, 2, down, _,
      Print["Problem in summing over the line types"]];
  LAusgabe);
Clear[vlc]
vlc[j_] := Switch[j, 1, 3, 2, 4, _, Print["Problem in summing over vlc"]];
Clear[Epm, EpmAusgabe]
Epm[j_] := (EpmAusgabe = ConstantArray[1, 2];
  For[i = 1, i < 3, i++,
    EpmAusgabe[[i]] = Switch[j[[i]], 1, plus, 2, minus, _,
      Print["Problem in summing over Epm"]];
  EpmAusgabe);
```

---

```

(* CalculateRate calculates all diagrams for a given combination
of two lines and integrates the result. Afterwards a sum over
all line combinations is carried out. *)
Clear[CalculateRate]
CalculateRate[x_] := Module[{Ergebnis}, Ergebnis = (*Sum[*)
  IntegrateDiagram[
    Simplify[Sum[
      ExpandDiagram[x, v[{v1, v2, v3, v4}], L[{{L11, L12}, {L21, L22}}],
      vlc[vlc1], Epm[{Epm1, Epm2}]]
      , {v1, 2}, {v2, 2}, {v3, 2}, {v4, 2}, {L11, 1, 4}, {L12, 2},
      {L21, 1, 4}, {L22, 2}, {vlc1, 2}, {Epm1, 2}, {Epm2, 2}]
    ]
  ];
  Simplify[Ergebnis]
];

```

## B Diagrams contributing to the resummation approach

In this appendix we exemplarily give all diagrams including the analytical expressions they represent for the rate  $W_{\uparrow\uparrow}^-(\omega)$  appearing in the resummation approach discussed in Sec. 5.2.2. We assume the temperature low enough to ensure  $f(\omega_1 < -\Delta) \approx 1$  and  $f(\omega_1 > \Delta) \approx 0$ . All diagrams that appear here are only segments of a superordinate diagram so that all diagrams in this appendix must not get the general prefactor  $(-i)$ . Diagrams, where the line associated with the superconductors is a backward line, are given by

$$\begin{array}{c}
 \text{---} \\
 \text{---} \quad \epsilon \\
 \text{---} \quad \omega_1 \\
 \text{---} \quad \omega \\
 \text{---} \\
 \uparrow \quad \text{---} \quad \uparrow \\
 \text{---} \quad \epsilon \\
 \text{---} \quad E_- \\
 \text{---} \\
 \omega \\
 \text{---} \\
 \uparrow \quad \text{---} \quad \uparrow \\
 \text{---} \quad \omega_1 \\
 \text{---} \quad E_{\pm}
 \end{array}
 = \sum_{\sigma} \int_{\Delta}^{\infty} \frac{d\omega_1}{4\pi} \frac{\left(1 + \frac{\delta}{2\epsilon_A}\right) \omega_1 \sum_S \Gamma_S}{\sqrt{\omega_1^2 - \Delta^2}(\omega - \omega_1)}, \quad (\text{B.1})$$

$$\begin{array}{c}
 \text{---} \\
 \text{---} \quad \epsilon \\
 \text{---} \quad E_- \\
 \text{---} \\
 \omega \\
 \text{---} \\
 \uparrow \quad \text{---} \quad \uparrow \\
 \text{---} \quad \omega_1 \\
 \text{---} \quad E_{\pm}
 \end{array}
 = \int_{\Delta}^{\infty} \frac{d\omega_1}{4\pi} \frac{\left(1 \pm \frac{\delta}{2\epsilon_A}\right) \omega_1 \sum_S \Gamma_S}{\sqrt{\omega_1^2 - \Delta^2}(\omega + \omega_1 + E_{\pm} - E_-)}. \quad (\text{B.2})$$

In case of the line being a forward line, the diagrams correspond to the expressions

$$\begin{array}{c}
 \text{---} \\
 \text{---} \quad \epsilon \\
 \text{---} \quad \omega_1 \\
 \text{---} \quad \omega \\
 \text{---} \\
 \uparrow \quad \text{---} \quad \uparrow \\
 \text{---} \quad \epsilon \\
 \text{---} \quad E_- \\
 \text{---} \\
 \omega \\
 \text{---} \\
 \uparrow \quad \text{---} \quad \uparrow \\
 \text{---} \quad \omega_1 \\
 \text{---} \quad E_{\pm}
 \end{array}
 = \sum_{\sigma} \int_{\Delta}^{\infty} \frac{d\omega_1}{4\pi} \frac{\left(1 - \frac{\delta}{2\epsilon_A}\right) \omega_1 \sum_S \Gamma_S}{\sqrt{\omega_1^2 - \Delta^2}(\omega - \omega_1)}, \quad (\text{B.3})$$

$$\begin{array}{c}
 \text{---} \\
 \text{---} \quad \epsilon \\
 \text{---} \quad E_- \\
 \text{---} \\
 \omega \\
 \text{---} \\
 \uparrow \quad \text{---} \quad \uparrow \\
 \text{---} \quad \omega_1 \\
 \text{---} \quad E_{\pm}
 \end{array}
 = \int_{\Delta}^{\infty} \frac{d\omega_1}{4\pi} \frac{\left(1 \mp \frac{\delta}{2\epsilon_A}\right) \omega_1 \sum_S \Gamma_S}{\sqrt{\omega_1^2 - \Delta^2}(\omega + \omega_1 + E_{\pm} - E_-)}. \quad (\text{B.4})$$

Additionally, the line could be an incoming line

$$\begin{array}{c}
 \begin{array}{c}
 \text{---} \epsilon \text{---} \\
 \text{---} \omega_1 \text{---} \\
 \text{---} \omega \text{---} \\
 \uparrow \epsilon \uparrow \\
 \text{---} E_- \text{---} \\
 \uparrow \omega_1 \uparrow \\
 \text{---} E_{\pm} \text{---}
 \end{array}
 \end{array}
 = \sum_{\sigma} \int_{\Delta}^{\infty} \frac{d\omega_1}{2\pi} \frac{\Delta \sqrt{1 - \frac{\delta^2}{4\epsilon_A^2}} |\chi|}{\sqrt{\omega_1^2 - \Delta^2} (\omega - \omega_1)}, \quad (\text{B.5})$$

$$\begin{array}{c}
 \begin{array}{c}
 \text{---} \epsilon \text{---} \\
 \text{---} E_- \text{---} \\
 \text{---} \omega \text{---} \\
 \uparrow \omega_1 \uparrow \\
 \text{---} E_{\pm} \text{---}
 \end{array}
 \end{array}
 = \pm \int_{\Delta}^{\infty} \frac{d\omega_1}{2\pi} \frac{\Delta \sqrt{1 - \frac{\delta^2}{4\epsilon_A^2}} |\chi|}{\sqrt{\omega_1^2 - \Delta^2} (\omega + \omega_1 + E_{\pm} - E_-)}, \quad (\text{B.6})$$

or an outgoing line

$$\begin{array}{c}
 \begin{array}{c}
 \text{---} \epsilon \text{---} \\
 \text{---} \omega_1 \text{---} \\
 \text{---} \omega \text{---} \\
 \uparrow \epsilon \uparrow \\
 \text{---} E_- \text{---} \\
 \uparrow \omega_1 \uparrow \\
 \text{---} E_{\pm} \text{---}
 \end{array}
 \end{array}
 = \sum_{\sigma} \int_{\Delta}^{\infty} \frac{d\omega_1}{2\pi} \frac{\Delta \sqrt{1 - \frac{\delta^2}{4\epsilon_A^2}} |\chi|}{\sqrt{\omega_1^2 - \Delta^2} (\omega - \omega_1)}, \quad (\text{B.7})$$

$$\begin{array}{c}
 \begin{array}{c}
 \text{---} \epsilon \text{---} \\
 \text{---} E_- \text{---} \\
 \text{---} \omega \text{---} \\
 \uparrow \omega_1 \uparrow \\
 \text{---} E_{\pm} \text{---}
 \end{array}
 \end{array}
 = \pm \int_{\Delta}^{\infty} \frac{d\omega_1}{2\pi} \frac{\Delta \sqrt{1 - \frac{\delta^2}{4\epsilon_A^2}} |\chi|}{\sqrt{\omega_1^2 - \Delta^2} (\omega + \omega_1 + E_{\pm} - E_-)}. \quad (\text{B.8})$$

Besides, a diagram exists that contains a cross vertex instead of a tunneling line associated with the superconducting leads. This diagram should have the width of a point, which is difficult to realize graphically. The expression evoked by the cross vertex is given by

$$\begin{array}{c}
 \begin{array}{c}
 \text{---} E_- \times E_- \text{---} \\
 \text{---} \omega \text{---} \\
 \uparrow \epsilon \uparrow
 \end{array}
 \end{array}
 = \sqrt{1 - \frac{\delta^2}{4\epsilon_A^2}} |\chi|. \quad (\text{B.9})$$

# Bibliography

- [1] S. De Franceschi, L. Kouwenhoven, C. Schönberger, and W. Wernsdorfer, *Nat. Nanotechnol.* **5**, 703 (2010).
- [2] A. Martín-Rodero and A. Levy Yeyati, *Adv. Phys.* **60**, 899 (2011).
- [3] L. P. Kouwenhoven, C.M. Marcus, P. L. McEuen, S. Tarucha, R. M. Westervelt, and N. S. Wingreen, *Kluwer Series*, **E345**, Proceedings of the NATO Advanced Study Institute on Mesoscopic Electron Transport, 105 (1997).
- [4] V. Mourik, K. Zuo, S. M. Frolov, S. R. Plissard, E. P. A. M. Bakkers, and L. P. Kouwenhoven, *Science* **336**,1003 (2012).
- [5] L. Hofstetter, S. Csonka, J. Nygård, and C. Schönberger, *Nature* **461**, 960 (2009).
- [6] L. G. Herrmann, F. Portier, P. Roche, A. Levy Yeyati, T. Kontos, and C. Strunk, *Phys. Rev. Lett.* **104**, 026801 (2010).
- [7] L. Hofstetter, S. Csonka, A. Baumgartner, Fülöp, S. d'Hollosy, J. Nygård, C. Schönberger *Phys. Rev. Lett.* 107, 136801 (2011).
- [8] A. Das, Y. Ronen, M. Heiblum, D. Mahalu, A. V. Kretinin, and H. Shtrikman, *arXiv:1205.2455* (2012).
- [9] J.-D. Pillet, C. Quay, P. Morfin, C. Bena, A. L. Yeyati, and P. Joyez, *Nature Phys.* **6**, 965 (2010).
- [10] T. Dirks, T. L. Hughes, S. Lal, B. Uchoa, Y.-F. Chen, C. Chialvo, P. M. Goldbart, and N. Mason, *Nature Phys.* **7**, 386 (2011).
- [11] S. Sahoo, T. Kontos, J. Furer, C. Hoffmann, M. Gräber, A. Cottet, and C. Schönberger, *Nat. Phys.* **1**, 99 (2005).
- [12] J. R. Hauptmann, J. Paaske, and P. E. Lindelof, *Nat. Phys.* **4**, 373 (2008).
- [13] C. A. Merchant and N. Marković, *Phys. Rev. Lett.* **100**, 156601 (2008).
- [14] L. Hofstetter, A. Geresdi, M. Aagesen, J. Nygård, C. Schönberger, and S. Csonka, *Phys. Rev. Lett.* **104**, 246804 (2010).
- [15] C. W. J. Beenakker, in: *Mesoscopic Quantum Physics*, edited by E. Akkermans, G. Montambaux, J.-L. Pichard, and J. Zinn-Justin (North-Holland, Amsterdam, 1995): pp. 279-324.

- [16] R. Fazio and R. Raimondi, Phys. Rev. Lett. **80**, 2913 (1998).
- [17] P. Schwab and R. Raimondi, Phys. Rev. B **59**, 1637 (1999).
- [18] A. A. Clerk and V. Ambegaokar, Phys. Rev. B **61**, 9109 (2000).
- [19] J. C. Cuevas, A. L. Yeyati, and A. Martín-Rodero, Phys. Rev. B **63**, 094515 (2001).
- [20] Y. Avishai, A. Golub, and A. D. Zaikin, Phys. Rev. B **67**, 041301(R) (2003).
- [21] V. Koerting, B. M. Andersen, K. Flensberg, and J. Paaske, Phys. Rev. B **82**, 245108 (2010).
- [22] M. G. Pala, M. Governale, and J. König, New. J. Phys. **9**, 278 (2007).
- [23] M. Governale, M. G. Pala, and J. König, Phys. Rev. B **77**, 134513 (2008).
- [24] C. Karrasch, A. Oguri, and V. Meden, Phys. Rev. B **77**, 024517 (2008).
- [25] A. V. Rozhkov and D. P. Arovas, Phys. Rev. B **62**, 6687 (2000).
- [26] Y. Tanaka, A. Oguri, and A. C. Hewson, New J. Phys. **9**, 115 (2007).
- [27] T. Meng, S. Florens, and P. Simon, Phys. Rev. B **79**, 224521 (2009).
- [28] D. Futterer, M. Governale, M. G. Pala, and J. König, Phys. Rev. B **79**, 054505 (2009).
- [29] B. Sothmann, D. Futterer, M. Governale, and J. König, Phys. Rev. B **82**, 094514 (2010).
- [30] J. Eldridge, M. G. Pala, M. Governale, and J. König, Phys. Rev. B **82**, 184507 (2010).
- [31] B. Hiltcher, M. Governale, J. Splettstoesser, and J. König, Phys. Rev. B **84**, 155403 (2011).
- [32] A. G. Moghaddam, M. Governale, and J. König, Phys. Rev. B **85**, 094518 (2012).
- [33] A. Martín-Rodero and A. Levy Yeyati, J. Phys.: Condens. Matter **24**, 385303 (2012).
- [34] The NRG data, some of them presented in Ref. 33, were kindly provided by A. Martín-Rodero and A. Levy Yeyati.
- [35] G. E. Blonder, M. Tinkham, and T. M. Klapwijk, Phys. Rev. B **25**, 4515 (1982).
- [36] P. G. de Gennes, *Superconductivity of Metals and Alloys* (Addison-Wesley, Reading, MA, 1989).
- [37] H. K. Onnes, Nobel Lecture (1913).

## Bibliography

---

- [38] J. G. Bednorz and K. A. Müller, *Z. Phys. B* **64**, 189 (1986).
- [39] Y. Kamihara, T. Watanabe, M. Hirano, and H. Hosono, *J. Am. Chem. Soc.* **130**, 3296 (2008).
- [40] G. Czycholl, *Theoretische Festkörperphysik*, 3rd edition, Springer (2008).
- [41] A. P. Mackenzie and Y. Maeno, *Rev. Mod. Phys.* **75**, 657 (2003).
- [42] F. S. Bergeret, A. F. Volkov, and K. B. Efetov, *Rev. Mod. Phys.* **77**, 1321 (2005).
- [43] J. Bardeen, L. N. Cooper, and J. R. Schrieffer, *Phys. Rev.* **106**, 162 (1957).
- [44] J. Bardeen, L. N. Cooper, and J. R. Schrieffer, *Phys. Rev.* **108**, 1175 (1957).
- [45] B. D. Josephson, *Phys. Lett.* **1**, 251 (1962).
- [46] A. F. Andreev, *Zh. Eksp. Teor. Fiz.* **46**, 1823 (1964) [*Sov. Phys. JETP* **19**, 1228 (1964)].
- [47] P.-G. de Gennes and D. Saint-James, *Phys. Lett.* **4**, 151 (1963).
- [48] M. Tinkham, *Introduction to superconductivity*, 2nd edition, Dover (1996).
- [49] C. W. J. Beenakker, *Phys. Rev. B* **44**, 1646 (1991).
- [50] P. W. Anderson, *Phys. Rev.* **124**, 41 (1961).
- [51] S. De Franceschi, S. Sasaki, J. M. Elzerman, W. G. van der Wiel, S. Tarucha, and L. P. Kouwenhoven, *Phys. Rev. Lett.* **86**, 878 (2001).
- [52] J. Kondo, *Prog. Theor. Phys.* **32**, 37 (1964).
- [53] T. K. Ng and P. A. Lee, *Phys. Rev. Lett.* **61**, 1768 (1988).
- [54] L. I. Glazman and M. E. Raikh, *Pis'ma Zh. Eksp. Teor. Fiz.* **47**, 378 (1988) [*JETP Lett.* **47**, 452 (1988)].
- [55] D. Goldhaber-Gordon, H. Shtrikman, D. Mahalu, D. Abusch-Madger, U. Meirav, and M. A. Kastner, *Nature* **391**, 156 (1998).
- [56] M. R. Buitelaar, T. Nussbaumer, and C. Schönenberger, *Phys. Rev. Lett.* **89**, 256801 (2002).
- [57] M. R. Buitelaar, W. Belzig, T. Nussbaumer, B. Babić, C. Bruder, and C. Schönenberger, *Phys. Rev. Lett.* **91**, 057005 (2003).
- [58] J.-P. Cleuziou, W. Wernsdorfer, V. Bouchiat, T. Ondarçuhu, and M. Monthieux, *Nature Nanotechnology* **1**, 53 (2006).
- [59] P. Jarillo-Herrero, J. A. van Dam, and L. P. Kouwenhoven, *Nature* **439**, 953 (2006).

- 
- [60] H. I. Jørgensen, K. Grove-Rasmussen, T. Novotný, K. Flensberg, and P. E. Lindelof, Phys. Rev. Lett. **96**, 207003 (2006).
- [61] K. Grove-Rasmussen, H. Ingerslev Jørgensen, and P. E. Lindelof, New J. Phys. **9**, 124 (2007).
- [62] H. Ingerslev Jørgensen, T. Novotný, K. Grove-Rasmussen, K. Flensberg, and P. E. Lindelof, Nano Lett. **7**, 2441 (2007).
- [63] A. Eichler, M. Weiss, S. Oberholzer, C. Schönenberger, A. Levy Yeyati, J. C. Cuevas, and A. Martín-Rodero, Phys. Rev. Lett. **99**, 126602 (2007).
- [64] T. Sand-Jespersen, J. Paaske, B. M. Andersen, K. Grove-Rasmussen, H. I. Jørgensen, M. Aagesen, C. B. Sørensen, P. E. Lindelof, K. Flensberg, and J. Nygård Phys. Rev. Lett. **99**, 126603 (2007).
- [65] A. Eichler, R. Deblock, M. Weiss, C. Karrasch, V. Meden, C. Schönenberger, and H. Bouchiat, Phys. Rev. B **79**, 161407(R) (2009).
- [66] R. S. Deacon, Y. Tanaka, A. Oiwa, R. Sakano, K. Yoshida, K. Shibata, K. Hirakawa, and S. Tarucha, Phys. Rev. Lett. **104**, 076805 (2010).
- [67] R. S. Deacon, Y. Tanaka, A. Oiwa, R. Sakano, K. Yoshida, K. Shibata, K. Hirakawa, and S. Tarucha, Phys. Rev. B **81**, 121308(R) (2010).
- [68] J. A. van Dam, Y. V. Nazarov, E. P. A. M. Bakkers, S. De Franceschi, and L. P. Kouwenhoven, Nature **442**, 667 (2006).
- [69] C. W. J. Beenakker and H. van Houten, in *Single-Electron Tunneling and Mesoscopic Devices*, edited by H. Koch and H. Lübbig (Springer, Berlin, 1992).
- [70] B. I. Spivak and S. A. Kivelson, Phys. Rev. B **43**, 3740 (1991).
- [71] A. V. Rozhkov, D. P. Arovas, and F. Guinea, Phys. Rev. B **64**, 233301 (2001).
- [72] K. Kang, Phys. Rev. B **58**, 9641 (1998).
- [73] R. Fazio and R. Raimondi, Phys. Rev. Lett. **82**, 4950 (1999).
- [74] A. A. Clerk, V. Ambegaokar, and S. Hershfield, Phys. Rev. B **61**, 3555 (2000).
- [75] S. Shapira, E. H. Linfield, C. J. Lambert, R. Seviour, A. F. Volkov, and A. V. Zaitsev, Phys. Rev. Lett. **84**, 159 (2000).
- [76] A. Levy Yeyati, J. C. Cuevas, A. López-Dávalos, and A. Martín-Rodero, Phys. Rev. B **55**, R6137 (1997).
- [77] L. Dell'Anna, A. Zazunov, and R. Egger, Phys. Rev. B **77**, 104525 (2008).
- [78] L. I. Glazman and K. A. Matveev, JETP Lett. **49**, 659 (1989).
- [79] G. Sellier, T. Kopp, J. Kroha, and Y. S. Barash, Phys. Rev. B **72**, 174502 (2005).

## Bibliography

---

- [80] F. S. Bergeret, A. L. Yeyati, and A. Martin-Rodero, Phys. Rev. B **74**, 132505 (2006).
- [81] R. López, Mahn-Soo Choi, and R. Aguado, Phys. Rev. B **75**, 045132 (2007).
- [82] J. König, H. Schoeller, and G. Schön, Phys. Rev. Lett. **76**, 1715 (1996).
- [83] J. König, J. Schmid, H. Schoeller, and G. Schön, Phys. Rev. B **54**, 16820 (1996).
- [84] J. König, *Quantum Fluctuations in the Single-Electron Transistor* (Shaker, Aachen, 1999).
- [85] M. Braun, J. Martinek und J. König, Phys. Rev. B **70**, 195345 (2004).
- [86] G. C. Wick, Phys. Rev. **80**, 268 (1950).
- [87] D. Futterer, J. Swiebodzinski, M. Governale, and J. König, Phys. Rev. B **87**, 014509 (2013).
- [88] M. Jullière, Phys. Lett. **54A**, 225 (1975).
- [89] B. R. Bulka, Phys. Rev. B **62**, 1186 (2000).
- [90] W. Rudziński, J. Barnaś, R. Świrkowicz, and M. Wilczyński, Phys. Rev. B **71**, 205307 (2005).
- [91] S. Braig and P. W. Brouwer, Phys. Rev. B **71**, 195324 (2005).
- [92] G. Falci, D. Feinberg, and F. W. J. Hekking, Europhys. Lett. **54**, 255 (2001).
- [93] G.B. Lesovik, T. Martin, and G. Blatter, Eur. Phys. J. B **24**, 287 (2001).
- [94] D. Sánchez, R. López, P. Samuelsson, and M. Büttiker, Phys. Rev. B **68**, 214501 (2003).
- [95] R. Mélin, and D. Feinberg, Phys. Rev. B **70**, 174509 (2004).
- [96] M. S. Kalenkov, and A. D. Zaikin, Phys. Rev. B **76**, 224506 (2007).
- [97] S. Das, S. Rao, and A. Saha, Europhys. Lett. **81**, 67001 (2008).
- [98] D. Futterer, M. Governale, and J. König, Europhys. Lett. **91**, 47004 (2010).
- [99] A. Braggio, M. Governale, M.G. Pala, and J. König, Solid State Commun. **151**, 155 (2011).
- [100] B. Hiltcher, M. Governale, and J. König, arXiv:1208:1843
- [101] M. R. Gräber, T. Nussbaumer, W. Belzig, and C. Schönenberger, Nanotechnology **15**, S479 (2004).
- [102] S. Y. Cho, K. Kang, and C.-M. Ryu, Phys. Rev. B **60**, 16874 (1999).

- 
- [103] Q.-F. Sun, H. Guo, and T.-H. Lin, Phys. Rev. Lett. **87**, 176601 (2001).
- [104] T. Aono, A. Golub, and Y. Avishai, Phys. Rev. B **68**, 045312 (2003).
- [105] F. Siano and R. Egger, Phys. Rev. Lett. **93**, 047002 (2004).
- [106] M. Krawiec and K. I. Wysokiński, Supercond. Sci. Technol. **17**, 103 (2004).
- [107] J. Splettstoesser, M. Governale, J. König, F. Taddei, and R. Fazio, Phys. Rev. B **75**, 235302 (2007).
- [108] Y. Tanaka, N. Kawakami, and A. Oguri, J. Phys. Soc. Jpn. **76**, 074701 (2007).
- [109] T. Domański and A. Donabidowicz, Phys. Rev. B **78**, 073105 (2008).
- [110] T. Domański, A. Donabidowicz, and K. I. Wysokiński, Phys. Rev. B **78**, 144515 (2008).
- [111] Y. Yamada, Y. Tanaka, and N. Kawakami, J. Phys. Soc. Jpn. **79**, 043705 (2010).
- [112] Y. Yamada, Y. Tanaka, and N. Kawakami, Phys. Rev. B **84**, 075484 (2011).
- [113] T. Yoshioka and Y. Ohashi, J. Phys. Soc. Japan **69**, 1812 (2000).
- [114] J. Bauer, A. Oguri, and A.C. Hewson, J. Phys.: Condens. Matter **19**, 486211 (2007).
- [115] T. Hecht, A. Weichselbaum, J. von Delft, and R. Bulla, J. Phys.: Condens. Matter **20**, 275213 (2008).
- [116] J.S. Lim and M.S. Choi, J. Phys.: Condens. Matter **20**, 415225 (2008).
- [117] F. W. J. Hekking, G. Schön, and D. V. Averin (Eds.), *Mesoscopic Superconductivity* (Elsevier Science, Amsterdam, 1994), Special Issue of Physica B **203**.
- [118] C. W. J. Beenakker, in E. Akkermans, G. Montambaux, J.-L. Pichard, and J. Zinn-Justin (Eds.), *Mesoscopic Quantum Physics* (Elsevier, Amsterdam, 1995), pp. 291–324.
- [119] L. L. Sohn, L. P. Kouwenhoven, and G. Schön (Eds.), *Mesoscopic Electron Transport*, vol. 345 of *NATO ASI Series E* (Kluwer Academic, Dordrecht, 1997).
- [120] C. J. Lambert and R. Raimondi, J. Phys.: Condens. Matter **10**, 901 (1998).
- [121] T. Schäpers, *Superconductor/Semiconductor Junctions* (Springer, Berlin, 2001).
- [122] H. Takayanagi, J. Nitta, and H. Nakano (Eds.), *Controllable Quantum States: Mesoscopic Superconductivity and Spintronics* (World Scientific, Singapore, 2008).
- [123] H. Takayanagi and T. Kawakami, Phys. Rev. Lett. **54**, 2449 (1985).
- [124] N. T. Bagraev, L. E. Klyachkin, A. A. Koudryavtsev, A. M. Malyarenko, G. A. Oganessian, and D. S. Poloskin, Semiconductors **43**, 1455 (2009).

## Bibliography

---

- [125] P. Y. Yu and M. Cardona, *Fundamentals of Semiconductors*, 4th Ed (Springer, Berlin, 2010).
- [126] R. Winkler, *Spin-Orbit Coupling Effects in Two-Dimensional Electron and Hole Systems* (Springer, Berlin, 2003).
- [127] J. P. Lu, J. B. Yau, S. P. Shukla, M. Shayegan, L. Wissinger, U. Rössler, and R. Winkler, *Phys. Rev. Lett.* **81**, 1282 (1998).
- [128] S. J. Papadakis, E. P. de Poortere, M. Shayegan, and R. Winkler, *Phys. Rev. Lett.* **84**, 5593 (2000).
- [129] R. Danneau, O. Klochan, W. R. Clarke, L. H. Ho, A. P. Micolich, M. Y. Simmons, A. R. Hamilton, M. Pepper, D. A. Ritchie, and U. Zülicke, *Phys. Rev. Lett.* **97**, 026403 (2006).
- [130] B. Grbić, R. Leturcq, T. Ihn, K. Ensslin, D. Reuter, and A. D. Wieck, *Phys. Rev. Lett.* **99**, 176803 (2007).
- [131] S. P. Koduvayur, L. P. Rokhinson, D. C. Tsui, L. N. Pfeiffer, and K. W. West, *Phys. Rev. Lett.* **100**, 126401 (2008).
- [132] C. H. L. Quay, T. L. Hughes, J. A. Sulpizio, L. N. Pfeiffer, K. W. Baldwin, K. W. West, D. Goldhaber-Gordon, and R. de Picciotto, *Nat. Phys.* **6**, 336 (2010).
- [133] H. De Raedt, K. Michielsen, and T. M. Klapwijk, *Phys. Rev. B* **50**, 631 (1994).
- [134] S. Chaudhure and P. F. Bagwell, *Phys. Rev. B* **51**, 16936 (1995).
- [135] M. Kupka, *Physica C* **281**, 91 (1997).
- [136] N. A. Mortensen, K. Flensberg, and A.-P. Jauho, *Phys. Rev. B* **59**, 10176 (1999).
- [137] M. J. M. de Jong and C. W. J. Beenakker, *Phys. Rev. Lett.* **74**, 1657 (1995).
- [138] F. Taddei, S. Sanvito, and C. J. Lambert, *J. Low Temp. Phys.* **124**, 305 (2001).
- [139] K. Xia, P. J. Kelly, G. E. W. Bauer, and I. Turek, *Phys. Rev. Lett.* **89**, 166603 (2002).
- [140] M. Eschrig, *Phys. Rev. B* **80**, 134511 (2009).
- [141] R. Grein, T. Löfwander, G. Metalidis, and M. Eschrig, *Phys. Rev. B* **81**, 094508 (2010).
- [142] J. N. Kupferschmidt and P. W. Brouwer, *Phys. Rev. B* **83**, 014512 (2011).
- [143] D. Futterer, M. Governale, U. Zülicke, and J. König, *Phys. Rev. B* **84**, 104526 (2011).

# List of Publications

- (A)** *Non-local Andreev transport through an interacting quantum dot,*  
D. Futterer, M. Governale, M. G. Pala, and J. König, Phys. Rev. B **79**, 054505 (2009).
- (B)** *Generation of pure spin currents by superconducting proximity effect in quantum dots,*  
D. Futterer, M. Governale, and J. König, EPL **91**, 47004 (2010).
- (C)** *Probing the exchange field of a quantum-dot spin valve by a superconducting lead,*  
B. Sothmann, D. Futterer, M. Governale, and J. König, Phys. Rev. B **82**, 094514 (2010).
- (D)** *Band-mixing-mediated Andreev reflection of semiconductor holes,*  
D. Futterer, M. Governale, Z. Zülicke, and J. König, Phys. Rev. B **84**, 104526 (2011).
- (E)** *Renormalization effects in proximized interacting quantum dots,*  
D. Futterer, J. Swiebodzinski, M. Governale, and J. König, Phys. Rev. B **87**, 014509 (2013).

Parts of this thesis have been published. The contents of Chapter 4 have been published in Ref. **(A)**. The results presented in Chapter 5 have been published in Ref. **(E)** and the results of Chapter 6 have been published in Ref. **(D)**.



# Acknowledgements

I wish to express my greatest thanks to the following people:

**Prof. Dr. Jürgen König** for being a great supervisor and for opening the possibility for my PhD studies in his group. He has always been open for physical discussions which typically turned out to be expedient and he gave me the opportunity to be part of the physical community.

**Prof. Dr. Michele Governale** for inviting me to Victoria University of Wellington, New Zealand at the first place. Furthermore, for our scientific discussions and collaborations over the last years as well as for the fine time we spent together in Wellington.

**Dr. Björn Sothmann, Dr. Jacek Swiebodzinski, and Prof. Dr. Ulrich Zülicke** for fruitful discussions and successful collaborations.

**A. Martín-Rodero and A. Levy Yeyati** for fruitful discussions and for providing their NRG data.

**Dr. Arijit Saha** for scientific discussions.

**Dr. Bastian Hiltcher and Dr. Stephan Lindebaum** for their personal friendship. They helped me solving numerous physical problems and each day in office with them was an enrichment.

**Stephan Rojek** for many discussions and the time spent during, between, and after work.

**Dr. Alfred Hucht** for helping me with uncounted 'Mathematica' problems.

**All members of the AG König and AG Entel** for the nice working environment.

**Mascha Katharina Wolf and my complete family** for their support and care.



# Lebenslauf

Der Lebenslauf ist in der Onlineversion aus Gründen des Datenschutzes nicht enthalten.



Duisburg, 30.01.2013

### **Erklärung**

Ich bestätige mit meiner Unterschrift, dass ich die vorliegende Dissertation „Transport through Hybrid Superconducting/Normal Nanostructures“ selbstständig verfasst habe und dabei nur die angegebenen Hilfsmittel verwendet habe. Wörtlich oder inhaltlich übernommene Stellen sind als solche gekennzeichnet.

Darüber hinaus bestätige ich, dass die vorliegende Dissertation „Transport through Hybrid Superconducting/Normal Nanostructures“ nur in diesem Promotionsverfahren an der Fakultät für Physik der Universität Duisburg-Essen eingereicht wurde.

David Futterer